Martin Jakob Ganahl

Simulation of Spin Transport in One Dimensional Quantum Heisenberg Spin 1/2 Systems in Real Time

DIPLOMARBEIT

zur Erlangung des akademischen Grades
Diplom-Ingenieur
Diplomstudium Technische Physik

Technische Universität Graz

Betreuer:
Ao.Univ.-Prof. Dipl.-Ing. Dr.rer.nat. Hans Gerd Evertz
Institut für Theoretische Physik - Computational Physics

Graz, Mai 2010

To my family and my friends

Zusammenfassung

Die Ausbreitungseigenschaften von Spinanregungen in ein dimensionalen Heisenbergsystemen werden mithilfe exakter Diagonalisierung und Matrix Produkt Zuständen untersucht. Es stellt sich heraus, dass Zwei- und Mehrteilchenanregungen aus dem ferromagnetischen Grundzustand des Heisenberg Systems in ungebundene und gebundene Spinzustände zerfallen die sich mit unterschiedlichen Geschwindigkeiten fortbewegen. Die numerischen Ergebnisse werden mithilfe der analytisch exakten Lösungen des Bethe Ansatzes interpretiert. In einem zweiten Teil der Arbeit wird die Ausbreitung von Magnetisierungsanregungen in zwei gekoppelten Spinketten untersucht. Die Ketten sind dabei an einer Stelle über eine S_z und S_{xy} Kopplung miteinander verbunden. Als Startzustand wird eine gaußförmige Dichteanregung aus dem Grundzustand bei Halbfüllung mithilfe eines Magnetfeldes erzeugt. Bei t = 0 wird dieses Magnetfeld abgeschaltet und die Ausbreitung der Anregung verfolgt. Es ergibt sich, dass die Transmissivität über die Störstelle über die Kopplungsparameter zwischen den Ketten variiert werden kann.

Abstract

Spin transport in one dimensional Heisenberg spin 1/2 systems are investigated with exact diagonalization and matrix product state techniques (time evolving block decimation). In the quantum Heisenberg chain, single and many-particle excitations from the ferromagnetic, aligned state decay into bound and unbound states which travel at different speed. Numerical results are compared to the analytical solution from the Bethe Ansatz. In a second part, real time propagation of spin density excitations in two coupled Heisenberg chains is investigated. The chains are coupled at one site by a S_z and S_{xy} coupling. As initial state the chains were prepared in the ground state at half filling with a gauss shaped spin-density excitation, created with a magnetic field. At t=0, the magnetic field is switched off and the time evolution of the state is observed. As it turns out, the scattering of the emerging spin-density waves at the connection can be varied with the coupling strength between the chains.

Contents

List of Figures

Chapter 1

Introduction

Our understanding of Nature rests on the foundations of Quantum Mechanics, and many phenomena can only be understood in its framework. Thus the ability to simulate quantum systems is not only an interesting topic on its own but also of fundamental importance for developing new materials and devices with yet unknown properties like quantum computers, organic superconductors, biomolecules with special properties, nano wires, quantum circuits and so on. Though the equations describing the properties of quantum systems can readily be deduced, their solution in general is a close to impossible task because the number of degrees of freedom of quantum systems grows exponentially in system size, and unluckily all physical systems of interest are essentially large (in a quantum mechanical sense).

Of course, approximation methods have been developed with the aid of which answers to interesting and important question on the structure and on the properties of many physical systems could be found. Many of these methods however neglect correlation effects and thus can only be applied to a limited number of systems (weakly correlated ones). The band structures of many metals like the rare earth metals can for example not be understood from such simple model systems and strong interactions and long range correlation have to be taken into account.

Simulation of strongly correlated materials on the other hand is one of the biggest challenges in physics, and some of the most efficient algorithms in computer science have been developed to compute properties of such systems, like Quantum Monte Carlo methods (QMC), Numerical Renormalization Methods (NRT) or , for 1-d systems, the Density Matrix Renormalization Group (DMRG). Two typical model systems for strongly correlated materials are the Hubbard model and the Heisenberg model, but of course there are many more. The Hubbard model for example is used to describe high temperature superconductors or magnetic properties of solids. The Heisen-

berg model captures the Coulomb interaction of electrons in an effective spin interaction and is used to describe magnetic properties of ferromagnets, anti ferromagnets and also ferrimagnets.

With methods like QMC, NRG or DMRG (in one dimension), systems in equilibrium have been intensively investigated, but despite the great success of these methods in the equilibrium case, little progress has been made in the area of simulating far from equilibrium dynamics of strongly correlated quantum systems. The reason for this again is the large Hilbert space dimension of the underlying system. A suitable approximation scheme for non equilibrium quantum states was unknown for a long time. The structure of a non equilibrium state is hard to analyze and in general a very large number of basis states contributes to it. Standard methods to time evolution of quantum systems used to be full and exact diagonalization (Lanzcos-method) which are restricted to small systems of $\approx$ 20-25 sites (see [1] for a review).

This changed when in 2003/2004, White and Feiguin and Vidal et al. ([2, 3, 4]) published a number of papers which introduced an efficient time evolution scheme for one dimensional quantum system on a DMRG basis. In the present work, we will discuss this method in two of its variants and apply one of them to the Heisenberg system to study spin transport in one dimension.

In general, simulation of transport in one dimensional structures has been experiencing increasing attention: the scale on which electronic devices can be produced is already at a threshold where quantum effects start to play a crucial role. Understanding the physics of such systems is thus of fundamental importance for future applications and construction of small and efficient quantum circuits; new materials like nano tubes offer new ways of electron transport on a quantum scale; systems with quantum dots could be used as quantum gates; ... . The physics of such systems are highly complex and the equations in general are very complicated. Simulation tools are thus indispensable to gain insight into the various physical processes.

Especially since the successful trapping of ultra cold quantum gases in optical lattices with variable coupling strengths has become possible, new challenging experiments on quantum many body systems have enabled experimentalists to investigate many body effects in simple systems. In combination with new, effective simulation tools for quantum many body systems, this opens a new and rich field for research of all kinds ([5, 6, 7]).

Part I

The Model

In this work we investigate spin transport in the one dimensional Heisenberg spin 1/2 system. Since its invention it has attracted many theorists since it is one of the simplest quantum models on which one can study strong interaction effects in condensed matter. In one dimension there even exists an analytical solution (though it is somewhat cumbersome and unhandy) which was first formulated by Hans Bethe (the famous Bethe ansatz). It has since then also been applied to other models, like the one dimensional Hubbard model.

In recent years the model has again experienced a revival with the advent of efficient simulation techniques for time evolution (tDMRG and TEBD) which allow for a quantitative investigation of time evolution of all kinds of one dimensional systems. The transport properties of spin chains are interesting from a quantum computational view. A successful implementation of quantum algorithms needs a communication channel with the core processor, where quantum states can be read out with high fidelity. Recent investigations on spin and entanglement transport in spin chains propose that spin chains could serve as quantum wires for information transfer ([8, 9]).

Chapter 2

The Heisenberg Model in One Dimension

2.1 General Properties

The Heisenberg model is one of the simplest models on which one can study effects of strong interaction in solids. Here we will give a very brief discussion of the model and its basic features.

Let's start with the Hamiltonian. The most general case is the complete anisotropic one with the Hamiltonian H

$$H = \sum_{i=1}^{N} J_x S_i^x S_{i+1}^x + J_y S_i^y S_{i+1}^y + J_z S_i^z S_{i+1}^z + \mu \mathbf{B}\hat{\mathbf{S}} \tag{2.1}$$

where $\mathbf{B}$ is a magnetic field which couples to the magnetic moments of the spins. The behavior of the system depends very much on the coupling constants and also on the spacial dimensions. In this document, we will only be concerned with the 1 dimensional model. In general, one simplifies the problem by restriction of the parameters. Common choices are

$$\begin{aligned} J_y = J_x, J_z = 0 \quad &\text{XX model} \\ J_x = J_y, J_z \neq 0 \quad &\text{XXZ model} \end{aligned}$$

with $\mathbf{B} = 0$. The model shows a very rich spectrum of phenomena. Since we will look at propagation of spins in the XXZ chain, we will state some of the more important features for this model.

The XXZ model is critical for $|\Delta| \leq 1$. For $|\Delta| > 1$, there is an excitation gap from the ground state. The criticality of the system manifests itself in the divergence of the correlation length $\xi = \infty$ for all kinds of correlations. The

case $\Delta = 0$ corresponds to free particles on the chain. There has recently been a lot of interest in the entanglement properties of the ground states of such spin chains (see for example [10]). A quantity of interest is the entanglement entropy S (also known as von Neumann entropy) of a sub system I of an infinite system (a chain, in our case). It is defined as

$$S = \mathrm{tr}(\hat{\rho}_I \log_2(\hat{\rho}_I))$$

and is a measure of how strongly the system is entangled with its environment. For Heisenberg chains, these entanglement properties are closely related to whether or not the system is at a critical point. Handwavingly, one can argue that since critical system have infinite correlation length, and quantum correlations are due to the fact that separated parts of the system "feel" each other due to entanglement, the system is entangled over an infinite distance. For the von Neumann entropy $S(\hat{\rho}_I(L))$ (for shortness we will denote it by $S(L)$ in the following) of a system of length L, this means that $S(L)$ diverges for L$\rightarrow \infty$. Reality is however not always as bad as one might expect, and for many systems the divergence of $S(L)$ takes on the best possible behavior, namely it is logarithmic in L. Even more well behaved are system which are away from criticality. The XX model with transverse magnetic B_z field for example can be driven out of criticality by suitably chosen B_z, and in this case $S(L)$ saturates for large L at a finite value.

2.2 Transport and Entanglement in Spin Chains

Transport properties in Heisenberg chains have attracted many scientist. Especially interesting is the XX chain with and without transversal fields because it can be treated analytically. The time evolution of initial states with step like magnetization profile has been investigated and it has been shown by Hunyadi et al. and Antal et al.([11, 12]) that the magnetization fronts emerging from such a step like profile obey a scaling relation and that the magnetization transport in such chains is quantized.

Besides analytical work on spin chains, there has also been work done on real time evolution using time dependent density matrix renormalization methods. [13] investigated the dynamics and the transport properties of the half filled product state $|\uparrow \cdots \uparrow\downarrow \cdots \downarrow\rangle$ for different Heisenberg models with adaptive time-dependent DMRG which showed ballistic behavior for $|J_z| < 1$. Studies of the transition from ballistic to diffusive transport have also been done by [14]. They analyzed the dependence of the spatial width of a gauss-shaped magnetization excitation in the XXZ chain. The results indicate that in the massive regime of the XXZ chain ballistic transport occurred away from

half filling, whereas at half filling transport was observed to be diffusive, and in the massless regime of the XXZ chain, magnetization dynamics exhibit ballistic properties.

Another interesting topic is the propagation of entanglement in spin chains. Especially in the area of quantum information and quantum computation entanglement plays a crucial role. Spin chains have attracted attention because of their transport properties. For a successful implementation of quantum computing protocols, one needs a quantum "wire" which makes it possible to communicate with the core processor. This quantum wire should be a good "entanglement conductor". Spin chains are potential candidates for such quantum wires. [8] have investigated singlet transport in Heisenberg XX chains in staggered transverse field. They prepared the system in a Neel state and at t = 0 entangled two sites of one sublattice in a spin singlet. As it turns out, the propagation of such a state in a staggered field is largely confined to the sublattice and is proportional to the square of the magnetic field λ^2. They also looked at multiple singlet excitations in the staggered field configuration and found out that singlets on the same lattice interfered constructively whereas singlets on different sublattices do not interfere. If an XY anisotropy was introduced, they observed different propagation branches of singlets in the system. In [15], Duer et al investigated the time evolution of an initially unentangled state for long-range Ising type interactions, and were able to provide sufficient conditions under which the bipartite entanglement of blocks of spins of length L saturates at finite length scales.

A topic of utmost importance is entanglement in ground states of 1-d quantum systems and has been investigated by Latorre et al. and Vidal et al. ([10, 9]).. Ground state entanglement and simulatability of ground state properties are in close connection and have received great interest since the invention of density matrix renormalization group methods for 1-d systems. A consequence of these investigations is the insight that for many 1-d systems (especially non-critical ones), ground states of infinite chains are not entangled over infinite distances and that the entanglement of finite blocks of length L of these systems with the rest of the system (the environment) is finite in a certain sense for $L \to \infty$.

2.3 The Bethe Solution for the Dilute Limit

In this section I'm going to explain the major features of the Bethe solution of the Heisenberg magnet. Later on we will compare this solution to time evolution simulation of the spin chain. We will mainly follow the textbooks [16, 17] and the papers [18, 19, 20]. The Hamiltonian for the general 1-d

Heisenberg XXZ magnet is given by

$$H = \sum_i J_z \hat{S}_i^z \hat{S}_{i+1}^z + \frac{J_{xy}}{2}(\hat{S}_i^+ \hat{S}_{i+1}^- + \hat{S}_i^- \hat{S}_{i+1}^+) - \frac{\Delta N}{4} =$$
$$= J_{xy} \sum_i \Delta \hat{S}_i^z \hat{S}_{i+1}^z + \frac{1}{2}(\hat{S}_i^+ \hat{S}_{i+1}^- + \hat{S}_i^- \hat{S}_{i+1}^+) - \frac{\Delta N}{4} \tag{2.2}$$

where we have defined the anisotropy $\Delta = \frac{J_z}{J_{xy}}$ and the ladder operators $\hat{S}_i^+$ and $\hat{S}_i^-$ are

$$\hat{S}_i^+ = \hat{S}_i^x + i\hat{S}_i^y$$
$$\hat{S}_i^- = \hat{S}_i^x - i\hat{S}_i^y.$$

We'll look at the ferromagnetic phase of the system, which corresponds to $\Delta < 0$. For such a coupling, the ground state $|0\rangle$ of the magnet is the completely aligned (saturated) state

$$|0\rangle = |\downarrow \cdots \downarrow\rangle.$$

This state will represent our physical vacuum. Excitation from this vacuum are spin flips at certain sites. Note that the vacuum state is degenerate with the state where all spins point in the opposite direction (due to the spin flip symmetry of the Hamiltonian). For simplicity we will not deal with this problem and consider only the state with all spin pointing downwards.

For convenience we measure energies relative to the energy of the completely aligned state (which is the ground state of the ferromagnet). Usually J_{xy} is set to 1 and we will follow this convention in this document. A natural basis for this system is the product basis $|i_1 \dots i_N\rangle$ where $|i_k\rangle \in \{|\uparrow\rangle, |\downarrow\rangle\}$ are the eigenvectors of the $\hat{S}_k^z$ operator. However, we will adopt a different few where a spin up at site n is equivalent to a particle at site n. Please note that this is not the Jordan Wigner transformation but just convenient way of representing the state.

The Jordan Wigner transformation maps spins onto fermionic particles by introducing Fermi Dirac statistics for these particles. The Heisenberg Hamiltonian for the XXZ case can be transformed according to

$$\sigma_i^z = 2c_i^\dagger c_i - 1$$
$$\sigma_i^+ = \prod_{j<i} \sigma_j^z c_i$$
$$\sigma_i^- = \prod_{j<i} \sigma_j^z c_i^\dagger$$

We will however treat them as bosons so we don't need to care about the statistics. A state with M up spins thus corresponds to a state with M particles. For shortness, we will omit the basis states $|i_1 \cdots i_N\rangle$ in all equations and only work with the probability amplitude $\psi(x_1, x_2, \cdots x_M)$ of finding the M spins at the positions $x_1 < x_2 < \cdots < x_M$. (similar to the real space wave function). In the following, periodic boundary conditions are imposed. Lets first look at the case of only one up spin in the system. The eigenstates with one spin up are

$$\psi_k(x_1) = \frac{1}{\sqrt{N}} e^{ikx_1} \tag{2.3}$$

where k is quantized due to the pbc:

$$k = \frac{2\pi}{N} n, \quad n \in \mathbb{N}$$

and the dispersion relation is

$$E(k) = J_{xy}(\cos(k) - \Delta) \tag{2.4}$$

which is proved by a simple calculation. The one up-spin on the chain behaves like a free particle since there is only kinetic energy and no potential energy. These states are called one magnon states.

For two up spins, things get a bit more involved. Due to the $\hat{S}^z \hat{S}^z$ coupling, two adjacent spins feel a potential and hence can scatter (see [16]). An ansatz which takes such a possible scattering into account is

$$\psi(x_1, x_2) = \alpha e^{i(k_1 x_1 + k_2 x_2)} + \beta e^{i(k_2 x_1 + k_1 x_2)}. \tag{2.5}$$

This wave function is insensitive to the exchange of the momenta k_1 and k_2. The complex coefficients α and β have to be determined so that a set of conditions is fulfilled, two of which are translational invariance and normalizability for finite chains. The translational invariance of the system implies, that

$$\psi(x_1, x_2) = \psi(x_2, x_1 + N)$$

(this implicates that our particles are (hard core) bosons since moving one particle around the ring from the last to the first position does not change the wavefunction). Plugging in eq.(2.5) gives

$$\alpha = \beta e^{-ik_2 N} = \beta e^{ik_1 N} \tag{2.6}$$

which provides the quantization condition for the total momentum by

$$k = k_1 + k_2 = \frac{2\pi n}{N} \quad n \in \mathbb{N}.$$

A second condition inferred from eq.(2.6) is

$$\frac{\alpha}{\beta} = e^{ik_1 N}.$$

We distinguish now two situations for the wave function eq.(2.5): the two up-spins can either be so far apart that they cannot interact via the interaction potential, which means $|x_1 - x_2| > 1$, or they can be located at adjacent sites, thus $|x_1 - x_2| = 1$ (the case $x_1 = x_2$ is excluded because the spins cannot sit on the same site). For the first case, the wave function (2.5) is an eigenstate of eq.(2.2) for every ratio $\frac{\alpha}{\beta}$. Applying H to the wave function eq.(2.5) then yields

$$\begin{aligned} H\psi(x_1, x_2) &= J_{xy}\big(-2\Delta\psi(x_1, x_2) + \\ &+ \frac{1}{2}(\psi(x_1 - 1, x_2) + \psi(x_1 + 1, x_2) + \psi(x_1, x_2 - 1) + \psi(x_1, x_2 + 1))\big) \\ &= J_{xy}\big(-2\Delta + \cos(k_1) + \cos(k_2)\big) \end{aligned} \tag{2.7}$$

which has the exact same form as the dispersion of two non interacting single magnons with momenta k_1 and k_2 (see eq.(2.4)). Note however, that the pair (k_1, k_2) cannot take on all the values of the non interacting case because k_1 and k_2 have to meet further restrictions which single out the possible solutions. When the particles are not separated, they interact via the $\hat{S}^z\hat{S}^z$ term of the Hamiltonian. The action of H on a state $\psi(x_1, x_2 = x_1 + 1)$ is

$$\begin{aligned} H\psi(x_1, x_1 + 1) &= J_{xy}(-\Delta\psi(x_1, x_1 + 1) + \\ &+ \frac{1}{2}(\psi(x_1 - 1, x_1 + 1) + \psi(x_1, x_1 + 2)) \end{aligned} \tag{2.8}$$

since the particles can not hop onto the same site. Comparing eq.(2.8) to eq.(2.7), there are three terms missing: a $\Delta\psi(x, x + 1)$ and the two terms $\psi(x, x)$ and $\psi(x + 1, x + 1)$ where the particles would be at the same site. We can now recover the form of eq.(2.7) if we demand that

$$-\Delta\psi(x_1, x_1 + 1) + \frac{1}{2}(\psi(x_1, x_1) + \psi(x_1 + 1, x_1 + 1)) = 0 \tag{2.9}$$

because then we can add these two terms to eq.(2.8), thus arriving at eq.(2.7). The energy eigenvalues $E(k_1, k_2)$ for these states have the same form as for two superimposed magnons with energies $E(k_1) + E(k_2)$ and are given by

$$E(k_1, k_2) = J_{xy}(-2\Delta + \cos(k_1) + \cos(k_2))$$

where k_1, k_2 can now be complex and depend on the anisotropy Δ. Eq.(2.9) yields a condition for the ratio $\frac{\alpha}{\beta}$:

$$\frac{\alpha}{\beta} = -e^{i\Theta(k_1,k_2)} = -\frac{\Delta e^{i\frac{k_1-k_2}{2}} - \cos(\frac{k_1+k_2}{2})}{\Delta e^{-i\frac{k_1-k_2}{2}} - \cos(\frac{k_1+k_2}{2})}. \tag{2.10}$$

Equating this to the quantization condition eq.(2.6) yields the equations

$$\begin{aligned} k_1 &= \frac{2\pi}{N}\frac{2n_1+1}{2} + \Theta(k_1,k_2) \\ k_2 &= \frac{2\pi}{N}\frac{2n_2+1}{2} - \Theta(k_1,k_2) \quad n_1, n_2 \in \mathbb{N} \end{aligned} \tag{2.11}$$

which have to be solved consistently for every allowed value of the total momentum k. Computing the complete spectrum for the two spin-up case is a lengthy procedure, so we will only state the results and refer the reader to [16, 17, 18, 19]. The eigenstates of the system split up into two classes: The two magnon scattering states and the two magnon bound states. We will briefly state the main features of these classes:

- The two magnon scattering states are characterized by a set of real numbers k_1 and k_2 which are related to the total momentum k by $k = k_1 + k_2$. In the limit $N \to \infty$ they form a continuous spectrum of excitations. For $k_1 = 0$, the energy-momentum relation of the scattering states can be computed analytically and coincides with the superposition of two independent one magnon states with the same momenta k_1, k_2. We follow the convention of [18] and call these states C_1 states. The dispersion relation for the C_1 states is

  $$E_{C_1}(k_1 = 0, k_2) = J_{xy}(\cos(k_1 + k_2) - 2\Delta) = J_{xy}(\cos(k_2) - 2\Delta).$$

  The C_1 states can be interpreted as superpositions of two non-interacting magnons where one magnon rests with momentum $k_1 = 0$ and the other one moves with momentum k_2. Inspection of the dispersion of the rest of the scattering states (we call them C_2 states) shows, that the energy of a (k_1,k_2)-scattering state is slightly shifted away from that of an independent superposition of a k_1 and k_2 single magnon state. Hence the C_2 states are NOT independent superpositions of single magnon states because the two magnons can interact via the S^zS^z potential. Their energies are however close to the non-interacting case. In fig.2.1 we plotted the complete spectrum of the two particle excitations for the isotropic Heisenberg chain from [18] for 36 sites. The C1 states are denoted by the red circles.

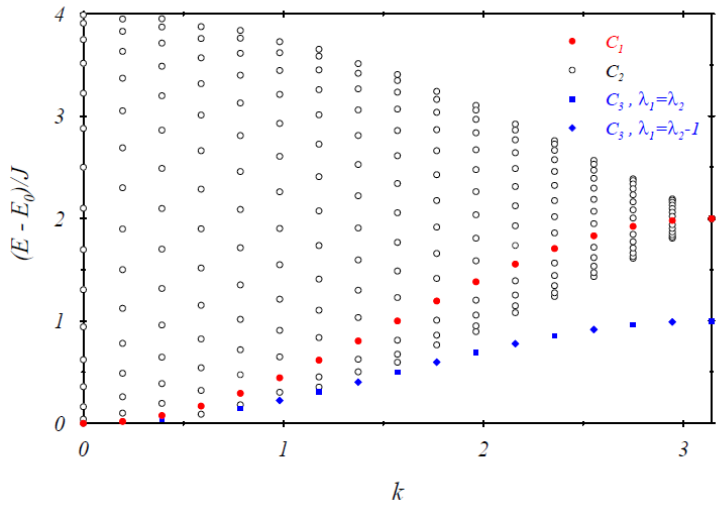

Figure 2.1: Two magnon excitation spectrum of the isotropic Heisenberg chain, taken from [18]. Red circles denote the C_1 states with $k_1 = 0, k_2 = k$; black circles are the rest of the two magnon scattering states. Blue circles denote the two magnon bound states.

- For the second class, the two magnon bound states, the k_1 and k_2 numbers are complex and are given by

$$k_1 = \frac{k}{2} - i\frac{\delta}{2} \qquad (2.12)$$
$$k_2 = \frac{k}{2} + i\frac{\delta}{2}$$

so that energy and momentum remain real. Without loss of generality we can assume $\delta > 0$. Their dispersion relation is given by

$$J_{xy}\big(-2\Delta + \cos(k/2)\cosh(\delta)\big) = -J_{xy}\big(\Delta - \frac{1}{2\Delta} - \frac{1}{2\Delta}\cos(k)\big) \qquad (2.13)$$

All states lie on a single branch in k-space (see fig.2.1). They are the lowest two particle excitations of the ferromagnet. We can rewrite

eq.(2.5) in terms of relative coordinates by defining

$$\begin{aligned} x &= x_1 + x_2 \\ r &= x_1 - x_2 \\ k &= k_1 + k_2 \\ \kappa &= k_1 - k_2 \\ \psi(x_1, x_2) &= e^{ixk}(e^{-i\kappa r/2} - e^{i\kappa r/2 - i\Theta}) \end{aligned}$$

If we take the limit $N \to \infty$, the second term $e^{i\kappa r/2} = e^{\delta r/2}$ diverges for $r \to \infty$. However, the two magnon bound states remain normalizable if we demand that the the term $e^{-i\Theta}$ vanishes (Remark: if we had chosen $\delta < 0$, we had to demand that $e^{i\Theta}$ vanishes). This leads us to the equation

$$\cos k/2 = \Delta e^{-\delta/2}$$

where δ denotes the imaginary part of k_1 (see above). Since $e^{-\delta/2} < 1$, this condition implies, that for $-1 < \Delta < 1$ there is a threshold so that bound states exist not for every value of k $\in [0, 2\pi)$ but only, if

$$\cos(k/2) < \Delta$$

which can be rewritten as

$$\cos(k) < 2\Delta^2 - 1. \tag{2.14}$$

In fig.2.2 we plotted the dispersion of the two magnon bound states for different values of Δ.

We have only considered two-particle excitations, but the Bethe ansatz can be applied to the full problem as well. The general ansatz for the wave function of the Heisenberg system with M particles (=up-spins) is

$$\psi(x_1, x_2, \cdots, x_M) = \sum_P A_P \prod_{n=1}^{M} \exp(ix_n k_{Pn})$$

where x_i denotes the location of particle i and the sum goes over all permutations of the M momenta k_l. From the translational invariance there follows a set of equations for the M momenta $k_1, ..., k_M$ and $M-1$ two body scattering phases $Theta(k_q, k_2)$ of the form of eq.(2.10) and (2.11). This system of equations has to be solved consistently for every allowed value of the total momentum $k = \sum_{i=1}^{M} k_i$. This is in general a formidable task and will

not be pursued any further. Remarkably, for a number $n < N/2$ up-spins in the system, these n up-spins form bound spin complexes (see end of [18] and [17]) which are called n-strings. These n-strings are stable only for a certain region of Δ, similar to the two magnon bound states (2-strings). The dispersion relation for these n-strings is given by

$$E(k) = -\frac{\sin\mu}{\sin(n\mu)}(\cos(n\mu) - (-1)^n \cos(k)) \tag{2.15}$$

whith

$$\Delta \quad (= J_z/J_{xy}) = -\cos(\mu).$$

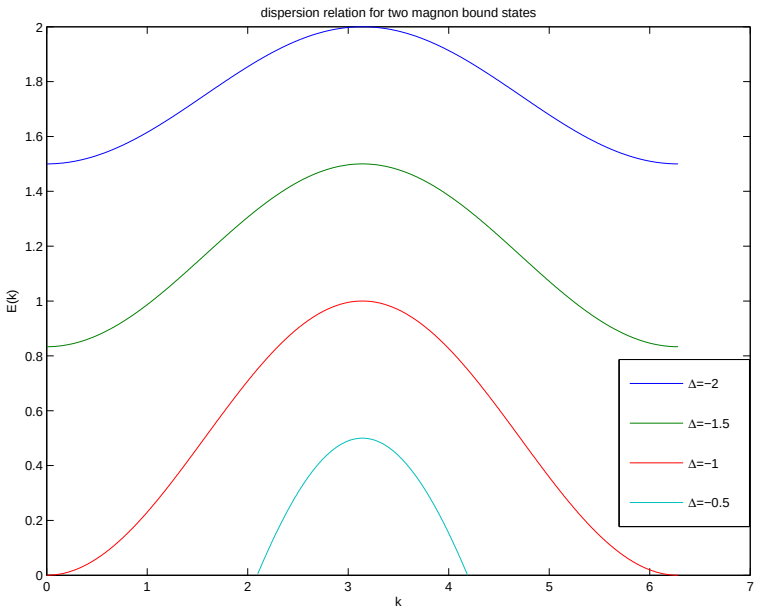

Figure 2.2: Dispersion for two magnon bound states for different values of the anisotropy Δ. For $\Delta < 1/\sqrt{2}$, not all values of k are allowed.

Part II

Approximate Description of 1-d Quantum Many Body States

Chapter 3

General Remarks

In this section we will develop the basic ideas that make strongly correlated quantum systems amenable to approximate time evolution. The most important concept is the representation of many body quantum states in terms of sets of matrices which gives rise to the definition of so called Matrix Product States (MPS). In this chapter, we will introduce the reader to the basic features of matrix product states. We will not give a complete review of the topic since there's no direct need for this. The interested reader who wants to delve deeper into the subject shall be referred to the reviews [21, 22].

Chapter 4

Matrix Product States (MPS)

4.1 What are MPS?

Before going into the mathematical details of such states, we will introduce them in a phenomenological way. Fig.4.2 shows the graphical representation of the following construction. Think of a one dimensional quantum system with obc like in fig.4.1.

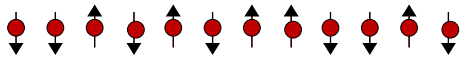

Figure 4.1: Scetch of a one dimensional spin system

We want to construct an "effective" basis for this system which is capable of approximating the ground state of a large chain. We can now diagonalize a small system of say $n = 4$ sites. In this way we get the ground state in some computational basis $|\beta\rangle$ of dimension χ. We can now add a site to this system and construct a basis for the new $n+1$ sites system from the outer products $|\beta\rangle \otimes |i_1\rangle$ with dimension χd, where d is the local Hilbert space dimension of $|i_1\rangle$. In the next step we now project these states $|\beta\rangle \otimes |i_1\rangle$ down to a lower dimensional subspace of dimension χ by applying a reduced basis transformation:

$$|\alpha_1\rangle = \sum_{\beta,i_1} A^{i_1}_{\beta\alpha_1} |\beta\rangle |i_1\rangle$$

If A is chosen properly, then this new reduced basis is able to accurately describe the ground state of the $n+1$ sites system. If we iterate these steps, we can thus construct an approximate basis which is able to describe the

ground state of a very large system of $n+N$ sites. This approximate ground state then can be written as

$$|\psi\rangle = \sum_{\{i_k\}\{\alpha_j\}} A^{i_1}_{\beta\alpha_1} A^{i_2}_{\alpha_1\alpha_2} \cdots A^{i_N}_{\alpha_{N-2}\alpha_{N-1}} |\beta\rangle\, |i_1 \cdots i_N\rangle$$

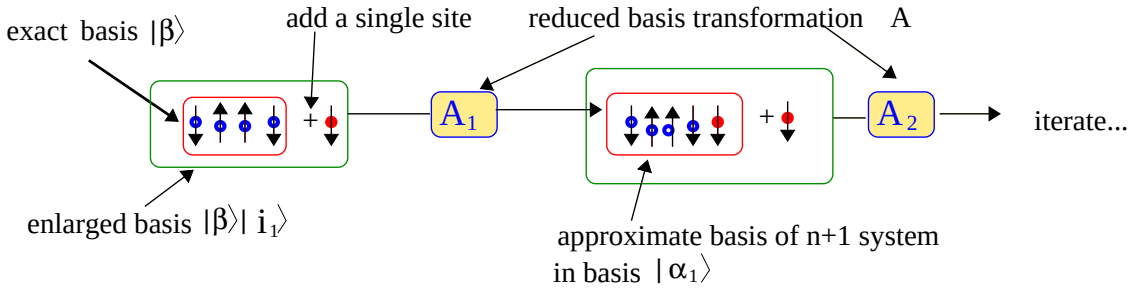

Figure 4.2: Construction of a MPS basis for description of the ground state of a quantum system.

After these preliminaries, let us now introduce MPS in a more mathematical fashion. Let

$$|\psi\rangle = \sum_{\{i_k\}} c_{i_1\cdots i_n} |i_1 \ldots i_N\rangle$$

be an arbitrary state in a many-particle Hilbert space with N the number of lattice points and let $|i_n\rangle$ denote a set of eigenstates of a local quantum system. We will only be concerned with one dimensional systems with open boundary conditions (obc). A very common case for $|i_n\rangle$ is the $|\uparrow\rangle, |\downarrow\rangle$ system of eigenstates of the spin-1/2 operator $\hat{S}_z$. Another choice could be a system of N electrons. Here, a many particle-state is specified by putting every electron into a certain single particle state, in this case a certain position on the lattice, and then antisymmetrize over the permutations of the electrons. In this way, we arrive at a state representation which looks like

$$|\psi\rangle = \sum_{n_1\cdots n_N=0,1} \alpha_{n_1\cdots n_N} |n_1 \cdots n_N\rangle,$$

where

$$|n_1 \cdots n_N\rangle = \frac{1}{\sqrt{n_1! \cdots n_N!}} (a_1^\dagger)^{n_1} \cdots (a_N^\dagger)^{n_N} |0\rangle$$

is a totally antisymmetric many particle state and $a_i^\dagger$ is the creation operator of a particle at site i. We can now treat the n_i as local quantum numbers

namely the eigenvalues of the (local) density operator $\hat{n}_i = a_i^\dagger a_i$. For the sake of simplicity, we will consider only the first case of a local basis of dimension $d = 2s + 1$ in the Hilbert space of an angular momentum operator $\vec{\hat{S}}$ with s the quantum number of $\vec{\hat{S}}^2$. In the following we will introduce so called Matrix Product States (MPS) as a new representation of quantum many body states of one dimensional systems.

A matrix product state with open boundary conditions is defined by the following equation:

$$|\psi\rangle = \sum_{\{i_k\}\{\alpha_j\}} \langle\phi_L| A^{[1]i_1}_{\alpha_1\alpha_2} \dots A^{[N]i_N}_{\alpha_{N-2}\alpha_{N-1}} |\phi_R\rangle \quad |i_1 \dots i_N\rangle \tag{4.1}$$

At every site of the system there are d matrices (one for every local state) with a so called auxiliary dimension χ. By computing the matrix-product of every combination of $i_1 \cdots i_N$ and sandwiching the resulting matrix between two auxiliary vectors $|\phi_L\rangle, |\phi_R\rangle$, one gets the "scalar" coefficients of the many particle state. Note that the matrices also carry a site index in square brackets. This site index will be omitted when we don't explicitly need it. We also will often omit the auxiliary indices α_k of the matrices to make the equations more readable.

It is a very common notation to write the left and right boundary expressions as

$$\begin{aligned} \langle\phi_L|A^{i_1} &= \sum_{\alpha_0} \phi^L_{\alpha_0} A^{i_1}_{\alpha_0\alpha_1} = A'^{i_1}_{\alpha_1} \\ A^{i_N}|\phi_R\rangle &= \sum_{\alpha_{N+1}} A^{i_N}_{\alpha_N\alpha_{N+1}} \phi^R_{\alpha_{N+1}} = A'^{i_N}_{\alpha_N} \end{aligned} \tag{4.2}$$

and rewrite eq. (4.1) as

$$|\psi\rangle = \sum_{i_1 \dots i_N} A'^{[1]i_1} A^{[2]i_2} \dots A'^{[N]i_N} |i_1 \dots i_N\rangle$$

where we treat $A'^{[1]i_1}$ and $A'^{[N]i_N}$ as vectors of dimension χ. For the rest of the document we will only consider MPS with obc. To make the equations more readable, we will omit the side index $[n]$ of the matrices and replace $A^{[n]i_n}$ by A^{i_n}.

Side remark: If we want to impose periodic boundary conditions, we can construct a periodic MPS (one which is invariant under translations) via

$$|\psi\rangle = \sum_{i_1 \dots i_N} \mathrm{tr}(\mathrm{A}^{[1]\mathrm{i}_1} \dots \mathrm{A}^{[\mathrm{N}]\mathrm{i}_\mathrm{N}}) |\mathrm{i}_1 \dots \mathrm{i}_\mathrm{N}\rangle.$$

Due to the cyclic invariance of the trace, the state is invariant under a transformation of the following kind:

$$\hat{T}_r : |i_1 \dots i_N\rangle \mapsto |i_{1+r} \cdots i_{N+r}\rangle$$
$$\hat{T}_r|\psi\rangle = |\psi\rangle$$

where $i + r = i + r - N$ for $i + r > N$, due to the periodicity of the system. Note that this holds for an arbitrary integer r.

For reasons we will discuss below, we introduce a further definition: we call a MPS left or right orthonormal respectively, if **all** of the matrices A^{s_i} satisfy **one** of the following conditions:

$$\sum_{i_n} A^{i_n} A^{\dagger i_n} = \mathbb{1} \quad \forall n \quad \text{right} - \text{handed} \tag{4.3}$$

$$\sum_{i_n} A^{\dagger i_n} A^{i_n} = \mathbb{1} \quad \forall n \quad \text{left} - \text{handed} \tag{4.4}$$

In practice, one often works with states which are composed of outer products of left and right orthonormalized MPS. As we will see later, the so called density matrix renormalization group (DMRG) uses such states of mixed orthonormality.

We can rearrange the sums in eq. (4.1) to

$$|\psi\rangle = \sum_{\alpha_n} \underbrace{\left(\sum_{i_1 \cdots i_n} \sum_{\alpha_1 \cdots \alpha_{n-1}} A^{i_1}_{\alpha_1} A^{i_2}_{\alpha_1 \alpha_2} \cdots A^{i_n}_{\alpha_{n-1} \alpha_n} |i_1 \cdots i_n\rangle \right)}_{|\phi_{\alpha_n}\rangle}$$
$$\underbrace{\left(\sum_{i_{n+1} \cdots i_N} \sum_{\alpha_{n+1} \cdots \alpha_N} A^{i_{n+1}}_{\alpha_n \alpha_{n+1}} \cdots A^{i_N}_{\alpha_{N-1}} |i_{n+1} \cdots i_N\rangle \right)}_{|\chi_{\alpha_n}\rangle}. \tag{4.5}$$

Now if **all** A-matrices belonging to the states $|\phi_{\alpha_n}\rangle$ (which are also MPS) are **left** orthonormalized, then the states $|\phi_{\alpha_n}\rangle$ are orthonormalized. Similarly, if all A-matrices belonging to $|\chi_{\alpha_n}\rangle$ are **right** orthonormalized, then the states $|\chi_{\alpha_n}\rangle$ are orthonormal. This is a very appealing feature, and later on we will see how we can use this to our advantage. The proof of this statement is straightforward (see appendix A for a detailed derivation).

4.2 Calculation of Observables for MPS

We want to compute the expectation value $\langle\psi|\hat{O}|\psi\rangle$ of a many sites operator which has the form

$$\hat{O} = \prod_{n=1}^{N} \hat{O}_n.$$

Now it is useful to define new tensors E for every site n as

$$E^n_{\hat{O}_n} = E^{\hat{O}_n}_{\alpha_{n-1}\alpha_n\alpha'_{n-1}\alpha'_n} = \sum_{i_n i'_n} A^{i_n}_{\alpha_{n-1}\alpha_n} A^{*i'_n}_{\alpha'_{n-1}\alpha'_n} \langle i'_n|\hat{O}_n|i_n\rangle.$$

For shortness, we will omit the auxiliary indices of the E-tensors in the following. In terms of these tensors, the expectation value $\langle\hat{O}\rangle$ reads

$$\langle\hat{O}\rangle = \prod_{n=1}^{N} E^n_{\hat{O}_n}. \tag{4.6}$$

Because A_1 and A_N at the left and right boundaries are vectors, $E^1_{\hat{O}_1}$ and $E^N_{\hat{O}_N}$ are matrices (tensors of rank 2) of dimension χ, and the product (4.6) therefore is a (real) number, which gives the expectation value $\langle\hat{O}\rangle$, if the state $|\psi\rangle$ is normalized. These E-tensors have a nice graphical representation, given in fig.4.3. From this representation, the expectation value can also be represented graphically like in fig.4.4.

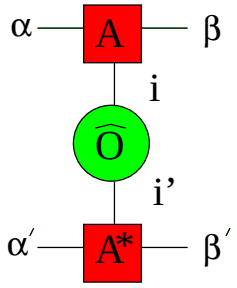

Figure 4.3: Graphical representation of an E-matrix. There is an implicit summation over connected lines. Lines with open ends correspond to uncontracted indices of the tensor.

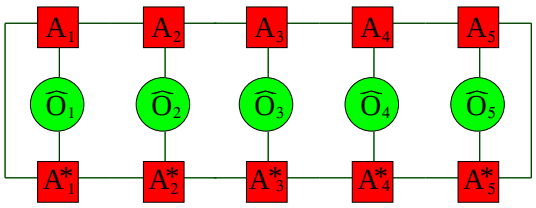

Figure 4.4: Graphical representation of the expectation value of a many sites operator $\prod_{n=1}^{N} \hat{O}_n$ with $N = 5$. There is an implicit summation over connected lines.

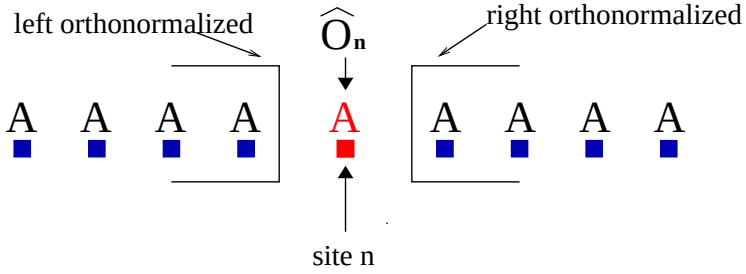

Figure 4.5: If the matrices are orthonormalized in the above way, calculation of $\langle \hat{O}_n \rangle$ of a single site operator at site n involves only contraction over the matrices A^{i_n} of site n (see also fig.4.6).

In practice, one often needs expectation values of single local operators, like S^i_z at site i. For a general MPS, if we want to calculate $\langle S^i_z \rangle$, we have to compute **all** E-matrices and contract them by means of eq. (4.6). On the other hand, if the MPS $|\psi\rangle$ has the property, that all A-matrices to the left of site i are left orthonormalized, and all matrices to the right of site i are right orthonormalized (see fig.4.5), then the evaluation of the expectation value does involve only the contraction of the matrices A^{i_n} at site n and is given by

$$\begin{aligned} \langle \hat{O}_n \rangle &= \sum_{\alpha_{n-1}\alpha_n\alpha'_{n-1}\alpha'_n} E^{\hat{O}_n}_{\alpha_{n-1}\alpha_n\alpha'_{n-1}\alpha'_n} \delta_{\alpha_n\alpha'_n}\delta_{\alpha_{n-1}\alpha'_{n-1}} = \\ &= \sum_{i_n,i'_n,\alpha_{n-1},\alpha_n} \langle i'_n|\hat{O}_n|i_n\rangle A^{i_n}_{\alpha_{n-1}\alpha_n} A^{*i'_n}_{\alpha_{n-1}\alpha_n}. \end{aligned} \tag{4.7}$$

Again, this is easiest remembered in the graphical representation of fig.4.6.

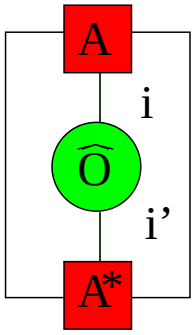

Figure 4.6: Graphical representation of the expectation value of a single site operator $\langle \hat{O}_n \rangle$ at site n for a state where A matrices to the left of site n are left orthonormalized and A matrices to the right of site n are right orthonormalized. Connected lines denote summation over a common index.

This can easily be reproduced by using a slightly modified eq. (4.5) of the MPS $|\psi\rangle$, where we pull out the matrices A^{i_n} at site n:

$$
\begin{aligned}
|\psi\rangle = & \\
= & \sum_{\alpha_n, i_n} \underbrace{\sum_{i_1 \cdots i_{n-1}} \sum_{\alpha_1 \cdots \alpha_{n-1}} A^{i_1}_{\alpha_1} \cdots A^{i_{n-1}}_{\alpha_{n-1}\alpha_{n-1}} |i_1 \cdots i_{n-1}\rangle}_{|\alpha_{n-1}\rangle} \quad A^{i_n}_{\alpha_{n-1}\alpha_n} |i_n\rangle \cdot \\
& \underbrace{\sum_{i_{n+1} \cdots i_N} \sum_{\alpha_{n+1} \cdots \alpha_N} A^{i_{n+1}}_{\alpha_n \alpha_{n+1}} \cdots A^{i_N}_{\alpha_{N-1}} |i_{n+1} \cdots i_N\rangle}_{|\alpha_n\rangle}
\end{aligned}
\tag{4.8}
$$

where due to the left and right orthonormality of the matrices the states $|\alpha_{n-1}\rangle$ and $|\alpha_n\rangle$ form an orthonormal set of states. From this representation, derivation of eq. (4.7) is straightforward.

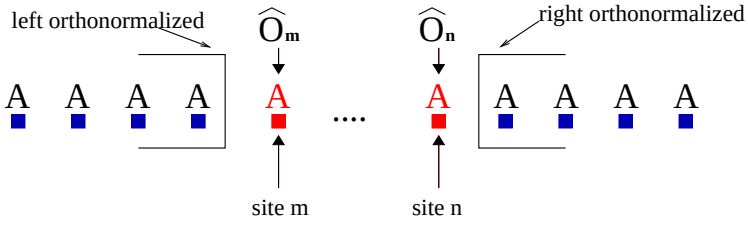

Figure 4.7: If the matrices are ortho normalized in the above way, calculation of $\langle \prod_{i=m}^{n} \hat{O}_i \rangle$ involves only contraction over the matrices $A^{[k]i_k}$ of sites k in between site m and site n.

The procedure can be extended to the calculation of k point correlators $\hat{O}_m\hat{O}_{m+1}\cdots\hat{O}_n$ with $m<n$. If again we assume that matrices to the left of site m are left orthonormalized, and those to the right of site n are right orthonormalized (see fig (4.7)), the $(n-m+1)$-point correlator $\langle\hat{O}_m\hat{O}_{m+1}\cdots\hat{O}_n\rangle$ reduces to a contraction over tensors that lie between the sites m and n and is given by

$$\langle\hat{O}_m\hat{O}_{m+1}\cdots\hat{O}_n\rangle=\prod_{k=m}^{n}E^k_{\hat{O}_k}$$

where the tensors $E^k_{\hat{O}_k}$ are

$$\begin{aligned}
E^m_{\hat{O}_m} &= \sum_{\alpha_{m-1}i_mi'_m} A^{i_m}_{\alpha_{m-1}\alpha_m}A^{*i'_m}_{\alpha_{m-1}\alpha'_m}\langle i'_m|\hat{O}_m|i_m\rangle && \text{site } m\\
E^k_{\hat{O}_k} &= \sum_{i_ki'_k} A^{i_k}_{\alpha_{k-1}\alpha_k}A^{*i'_k}_{\alpha'_{k-1}\alpha'_k}\langle i'_k|\hat{O}_k|i_k\rangle && m<k<n\\
E^n_{\hat{O}_n} &= \sum_{\alpha_ni_ni'_n} A^{i_n}_{\alpha_{n-1}\alpha_n}A^{*i'_n}_{\alpha'_{n-1}\alpha_n}\langle i'_n|\hat{O}_n|i_n\rangle && \text{site } n
\end{aligned}\qquad(4.9)$$

and E^m and E^n are matrices of dimension χ. To calculate the correlator, first compute the leftmost E-matrix E^m (tensor of rank 2). This matrix has two auxiliary indices. Then compute the E-tensor E^{m+1} at the next site and contract the two tensors over their common indices to obtain a new matrix. In fig. (4.8) you find a graphical representation of such a contraction. To this new matrix, add the matrix E^{m+2} in the same way as before. Iterate these steps until you reach the rightmost matrix E^n at which point the contraction results in a scalar. In this way, one arrives at a picture like in fig.4.4 where one only sums over the matrices $E^k_{\hat{O}_k}$ with $m\le k\le n$. Note that the matrices between sites m and n do not have to be orthonormal. However, the state has of course to be normalized.

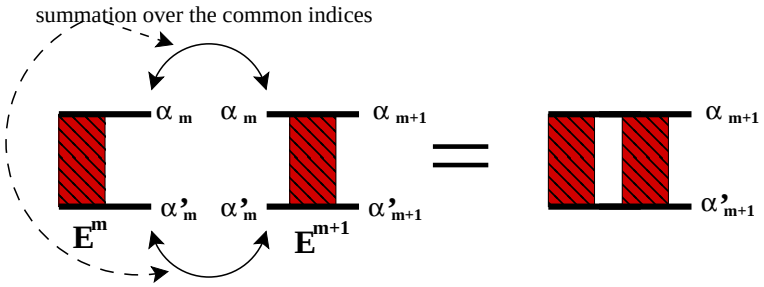

Figure 4.8: Graphical representation of contraction of E matrices. The right object is again a matrix with two indices.

Before we go further into examining the properties of MPS, we introduce the important concept of Schmidt decompositions.

4.3 The Schmidt Decomposition and the Canonical Representation of Quantum Many Body States

4.3.1 Schmidt Decomposition

The Schmidt decomposition is a special representation of a quantum many body state. It employs the fact that an arbitrary many particle system can always be cut into two distinct systems. Let us consider a general state $|\psi\rangle$ given by

$$|\psi\rangle = \sum_{i_1 \dots i_n} c_{i_1 \dots i_n} |i_1 \dots i_N\rangle$$

we now make a virtual cut of this system into two parts A and B by relabeling the indices $(i_1 \cdots i_l)$ and$(i_{l+1} \cdots i_N)$ in the following way:

$$\begin{aligned} (i_1 \cdots i_l) &= \alpha \\ (i_{l+1} \cdots i_N) &= \beta \\ |\psi\rangle = \sum_{(i_1 \dots i_l)(i_{l+1} \cdots i_N)} & c_{(i_1 \dots i_l)(i_{l+1} \cdots i_N)} |i_1 \dots i_l\rangle |i_{l+1} \dots i_N\rangle \end{aligned} \tag{4.10}$$

In this way we arrive at a representation of the state $|\psi\rangle$ of the form

$$|\psi\rangle = \sum_{\alpha,\beta} c_{\alpha,\beta} |\alpha\rangle |\beta\rangle \tag{4.11}$$

where $|\alpha\rangle$ and $|\beta\rangle$ are orthonormal bases for the two subsystem under consideration. The matrix $c_{\alpha\beta}$ contains information about the entanglement of the two subsystems. If for example $c_{\alpha\beta} = a_\alpha b_\beta$, the two blocks are completely unentangled. We now apply a singular value decomposition to the matrix c:

$$c = U \lambda V^\dagger.$$

Inserting this into eq. (4.11) we arrive at an expression

$$|\psi\rangle = \sum_i \lambda_{ii} \underbrace{(\sum_\alpha U_{\alpha i} |\alpha\rangle)}_{|\Phi_i^A\rangle} \underbrace{(\sum_\beta V_{i\beta}^\dagger |\beta\rangle)}_{|\Phi_i^B\rangle} \tag{4.12}$$

for $|\psi\rangle$ where we call $|\Phi_i^A\rangle$ and $|\Phi_i^B\rangle$ the Schmidt vectors and λ_{ii} the Schmidt eigenvalues (or Schmidt coefficients) of the systems A and B respectively. From the unitarity properties of U and V and the orthonormality of the states $|\alpha\rangle$ and $|\beta\rangle$ one can easily deduce the orthonormality of the set of Schmidt states for each subsystem:

$$\begin{aligned}\langle\Phi_j^A|\Phi_i^A\rangle &= \sum_{\alpha\alpha'} U^*_{\alpha' j} \underbrace{\langle\alpha'|\alpha\rangle}_{\delta_{\alpha'\alpha}} U_{\alpha i} \\ &= \sum_{\alpha} U^\dagger_{j\alpha} U_{\alpha i} = \delta_{ij}\end{aligned}$$

and for system B

$$\begin{aligned}\langle\Phi_j^B|\Phi_i^B\rangle &= \sum_{\beta\beta'} V^{\dagger *}_{j\beta'} \underbrace{\langle\beta'|\beta\rangle}_{\delta_{\beta'\alpha}} V^\dagger_{i\beta} \\ &= \sum_{\beta} V^\dagger_{i\beta} V_{\beta j} = \delta_{ij}\end{aligned}$$

The completeness relation for, say, subsystem A reads

$$\sum_i |\Phi_i^A\rangle\langle\Phi_i^A| = \mathbb{1} \tag{4.13}$$

and is proved by considering the action of $\sum_i |\Phi_i^A\rangle\langle\Phi_i^A|$ on an arbitrary state $|i_1 \cdots i_l\rangle$ of subsystem A. If this action results in the same state $|i_1 \cdots i_l\rangle$, then the completeness relation holds in system A:

$$\begin{aligned}\sum_\beta |\Phi_\beta^A\rangle\langle\Phi_\beta^A| \underbrace{|i_1 \cdots i_l\rangle}_{\equiv|\gamma\rangle} &= \sum_{\beta\alpha\alpha'} U_{\alpha\beta} U^\dagger_{\beta\alpha'} |\alpha\rangle \underbrace{\langle\alpha'|\gamma\rangle}_{\delta_{\alpha'\gamma}} = \\ \sum_\alpha \underbrace{\sum_\beta U_{\alpha\beta} U^\dagger_{\beta\gamma}}_{\delta_{\alpha\gamma}} |\alpha\rangle &= |\gamma\rangle\end{aligned}$$

which proves the above equation.

The λ_{ii} have also a physical interpretation: The squared norms $|\lambda_{ii}|^2$ of the Schmidt eigenvalues are the eigenvalues of the reduced density operator $\hat{\rho}^{(A,B)} = \mathrm{tr}_{(B,A)}(|\psi\rangle\langle\psi|)$ of the system in state $|\psi\rangle$ obtained by tracing out either subsystem A or B. This follows from eq.(4.12) and the orthonormality and completeness of the states $|\phi_\alpha\rangle$ and $|\phi_\beta\rangle$:

$$\hat{\rho}^B = \mathrm{tr}_A(|\psi\rangle\langle\psi|) = \tag{4.14}$$
$$= \sum_{ii'i''} \lambda_{i'i'} \lambda^*_{i''i''} \langle\phi^A_i|\phi^A_{i'}\rangle\langle\phi^A_{i''}|\phi^A_i\rangle|\phi^B_{i'}\rangle\langle\phi^B_{i''}| = \sum_i \lambda_i^2 |\phi^B_i\rangle\langle\phi^B_i|$$

This means that the states $|\phi^B_i\rangle$ are the eigenvectors of the reduced density matrix $\hat{\rho}^B$ of system B. A similar calculation shows that $|\phi^A_i\rangle$ are the eigenvectors of the reduced density matrix $\hat{\rho}^A$ of system A.

4.3.2 Canonical Matrix Product States

We will now construct a special representation of the state $|\psi\rangle$ which we will later on use to develop a simulation scheme for the time evolution of quantum states (see also[2, 3]).

Start with a Schmidt decomposition where system A consists of only one site:

$$|\psi\rangle = \sum_{\alpha_1} \lambda^{[1]}_{\alpha_1} |\Phi^1_{\alpha_1}\rangle |\Phi^{2\cdots N}_{\alpha_1}\rangle$$

The eigenstates $|\Phi^1_{\alpha_1}\rangle$ of the reduced density matrix for the system with only one site are

$$|\Phi^1_{\alpha_1}\rangle = \sum_{i_1} \Gamma^{[1]i_1}_{\alpha_1} |i_1\rangle,$$

where we introduced some fancy notation $\Gamma^{[1]i_1}_{\alpha_1}$ for the coefficients of the state $|\Phi^1_{\alpha_1}\rangle$ We already proved the existence of a set of Schmidt eigenstates for a certain partition of the system. In the next step we use this fact to write $|\psi\rangle$ in terms of Schmidt states belonging to a partition at site 2 of the system and equate it to the first representation:

$$|\psi\rangle = \sum_{\alpha_2} \lambda^{[2]}_{\alpha_2} |\Phi^{1,2}_{\alpha_2}\rangle |\Phi^{3\cdots N}_{\alpha_2}\rangle = \sum_{\alpha_1} \lambda^{[1]}_{\alpha_1} |\Phi^1_{\alpha_1}\rangle |\Phi^{2\cdots N}_{\alpha_1}\rangle$$

We now expand $|\Phi^{1,2}_{\alpha_2}\rangle$ in terms of $|\Phi^1_{\alpha_1}\rangle$ and $|i_2\rangle$ and $|\Phi^{2\cdots N}_{\alpha_1}\rangle$ in terms of $|i_2\rangle$ and $|\Phi^{3\cdots N}_{\alpha_2}\rangle$. We then get

$$\sum_{\alpha_1\alpha_2 i_2} \lambda^{[1]}_{\alpha_1} c^{i_2}_{\alpha_1\alpha_2} |\Phi^1_{\alpha_1}\rangle |i_2\rangle |\Phi^{3\cdots N}_{\alpha_2}\rangle = \sum_{\alpha_1\alpha_2 i_2} \lambda^{[2]}_{\alpha_2} \tilde{c}^{i_2}_{\alpha_1\alpha_2} |\Phi^1_{\alpha_1}\rangle |i_2\rangle |\Phi^{3\cdots N}_{\alpha_2}\rangle \tag{4.15}$$

where $c^{i_2}_{\alpha_1\alpha_2}$ are the expansion coefficients of $|\Phi^{1,2}_{\alpha_2}\rangle$ and $\tilde{c}^{i_2}_{\alpha_1\alpha_2}$ are those of $|\Phi^{2\cdots N}_{\alpha_1}\rangle$. Comparing the coefficients leads to the equation

$$\lambda^{[1]}_{\alpha_1} c^{i_2}_{\alpha_1\alpha_2} = \lambda^{[2]}_{\alpha_2} \tilde{c}^{i_2}_{\alpha_1\alpha_2} \tag{4.16}$$

We satisfy this by setting

$$c^{i_2}_{\alpha_1\alpha_2} = \lambda^{[2]}_{\alpha_2} \Gamma^{[2]i_2}_{\alpha_1\alpha_2} \tag{4.17}$$

$$\tilde{c}^{i_2}_{\alpha_1\alpha_2} = \lambda^{[1]}_{\alpha_1} \Gamma^{[2]i_2}_{\alpha_1\alpha_2} \tag{4.18}$$

The matrix $\tilde{c}$ can be obtained in the following way: We write $|\psi\rangle$ as

$$|\psi\rangle = \sum_{(\alpha_1 i_2)(i_3\cdots N)} a_{(\alpha_1 i_2)(i_3\cdots N)} |\Phi^1_{\alpha_1}\rangle |i_2\rangle |i_3 \cdots i_N\rangle = \sum_{(\alpha_1 i_2)m} a_{(\alpha_1 i_2)m} |\Phi^1_{\alpha_1}\rangle |i_2\rangle |m\rangle$$

and insert a SVD of the matrix $a_{(\alpha_1 i_2)m}$:

$$|\psi\rangle = \sum_{\alpha_2} \lambda^{[2]}_{\alpha_2} \left(\sum_{(\alpha_1 i_2)} U_{(\alpha_1 i_2)\alpha_2} |\Phi^1_{\alpha_1}\rangle |i_2\rangle \right) \left(\sum_m V^\dagger_{\alpha_2 m} |m\rangle \right)$$

which yields the following equation for the Schmidt states of the left system:

$$\sum_{(\alpha_1 i_2)} U_{(\alpha_1 i_2)\alpha_2} \, |\Phi^1_{\alpha_1}\rangle \, |i_2\rangle = \sum_{(\alpha_1 i_2)} \tilde{c}^{i_2}_{\alpha_1\alpha_2} \, |\Phi^1_{\alpha_1}\rangle \, |i_2\rangle$$

and thus

$$\tilde{c}^{i_2}_{\alpha_1\alpha_2} = U_{(\alpha_1 i_2)\alpha_2}.$$

If we now insert eq. (4.18) into eq. (4.15) we get

$$|\psi\rangle = \sum_{i_1 i_2 \alpha_1 \alpha_2} \Gamma^{[1]i_1}_{\alpha_1} \lambda^{[1]}_{\alpha_1} \Gamma^{[2]i_2}_{\alpha_1\alpha_2} \lambda^{[2]}_{\alpha_2} |i_1 i_2\rangle |\Phi^{3\cdots N}_{\alpha_2}\rangle.$$

By iterating these steps, one finally arrives at

$$|\psi\rangle = \sum_{\{i_k\}\{\alpha_l\}} \Gamma^{[1]i_1}_{\alpha_1} \lambda^{[1]}_{\alpha_1} \Gamma^{[2]i_2}_{\alpha_1\alpha_2} \lambda^{[2]}_{\alpha_2} \cdots \Gamma^{[N-1]i_{N-1}}_{\alpha_{N-2}\alpha_{N-1}} \lambda^{[N-1]}_{\alpha_{N-1}} \Gamma^{[N]i_N}_{\alpha_N - 1} |i_1 \ldots i_N\rangle \tag{4.19}$$

which surely is not the world's most handsome state representation, but despite its ugliness, this formula proves to be of considerable usefulness (we will come to this later).

In the above derivation we introduced the tensors $\Gamma^{[n]i_n}$ and λ. These tensors are of rank χ, where χ is the maximum number of non-zero Schmidt eigenvalues, taken over all bipartitions A:B:

$$\chi = max_{\text{all partitions A:B}}(\chi_A)$$

Note that the tensors $\Gamma^{[1]i_1}$ and $\Gamma^{[N]i_N}$ are vectors of dimension χ. All λ are diagonal matrices, that's why they carry only one index (apart from the site index).

It is a crucial feature of many local 1-d systems that the Schmidt eigenvalues λ of a bipartition A:B decay roughly exponentially in their indices, that is

$$\lambda_\alpha \propto \exp(-const.\alpha).$$

One can use this feature to develop an efficient simulation scheme for quantum many body systems.

Some remarks: The representation we derived is exact, as long as the dimension of the matrices is high enough. We could for example approximate the state eq.(4.19) by taking only those λ_α which are above a certain threshold, thus reducing the dimension of the matrices Γ and λ. In this way we get an approximation of the true state $|\psi\rangle$, which is the basic idea of all approximations done with MPS. This in turn affects the completeness relation eq. (4.13), because it holds only if the dimension of the matrices Γ is chosen large enough to faithfully represent the quantum state of the system. In the approximated scenario, the equality sign in eq. (4.13) is no more valid (but eq. (4.13) can still be very close to the identity in the relevant space). Especially if two blocks are highly entangled, we need many Schmidt eigenvalues which leads to a large dimension χ for the Γ-matrices. So if we discard some of the eigenvalues (thus reducing the dimension), the identity in equation (4.13) will only hold approximately. The so called state prediction method invented by White and used in time evolution simulations on DMRG basis uses eq. (4.13) as an approximate identity in the truncated Hilbert space of the subsystem A (see [23]).

If a state has been cast into the form of eq. (4.19) we call it a canonical state. Let's summarize this in a definition (see [24, 25])

Definition 1 *A state is in a canonical form for a bipartition A:B if the weights connecting these bipartitions are given by the Schmidt coefficients of the corresponding Schmidt decomposition. The state is canonical if it is canonical for every bipartition.*

In fig.4.9 you can see the graphical representation of such a canonical state.

A canonical state satisfies both of the following two conditions for arbi-

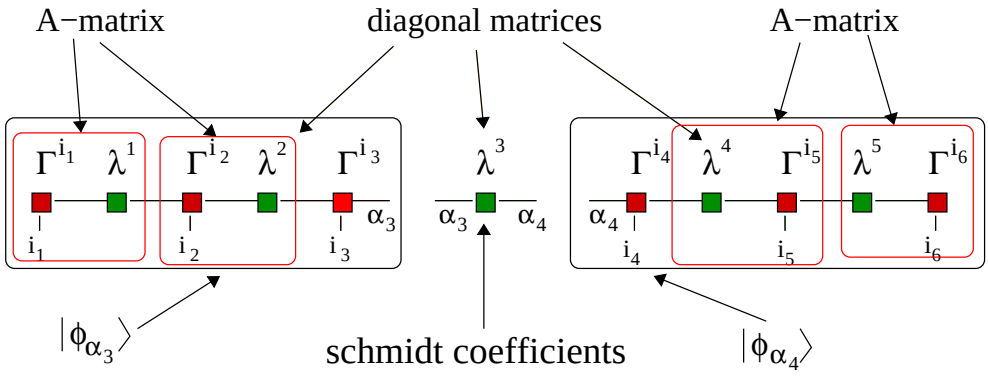

Figure 4.9: Graphical representation of a canonical matrix product state. $\lambda^{[i]}$ are diagonal matrices containing the Schmidt coefficients of the corresponding site. From the red squares, the original A-matrices from above can be computed. The A-matrices in the left block are left orthonormalized, the A-matrices in the right block are right orthonormalized. The states $|\phi_{\alpha_3}\rangle$ and $|\phi_{\alpha_4}\rangle$ are the Schmidt eigenstates for the left and right block respectively.

trary sites l of the system:

$$\sum_{i_l,\beta,\beta'} (\Gamma^{[l]i_l}_{\alpha\beta}\lambda^{[l]}_{\beta})(\Gamma^{[l]i_l}_{\alpha'\beta'}\lambda^{[l]}_{\beta'})^*\delta_{\beta\beta'} = \eta\delta_{\alpha\alpha'}$$
$$\sum_{i_l,\alpha,\alpha'} (\lambda^{[l-1]}_{\alpha}\Gamma^{[l]i_l}_{\alpha\beta})(\lambda^{[l-1]}_{\alpha'}\Gamma^{[l]i_l}_{\alpha'\beta'})^*\delta_{\alpha\alpha'} = \eta\delta_{\beta\beta'}$$

where $\eta = 1$ if and only if the state is normalized ([25]). Later on we will see that this orthonormality property of the Schmidt eigenstates for a certain bipartition is a crucial property used in the yet to explain time evolution algorithm called TEBD. Def. 1 is equivalent to the orthonormality condition of ordinary MPS (eq.(4.3) and (4.4)).

4.4 MPS and their Canonical Representation

The state representation introduced in section 4.3 is closely related to a matrix product representation. For simplicity we only consider open boundary conditions. Let $|\psi\rangle$ be an arbitrary state in some product Hilbert space of local Hilbert spaces $|i_j\rangle$ of dimension d:

$$|\psi\rangle = \sum_{i_1\cdots i_N} c_{i_1\cdots i_N}|i_1\ldots i_N\rangle$$

This state can be rewritten as

$$|\psi\rangle = \sum_{\{i_k\}\{\alpha_l\}} \Gamma^{[1]i_1}_{\alpha_1}\lambda^{[1]}_{\alpha_1}\Gamma^{[2]i_2}_{\alpha_1\alpha_2}\lambda^{[2]}_{\alpha_2}\cdots\Gamma^{[N-1]i_{N-1}}_{\alpha_{N-2}\alpha_{N-1}}\lambda^{[N-1]}_{\alpha_{N-1}}\Gamma^{[N]i_N}_{\alpha_N-1}|i_1\ldots i_N\rangle. \quad (4.20)$$

by defining new matrices $A^{[k]i_k}_{\alpha_{k-1}\alpha_k}$ for every site k (1<k<N) in the bulk

$$A^{[k]i_k}_{\alpha_{k-1}\alpha_k} = \Gamma^{[k]i_k}_{\alpha_{k-1}\alpha_k}\lambda^{[k]}_{\alpha_k}$$

and "boundary matrices" $A^{[1]i_1}_{\alpha_0\alpha_1}$ and $A^{[N]i_N}_{\alpha_{N-1}\alpha_N}$

$$\sum_{\alpha_0}\Phi^L_{\alpha_0}A^{[1]i_1}_{\alpha_0\alpha_1} = \Gamma^{[1]i_1}_{\alpha_1}\lambda^{[1]}_{\alpha_1} \quad (4.21)$$

$$\sum_{\alpha_N}\Phi^R_{\alpha_N}A^{[N]i_N}_{\alpha_{N-1}\alpha_N} = \Gamma^{[N]i_N}_{\alpha_{N-1}} \quad (4.22)$$

for suitable coefficients Φ^R_α and Φ^L_α. In equations (4.21) and (4.22) rewrite the sums on the left side as

$$\sum_{\alpha_0}\Phi^L_{\alpha_0}A^{[1]i_1}_{\alpha_0\alpha_1} = \langle\phi_L|A^{[1]i_1}$$

$$\sum_{\alpha_N}\Phi^R_{\alpha_N}A^{[N]i_N}_{\alpha_{N-1}\alpha_N} = A^{[N]i_N}|\phi_R\rangle$$

By inserting this into eq. (4.20) we arrive at the right orthonormalized MPS like in eq.(4.1).

Similarly, one could define $\tilde{A}$ matrices by grouping in the following way:

$$\tilde{A}^{[k]i_k}_{\alpha_{k-1}\alpha_k} = \lambda^{[k-1]}_{\alpha_{k-1}}\Gamma^{[k]i_k}_{\alpha_{k-1}\alpha_k}$$

which results in a switched definition of the boundary matrices $\tilde{A}^{[1]i_1}_{\alpha_0\alpha_1}$ and $\tilde{A}^{[N]i_N}_{\alpha_{N-1}\alpha_N}$:

$$\sum_{\alpha_0}\Phi^L_{\alpha_0}\tilde{A}^{[1]i_1}_{\alpha_0\alpha_1} = \Gamma^{[1]i_1}_{\alpha_1} \quad (4.23)$$

$$\sum_{\alpha_N}\Phi^R_{\alpha_N}\tilde{A}^{[N]i_N}_{\alpha_{N-1}\alpha_N} = \lambda^{[N-1]}_{\alpha_{N-1}}\Gamma^{[N]i_N}_{\alpha_{N-1}} \quad (4.24)$$

This MPS now obeys the left handed orthonormality constraint eq.(4.4). We see that a canonical state has the feature, that either the left or the right orthonormalized MPS representation of a quantum many body state can be extracted immediately. This is of advantage if we want to compute observables like n-point correlators. In section 4.2 we saw, that if we can divide a

MPS into a left and right orthonormalized part, the calculation of such observables becomes easier. In terms of our canonical form of a quantum many body state, the orthonormality conditions (see def.1 and below) guarantees, that for an arbitrary cut of the system at site i the diagonal matrices $\lambda^{[i]}$ are the Schmidt coefficients. Furthermore, the Schmidt states of the left and right system can immediatly be obtained as products of Γ and λ matrices. This in turn makes calculations of observables easy because in case of one site observables, we do not have to contract the whole tensor network but can use the orthonormality of the Schmidt states to reduce this contraction to one over only those tensors belonging to this site, which is a much faster operation. Another advantage of a canonical representation of a quantum many body state is the fact, that the action of one and two site operators can easily be calculated. As we saw above, the Schmidt eigenvalues λ_i are exactly the square roots of the eigenvalues of the reduced density matrices of the left and right subsystems at site i. From DMRG we know, that truncating the small eigenvalues does not change the expectation value of observables significantly. Applying a two site operator to a state leads to a change of the Schmidt eigenvalues at the corresponding bond, and because we can calculate this change very easily in our canonical MPS picture, we can approximate the new state by discarding all eigenvalues beyond a certain threshold. This is the basic principle used in our time evolution algorithms.

4.5 MPS and Entanglement

In this section we will talk about entanglement and its connection to MPS. For more details on the subject of entanglement entropy and area laws for physical systems, we refer the reader to the review [26]. Let's start with the formal definition of entanglement in terms of the von Neumann entropy S_{vN}. For a quantum mechanical system which is in a state described by a density matrix $\hat{\rho}$, we define the von Neumann entropy as

$$S_{vN}(\hat{\rho}) = -\mathrm{tr}[\hat{\rho}\log_2(\hat{\rho})] \tag{4.25}$$

It yields a natural measure of how entangled this system is with its environment. Suppose for example that the subsystem is in a pure state, then $S_{vN} = 0$. This is only the case if the wave function $|\psi\rangle$ of the whole system (subsystem + environment) can be written as $|\psi\rangle = |\phi_S\rangle \otimes |\phi_E\rangle$. If on the other hand subsystem and environment are entangled, then such a decomposition of the system wave function into a product state wave function is per definition not possible and $S_vN > 0$. The subsystem then is in a mixed

state of the form

$$\hat{\rho} = \sum_i \lambda_i^2 \left|\lambda_i\right\rangle \left\langle\lambda_i\right| .$$

If the weights of the density matrix are uniformly distributed, then S_{vN} has a maximum. MPS states have the property, that the amount of entanglement in the sense of eq.(4.25) of a MPS with its environment is bounded by a constant given by

$$S_{vN}(\hat{\rho}) < 2\log(\chi)$$

(see [26]). Suppose you have a system of N sites and a MPS approximation for its ground state, then the entangled entropy of a block of length $L \ll N$ (computed from the MPS) is bounded by that constant. Latorre et al. ([10]) have shown that the entanglement entropy of a block of spins embedded in an infinite chain saturates as a function of the block size if the system is away from criticality. At criticality, the entropy grows as

$$S_{vN}(L) = k\log_2(L) + const.$$

If the system is not critical, MPS should thus be able to yield good approximations to the true ground state.

The construction of MPS allows for a simple way of measuring the entanglement of a block of size L with the rest of the system, especially if it is in its canonical form, because then, the eigenvalues of the reduced density are immediately available and S_{vN} can be computed according to

$$S_{vN} = -\sum_{\alpha_L} \lambda_{\alpha_L} \log_2 \lambda_{\alpha_L} \tag{4.26}$$

where λ_{α_L} are the Schmidt eigenvalues of the partition at site L. Due to the logarithmic divergence of S_{vN}, the MPS approximation will still yield good results if the system is not too large. In practice system sizes up to one hundred and more sites can easily be handled.

4.6 Matrix Product Operators

In the same way we can define a MPS we can also define a Matrix Product Operator (MPO) (see [21, 27]; we will mainly follow these two reviews). The difference to a MPS is only the local basis: A MPS lives on a product Hilbert space of local Hilbert spaces. Similarly, the MPO lives on the product operator-space of the local operator spaces. To make this clear consider a spin 1/2 chain. The local Hilbert space is spanned by the $|+z\rangle, |-z\rangle$ basis, and unless we introduce some further degrees of freedom, the physics of the

local site (and hence of the chain) is completely determined by the three Pauli matrices σ_i and the 2×2 identity matrix, since these form an orthonormal basis of the vector space of 2×2 matrices. Any operator $\hat{O}$ acting on the chain can be written as

$$\hat{O} = \sum_{i_1 \cdots i_N \in \{1,2,3,4\}} C_{i_1 \cdots i_N} \sigma_{i_1} \otimes \sigma_{i_2} \otimes \cdots \sigma_{i_N}.$$

Like above for MPS, we can write the coefficients of the MPO as matrix products. If we do so, we arrive at

$$\begin{aligned} \hat{O} &= \sum_{i_1 \cdots i_N \in \{1,2,3,4\}} \sum_{\alpha_1 \cdots \alpha_{N-1}} A^{i_1}_{\alpha_1} A^{i_2}_{\alpha_1 \alpha_2} \cdots A^{i_N}_{\alpha_{N-1}} \sigma_{i_1} \otimes \sigma_{i_2} \otimes \cdots \sigma_{i_N} \\ &= \sum_{i_1 \cdots i_N \in \{1,2,3,4\}} A^{i_1} A^{i_2} \cdots A^{i_N} \sigma_{i_1} \otimes \sigma_{i_2} \otimes \cdots \sigma_{i_N} \end{aligned} \tag{4.27}$$

were A^{i_1} and A^{i_N} are again vectors of dimension χ and A^{i_n} are $\chi \times \chi$ matrices for $1 < n < N$. Another useful way of writing is in terms of the local basis states:

$$\hat{O} = \sum_{s_1, s_1' \cdots s_N s_N' \in \{1,2\}} M^{s_1, s_1'} M^{s_2 s_2'} \cdots M^{s_N s_N'} |s_1\rangle\langle s_1'| \otimes \cdots \otimes |s_N\rangle\langle s_N'|.$$

$M^{s_n, s_n'}$ are matrices of dimension $\chi_M \times \chi_M$ for $1 < n < N$, and $M^{s_1, s_1'}$ and $M^{s_N s_N'}$ are vectors of dimension χ_M. The reason for introducing MPO's is that the action of a MPO on a MPS gives a new MPS and the calculation of the new A-matrices of the MPS is straightforward. Let $|A\rangle$ be a MPS with matrices A^{i_n} of dimension χ_A. The action of the (matrix product) operator $\hat{O}$ results in a new state:

$$\begin{aligned} \hat{O}|A\rangle &= \sum_{\{s_i\},\{s_i'\}\{\tilde{s}_i\}} M^{s_1, s_1'} \cdots M^{s_N s_N'} A^{\tilde{s}_1} \cdots A^{\tilde{s}_N} |s_1\rangle \underbrace{\langle s_1' | \tilde{s}_1 \rangle}_{\delta_{s_1' \tilde{s}_1}} \cdots |s_N\rangle\langle s_N' | \tilde{s}_N \rangle = \\ &= \sum_{\{s_i\},\{s_i'\}} M^{s_1, s_1'} \cdots M^{s_N s_N'} A^{s_1'} \cdots A^{s_N'} |s_1\rangle \cdots |s_N\rangle \\ &= \sum_{\{s_i\}} \underbrace{\left(\sum_{s_1'} M^{s_1, s_1'} A^{s_1'} \right)}_{B^{s_1}} \cdots \underbrace{\left(\sum_{s_N'} M^{s_N s_N'} A^{s_N'} \right)}_{B^{s_N}} |s_1\rangle \cdots |s_N\rangle \end{aligned} \tag{4.28}$$

Note that for brevity we did not write the sums over the auxiliary indices. If these are reinserted, the matrices B of the new MPS $|B\rangle = \hat{O}\,|A\rangle$ are given by

$$B^{s_{n+1}}_{(\alpha_n\alpha'_n);(\alpha_{n+1}\alpha'_{n+1})} = \sum_{s'_{n+1}} M^{s_{n+1}s'_{n+1}}_{\alpha_n\alpha_{n+1}} A^{s'_{n+1}}_{\alpha'_n\alpha'_{n+1}} = \sum_{s'_{n+1}} M^{s_{n+1}s'_{n+1}} \otimes A^{s'_{n+1}} \quad (4.29)$$

and have an increased dimension $\chi_A\chi_M$. Please note that the new MPS $|B\rangle$ is in general not orthonormal in the sense of eqs. (4.3) and (4.4).

4.7 Matrix Product Representation for One and Two Site Operators

In this section we will explain how to construct matrix product representations for operators consisting of sums over one or two site operators. As usual, we will consider open boundary conditions. The transformation to periodic boundary conditions is straightforward. The operators shall be defined by

$$\hat{O}^{[1]} = \sum_{n=1}^{N} \hat{O}_n \quad (4.30)$$

$$\hat{O}^{[2]} = \sum_{n=1}^{N} \hat{O}_{n,n+1} = \sum_{n=1}^{N} \hat{A}_n \hat{B}_{n+1} \quad (4.31)$$

$\hat{O}^{[1]}$ consists only of operators $\hat{O}_n$ that act on one local site n, like $\hat{S}^z_i$ for example, whereas $\hat{O}^{[2]}$ consists of a product of one site operators $\hat{A}_n$ and $\hat{B}_{n+1}$. An example for this kind of operator is the Heisenberg coupling $\vec{\hat{S}}_i\vec{\hat{S}}_{i+1}$. The M-matrices of the MPO representation of operators of the kind of eq.(4.30) are given by

$$M^n = \begin{cases} \begin{pmatrix} O_1 & \mathbb{1} \end{pmatrix} & \text{left boundary, } n = 1 \\ \begin{pmatrix} \mathbb{1} & 0 \\ O_n & \mathbb{1} \end{pmatrix} & \text{bulk } 1 < n < N \\ \begin{pmatrix} \mathbb{1} \\ O_N \end{pmatrix} & \text{right boundary, } n = \mathrm{N} \end{cases}$$

for one site operators of eq.(4.30), where $\mathbb{1}$ and O_n are the d dimensional representations of the identity and the local operators in the local Hilbert space respectively. The auxiliary dimension χ of the MPO apparently is 2. For two site operators, the M-matrices are given by

$$M^n = \begin{cases} \begin{pmatrix} 0 & A_1 & \mathbb{1} \end{pmatrix} & \text{left boundary, } n = 1 \\ \begin{pmatrix} \mathbb{1} & 0 & 0 \\ A_n & 0 & 0 \\ 0 & B_n & \mathbb{1} \end{pmatrix} & \text{bulk } 1 < n < N \\ \begin{pmatrix} \mathbb{1} \\ B_N \\ 0 \end{pmatrix} & \text{right boundary, } n = N \end{cases}$$

where A_n and B_n are the d dimensional matrix representations of the operators $\hat{A}_n$ and $\hat{B}_n$. The auxiliary dimension for this operator is $\chi = 3$. To verify, that these matrices actually produce eq.(4.30) and (4.31), one only has to calculate the matrix product

$$\hat{O} = \prod_{n=1}^{N} M^n \tag{4.32}$$

We finish the introduction to MPO by showing a nice application of it.

4.8 An Example for MPO Application

As an example for the application of MPO, we studied the time evolution of a gauss-like one-particle excitation in the vacuum of the free fermion model, since this model can also be solved exactly. The excitation is created by the operator

$$g(k) = \sum_k e^{-\frac{(k-k_0)^2}{2\sigma^2}} c_k^\dagger = \sum_x e^{-2\pi^2\sigma^2(x-x_0)^2} e^{\frac{2i\pi(x-x_0)}{N}k_0} c_x^\dagger. \tag{4.33}$$

where $c_x^\dagger$ creates a particle at site x. The free fermion model and the Heisenberg XX chain can be transformed into each other by the Jordan Wigner

transformation. This transformation just takes the difference of the particle statistics into account, since free fermions and spins in the XX model differ only by the imposed particle statistics. For one particle states, the statistics is however irrelevant and the ladder operators S_x^+ of the XX chain can be treated like the creation operators $c_x^\dagger$ of free fermions, so we can apply (4.33) with $c_x^\dagger$ replaced by S_x^+ to the XX chain. In fig.4.10, the exact time evolution of the mentioned gauss pulse is compared to the time evolution with MPS (details on time evolution with MPS see below). The red line shows the exact time evolution of a single particle excitation from vacuum in the free fermion chain. The green line is the approximate time evolution of such a gauss pulse in a XX Heisenberg chain. For the Heisenberg chain, the vacuum state is the saturated (ferromagnetic) state with all spins aligned. The excitation is centered around a value of $2\pi k_0/N = -\pi/2$ with a width of $\sigma = 0.03$. Apart from small deviations at the maximum value of the peak (in the MPS time evolution, one applies a Suzuki Trotter expansion to the time evolution operator, which is also a source of errors), the spin-density of the MPS approximation is in good agreement with the exact solution. The stability of the gauss packages is due to the linearity of the dispersion at $k = -\pi/2$. The time step for the exact solution is chosen twice the one of the MPS approximation because for $t_{i,i+1} = J_{xy}$, the prefactor of the dispersion of the free fermions is twice as high as that of the Heisenberg XX chain.

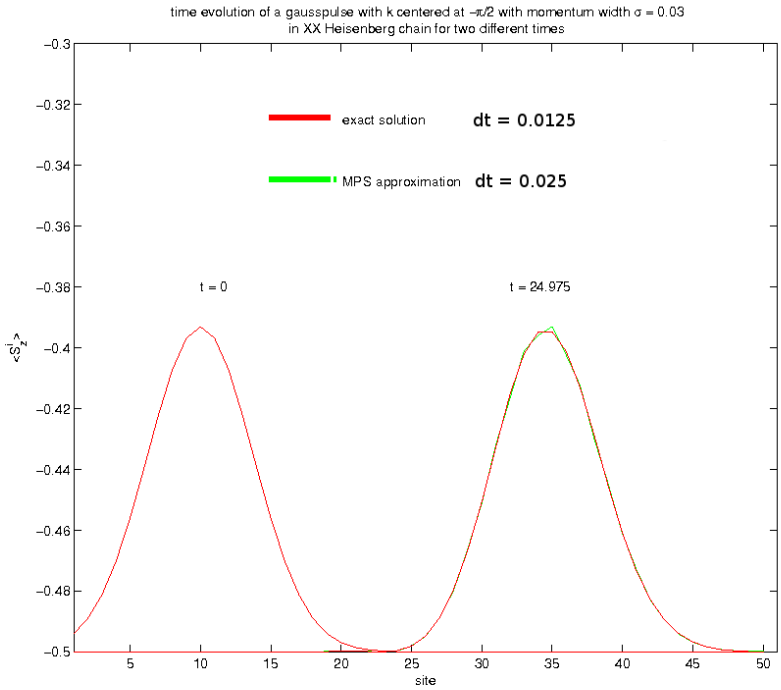

Figure 4.10: Time evolution of a ~~Gauss~~sian excitation centered at k $= -\pi/2$ in the free fermion system. The red line shows the exact solution, the green line is the TEBD solution of the $J_z = 0$ Heisenberg XX model ($J_{xy} = 1$). Due to the quasi-linear dispersion of the free fermions at k $= -\pi/2$, the gauss shaped density excitations is very stable.

4.9 Casting a MPS into its Canonical Representation

Above we saw how one can interpret a canonical state as a left or right ortho normalized MPS. The opposite is also possible: Starting from a arbitrary MPS, it is possible to render it into its canonical form by applying a sequence of transformations on its matrices. In this section, we will develop the algorithm with which this can be done. The following discussion can also be found in [21]. A MPS has the appealing feature that it is invariant under a auxiliary gauge transformation where one inserts the identity matrix between to arbitrary matrices (shown in fig. (4.11):

$$\cdots A_n^{i_n} A_{n+1}^{i_{n+1}} \cdots \mapsto \cdots A_n^{i_n} X_n X_n^{-1} A_{n+1}^{i_{n+1}} \cdots .$$

We now choose X_n in such a way, that the matrices $A^{i_n}X_n$ are left-orthonormalized. This can be achieved (see [28]) by choosing X_n to be

$$X_n^{-1} = \sqrt{\sum_{i_n} A^{i_n\dagger}A^{i_n}} = \sqrt{Q}.$$

Note that since the matrix Q is not necessarily non-singular, the inverse can not always be computed, and one has to use the pseudo-inverse instead (see again [28]). The procedure to obtain a left orthonormalized MPS now is as follows:

1. set $n = 1$
2. Calculate $X_n = \frac{1}{\sqrt{\sum_{i_n} A^{i_n\dagger}A^{i_n}}}$.
3. Replace $A^{i_n} \mapsto A^{i_n}X$ and $A^{i_{n+1}} \mapsto X_n^{-1}A^{i_{n+1}}$. Stop if n = N-1, else n = n+1.
4. Go to 2

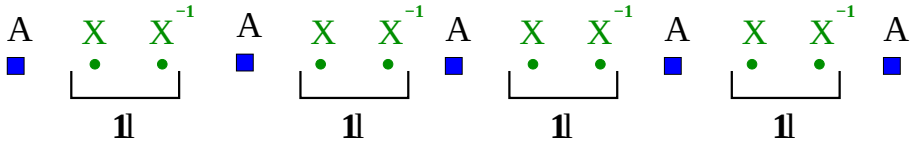

Figure 4.11: Graphical representation of left-orthonormalizing procedure of MPS. Between every pair of adjacent matrices A^i and A^{i+1}, one inserts a representation of the identity matrix $\mathbb{1} = X_iX_i^{-1}$. The matrices X_i are chosen so that A^iX_i is left orthonormalized (see text).

The resulting MPS then is left orthonormalized.

It is also possible to right-orthonormalize a MPS. The procedure is very much the same, but in this case one uses matrices Y_n with

$$Y_n^{-1} = \sqrt{\sum_{i_n} A^{i_n}A^{i_n\dagger}}$$

instead of X_n and, starting from the right-hand side of the system, iteratively applies the steps (see fig. (4.12))

1. $n = \mathrm{N}$
2. Calculate $Y_n = \frac{1}{\sqrt{\sum_{i_n} A^{i_n} A^{i_n \dagger}}}$.
3. Replace $A^{i_n} \mapsto Y_n A^{i_n}$ and $A^{i_{n-1}} \mapsto A^{i_{n-1}} Y_n^{-1}$. Stop if $n = 2$, else $n =$ n-1.
4. Go to 2

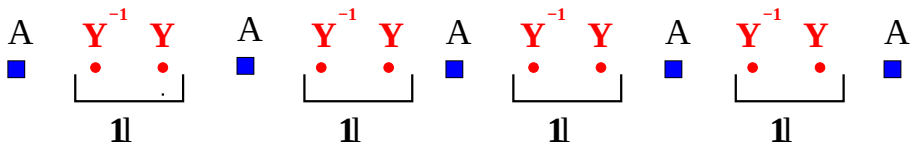

Figure 4.12: Graphical representation of right-orthonormalizing procedure of MPS. Again one inserts a matrix product $Y_i^{-1} Y_i = \mathbb{1}$ between to adjacent matrices A^i and A^{i+1} and chooses Y_i in such a way, that $Y_i A^{i+1}$ now is rightorthonormal.

If all matrices X_n and Y_n are at hand, one can compute the canonical representation thm. 1 by inserting 2(N-1) identities in the way

$$A^{i_1} A^{i_2} \cdots A^{i_N} \mapsto A^{i_1} X_1 \underbrace{X_1^{-1} Y_2^{-1}}_{U_1 \lambda_1 V_1^\dagger} Y_2 A^{i_2} X_2 \underbrace{X_2^{-1} Y_3^{-1}}_{U_2 \lambda_2 V_2^\dagger} Y_3 A_3 \cdots X_{N-1} \underbrace{X_{N-1}^{-1} Y_N^{-1}}_{U_N \lambda_N V_N^\dagger} Y_N A_N.$$

Then we SV-decompose the under braced expressions and collect terms in the way

$$V_{n-1}^\dagger Y_n A^{i_n} X_n U_n = \Gamma^{[n] i_n}$$

where λ is a diagonal matrix and U and V are unitary matrices which satisfy

$$U^\dagger U = U U^\dagger = \mathbb{1}$$
$$V V^\dagger = V^\dagger V = \mathbb{1}$$

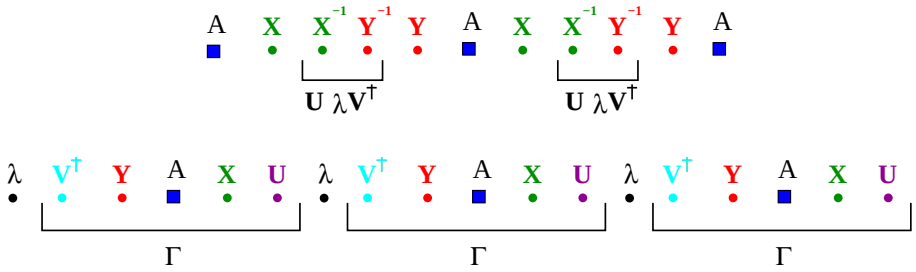

Figure 4.13: If we combine the procedures in fig.4.11 and fig.4.12, we can construct the canonical representation of a MPS: First left-orthonormalize it and store the X_i-matrices. Then do the right orthonormalization and store the Y_i matrices. Then apply an SVD to the product $X^{-1}Y^{-1} = U\lambda V^\dagger$. The Γ matrices are then given by the product $V^\dagger Y A X U$

Finally, this gives the canonical representation

$$\sum_{i_1 \cdots i_N} A^{[1]i_1} \cdots A^{[N]i_N} |i_1 \ldots i_N\rangle = \sum_{i_1 \cdots i_N} \Gamma^{[1]i_1} \lambda_1 \Gamma^{[2]i_1} \lambda_2 \cdots \Gamma^{[N]i_N} |i_1 \ldots i_N\rangle$$

where we dropped the summation over the auxiliary indices.

Chapter 5

Manipulation of Canonical Matrix Product States

For the rest of this document, we will only consider Schmidt representations of states with open boundary conditions. A very pleasant feature of a canonical state is the fact, that it can easily be manipulated. In this section, we will explain the basic operations needed to develop time evolution methods for these states.

5.1 Application of Unitary Single Site Operators to Canonical States

For starters we will look at the action of single-site operators on a canonical state $|\psi\rangle$. Let $\hat{\mathrm{O}}_n$ be some operator which acts only on site n of the system:

$$\hat{O}_n = \sum_{i_n, j_n} \langle i_n | O_n | j_n \rangle |i_n\rangle\langle j_n| \tag{5.1}$$

This operator transforms a state $|\psi\rangle$ into some state $|\psi'\rangle$ who's Schmidt decomposition can be computed from the Schmidt decomposition of state $|\psi\rangle$ by updating only the coefficients $\Gamma^{[n]i_n}_{\alpha_{n-1}\alpha_n}$. To find the new coefficients, we compute the action of $\hat{\mathrm{O}}_n$:

$$\hat{\mathrm{O}}_n|\psi\rangle = \sum_{\alpha_{n-1}} |\alpha_{n-1}^{1\cdots n-1}\rangle \sum_{\alpha_n l_n} \lambda_{\alpha_n} \left(\sum_{i_n} \Gamma^{[n]i_n}_{\alpha_{n-1}\alpha_n} O^{l_n i_n} \right) |l_n\rangle |\alpha_n^{n+1\cdots N}\rangle$$

The new $\Gamma^{[n]i_n}$-matrices are therefore given by the expression in the brackets:

$$\Gamma'^{[n]l_n}_{\alpha_{n-1}\alpha_n} = \sum_{i_n} \Gamma^{[n]i_n}_{\alpha_{n-1}\alpha_n} \langle l_n | O_n | i_n \rangle \tag{5.2}$$

Now one is tempted to treat the state $|\psi'\rangle$ as a canonical state, but in fact it is only canonical, if the operator $\hat{O}$ meets the condition that it is unitary:

$$\hat{O}\hat{O}^\dagger = \hat{O}^\dagger\hat{O} = \mathbb{1}$$

Why this condition? Above we explained, that a canonical state is a special form of a MPS where both, the left- and right-hand orthonormalized form of the MPS can be gained really easily. If you remember, this demands, that at **each bond** n of the system we have to satisfy **both** the conditions

$$\sum_{i_n} \left(\Gamma^{[n]i_n}\lambda^{[n]}\right)\left(\Gamma^{[n]i_n}\lambda^{[n]}\right)^\dagger = \mathbb{1} \tag{5.3}$$

$$\sum_{i_n} \left(\lambda^{[n-1]}\Gamma^{[n]i_n}\right)^\dagger\left(\lambda^{[n-1]}\Gamma^{[n]i_n}\right) = \mathbb{1}. \tag{5.4}$$

If one inserts the Γ' from eq.(5.2) into eq.(5.3), one arrives at

$$\begin{aligned}
&\sum_{i_n}\left(\Gamma'^{[n]i_n}\lambda^{[n]}\right)\left(\Gamma'^{[n]i_n}\lambda^{[n]}\right)^\dagger = \\
&\sum_{i_n,j_n,k_n}\left(\Gamma^{[n]j_n}\lambda^{[n]}\right)\left(\Gamma^{[n]k_n}\lambda^{[n]}\right)^\dagger\langle i_n|\hat{O}|j_n\rangle\langle i_n|\hat{O}|k_n\rangle^* = \\
&\sum_{i_n,j_n,k_n}\left(\Gamma^{[n]j_n}\lambda^{[n]}\right)\left(\Gamma^{[n]k_n}\lambda^{[n]}\right)^\dagger\langle k_n|\hat{O}^\dagger|i_n\rangle\langle i_n|\hat{O}|j_n\rangle = \\
&\sum_{j_n,k_n}\left(\Gamma^{[n]j_n}\lambda^{[n]}\right)\left(\Gamma^{[n]k_n}\lambda^{[n]}\right)^\dagger\langle k_n|\hat{O}^\dagger\hat{O}|j_n\rangle \stackrel{!}{=} \mathbb{1}
\end{aligned}$$

So if the operator $\hat{O}$ is right unitary, the right-orthonormalization is fulfilled (provided it was before the application of $\hat{O}$). Inserting eq.(5.2) into eq.(5.4) yields another condition for the operator:

$$\sum_{j_n,k_n}\left(\lambda^{[n-1]}\Gamma^{[n]j_n}\right)\left(\lambda^{[n-1]}\Gamma^{[n]k_n}\right)^\dagger\langle k_n|\hat{O}\hat{O}^\dagger|j_n\rangle \stackrel{!}{=} \mathbb{1}$$

which means that the operator has to be left unitary. $\hat{O}$ therefore has to be a unitary operator if the new state $|\psi'\rangle$ is to be canonical. For example, the spin 1/2 operators $\hat{S}_x, \hat{S}_y, \hat{S}_z$ do have this property. Still, the case of non-unitary operators $\hat{O}$ is also common (for example the operator S^+) and luckily, there are methods by which one can reorthonormalize the matrices and recover the canonical representation.

5.2 Application of Unitary Two Site Operators to Canonical States

The action of a two site operator $\hat{O}_{n,n+1}$ can be computed in a similar manner to single site operators. In the previous section we already mentioned, that application of non-unitary operators can cause difficulties and so we will in this section consider only unitary operators. Let the operator acting on two sites n and $n+1$ be defined by

$$\hat{O}_{n,n+1} = \sum_{ijkl} \langle ij|\hat{O}_{n,n+1}|kl\rangle |ij\rangle\langle kl|$$

where n and $n+1$ denote the two sites on which the operator acts. In the following we will drop these site indices for brevity. Like above we write the Schmidt vectors for a system $1 \cdots l$ as

$$|\alpha\rangle = |\phi_\alpha^{1\cdots l}\rangle$$

and for a system $l+1 \cdots N$ as

$$|\gamma\rangle = |\phi_\gamma^{l+1\cdots N}\rangle$$

In this notation the state $|\psi\rangle$ reads

$$|\psi\rangle = \sum_{\alpha\beta\gamma=1}^{\chi} \sum_{ij} \lambda_\alpha^{[n-1]} \Gamma_{\alpha\beta}^{[n]i} \lambda_\beta^{[n]} \Gamma_{\beta\gamma}^{[n+1]j} \lambda_\gamma^{[n+1]} |\alpha i j \gamma\rangle.$$

Application of $\hat{O}$ results in

$$|\psi'\rangle = \sum_{\alpha\gamma=1}^{\chi} \sum_{ij} \Theta_{\alpha\gamma}^{ij} |\alpha i j \gamma\rangle$$

where Θ is defined by

$$\Theta_{\alpha\gamma}^{ij} = \sum_{\beta=1}^{\chi} \sum_{kl} O_{kl}^{ij} \lambda_\alpha^{[n-1]} \Gamma_{\alpha\beta}^{[n]k} \lambda_\beta^{[n]} \Gamma_{\beta\gamma}^{[n+1]l} \lambda_\gamma^{[n+1]}.$$

Now there are two slightly different ways of obtaining the new $\Gamma' s$ and $\lambda' s$. Either one does a SVD of Θ which directly gives the new tensors or one diagonalizes the reduced density operator $\rho^{n+1\cdots N} = \mathrm{tr}^{1\cdots n}(|\psi'\rangle\langle\psi'|)$. The first possibility is favorable due to the existence of fast SVD-algorithms, whereas the implementation of conserved quantities such like total spin or total number of particles is easier in the reduced density operator picture. In the following we first will describe the second way because it highlights the physical background of the method and shows the similarities between the states produced by DMRG (see below for an introduction to DMRG) and the canonical states (Schmidt decompositions, respectively).

5.2.1 Updating the Γ Matrices via Diagonalization of the Reduced Density

The basic procedure is the following: First compute the reduced density matrix for either the left or the right system, then diagonalize it. From the diagonalization one obtains the eigenvalues of, for example, $\hat{\rho}^{n+1\cdots N}$ (which are the Schmidt eigenvalues), and a unitary matrix U, which basically contains the new Γ matrices for site n+1.

The reduced density operator for systems n+1$\cdots$ n reads

$$\rho^{n+1\cdots N} = \sum_{jj'\gamma\gamma'} \underbrace{\left(\sum_{\alpha i} \Theta^{ij}_{\alpha\gamma} (\Theta^{ij'}_{\alpha\gamma'})^* \right)}_{M} |j\gamma\rangle\langle j'\gamma'| \tag{5.5}$$

Diagonalizing the expression in brackets in the $|j\gamma\rangle$-space gives the new Schmidt coefficients $\lambda^{[n]}_\alpha$ for site n. Let Mdenote the matrix in brackets in eq.(5.5). Diagonalization of M yields

$$M_{(j\gamma)(j'\gamma')} = \sum_m U_{(j\gamma),m} D_{m,m} U^\dagger_{m,(j'\gamma')}$$

where $D_{m,m} = |\lambda^{'[n]}_m|^2$ denotes the the squared norm of the new Schmidt coefficients for site n. Insertion into eq.(5.5) results in

$$\hat{\rho}^{n+1\cdots N} = \sum_{jj'\gamma\gamma' m} U_{(j\gamma),m} D_{m,m} U^\dagger_{m,(j'\gamma')} |j\gamma\rangle\langle j'\gamma'|$$

By comparing this to the expression

$$\mathrm{tr}^{1\cdots n}(|\psi'\rangle\langle\psi'|) = \sum_m |\lambda'^{[n]}_m|^2 \sum_{j\gamma j'\gamma'} \Gamma'^{[n+1]j}_{m\gamma} \lambda^{[n+1]}_\gamma \left(\Gamma^{[n+1]j'}_{m\gamma'} \lambda^{[n+1]}_{\gamma'} \right)^* |j\gamma\rangle\langle j'\gamma'|$$

we see that the new $\Gamma^{'[n+1]i_{n+1}}_{\alpha_n\alpha_{n+1}}$ are

$$\Gamma'^{[n+1]i_{n+1}}_{\alpha_n\alpha_{n+1}} = \frac{U_{(i_{n+1}\alpha_{n+1}),\alpha_n}}{\lambda^{[n+1]}_{\alpha_{n+1}}}$$

The new $\Gamma'^{[n]i}$ can then be obtained from the scalar product

$$\begin{aligned} \lambda'_{\alpha_n} |\Phi^{1\cdots n}_{\alpha_n}\rangle &= \langle \Phi^{n+1\cdots N}_{\alpha_n} | \psi' \rangle \\ &= \sum_{\alpha,i} \left(\sum_{j\gamma} \Theta^{ij}_{\alpha\gamma} (\Gamma'^{[n+1]j}_{\alpha_n\gamma} \lambda^{[n+1]}_\gamma)^* \right) |\alpha i\rangle \\ &= \lambda'^{[n]}_{\alpha_n} \sum_{\alpha i} \lambda^{[n-1]}_\alpha \Gamma'^{[n]i}_{\alpha\alpha_n} |\alpha i\rangle. \end{aligned}$$

From this the formula the new coefficients $\Gamma'^{[n]i}_{\alpha\beta}$ are found to be

$$\Gamma'^{[n]i}_{\alpha\beta} = \frac{1}{\lambda'^{[n]}_{\beta}\lambda^{[n-1]}_{\alpha}} \sum_{j\gamma} \left(\Gamma'^{[n+1]j}_{\beta\gamma}\lambda^{[n+1]}_{\gamma}\right)^{*} \Theta^{ij}_{\alpha\gamma}. \tag{5.6}$$

5.2.2 Updating the Γ Matrices via SVD of the Matrix Θ

This procedure is shorter than the update via the diagonalization of the reduced density. The principle is visualized in fig. (5.1). One regroups the indices of the matrix $\Theta^{ij}_{\alpha\gamma}$ and applies a SVD to this matrix:

$$\Theta_{(i\alpha),(j\gamma)} = \sum_{\delta} U_{(i\alpha)\delta}\lambda'^{[n]}_{\delta\delta}V^{\dagger}_{\delta(j\gamma)}$$

The diagonal matrix $\lambda'^{[n]}$ contains the singular values of Θ, which are identical to the Schmidt eigenvalues. The matrices U and V in essential contain the new $\Gamma'^{[n]i}$ and $\Gamma'^{[n+1]j}$, up to a matrix multiplication by $\lambda^{[n-1]}$ and $\lambda^{[n+1]}$ respectively, which comes from the fact, that in the above derivation of Θ, we pulled the Schmidt eigenvalues of the bonds n-1 and n+1 into Θ. We get

$$\Gamma'^{[n]i_n}_{\alpha\delta} = \frac{U_{(i_n\alpha)\delta}}{\lambda^{[n-1]}_{\delta}}$$

$$\Gamma'^{[n+1]i_{n+1}}_{\delta\gamma} = \frac{V^{\dagger}_{\delta(i_{n+1}\gamma)}}{\lambda^{[n+1]}_{\delta}}$$

where we have relabeled i and j to i_n and i_{n+1}

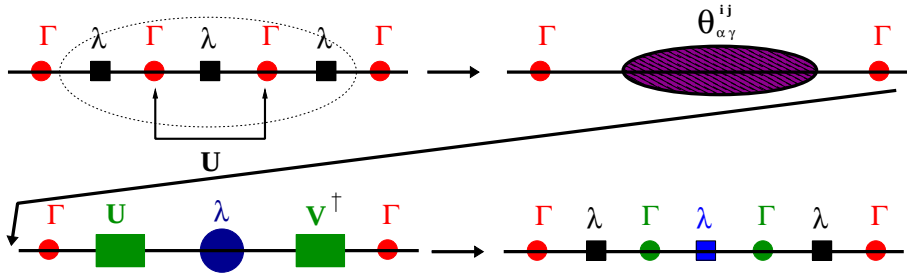

Figure 5.1: Graphical representation of the update of the Γ and λ matrices. Green and blue colors indicate the updated matrices.

5.3 Conserved Quantum Numbers

If the applied gate conserves certain quantum numbers, the procedure outlined above can be improved by taking into account that the reduced density operator is block diagonal in these conserved quantum numbers. If you look at

$$|\psi'\rangle = \sum_{\alpha\gamma=1}^{\chi} \sum_{ij} \Theta^{ij}_{\alpha\gamma} |\alpha i j \gamma\rangle$$

the tensor Θ has only non-zero elements for indices which conserve quantum numbers, that is, if Q(α), Q(γ) denotes the value of Q associated with the Schmidt vectors $|\alpha\rangle$ and $|\gamma\rangle$ and Q(i), Q(j) the value of Q for site $n, n+1$ if they are in state i and j, then conservation of the total value of Q implies

$$Q(\alpha) + Q(i) + Q(j) + Q(\gamma) = Q_0$$

where Q_0 is the conserved quantum number. For the reduced density matrix, this means that in eq.(5.5), $Q(j)+Q(\gamma) = Q(j')+Q(\gamma')$ and thus that $\hat{\rho}^{n+1\cdots N}$ is block diagonal and each block belongs to a certain value of Q(j)+Q(γ)=Q_R (=for example the number of up spins in the right block), and instead of diagonalizing the complete matrix, one just diagonalizes each of these blocks separately. All this sounds quite easy and intuitive, but the implementation of the algorithm can be quite tricky. As an example I will illustrate the procedure for the case of an abelian symmetry (non abelian symmetries are more complicated and tricky, but can also be handled, see [29] for a discussion of the full $SU(2)$ symmetry in the isotropic Heisenberg system). Let us assume, that we have a system of spin 1/2's which is in a state $|\psi\rangle$. Further more, we apply a gate between two sites m and $m+1$. This gate shall be such that it conserves the total spin $S^z = \sum_i S^z_i$ of the system (that is, the gate contains only spin flip and diagonal operators in terms of the two-site (m and $m+1$) Hilbert space).

All starts with the application of this quantum gate at a site m and $m+1$. Like above we denote the single site states at site m by $|i\rangle$ and the ones at site $m+1$ by $|j\rangle$, and those for the left and right block with $|\alpha\rangle$ and $|\gamma\rangle$ respectively. The thing we want to do is compute eq.(5.5), but only the blocks corresponding to a certain number $Q_R = Q(j) + Q(\gamma)$ of, say, up spins in the system $|j\gamma\rangle$. So we recognize, that we first need to know the number $Q(\gamma)$ (of up spins in system $|\gamma\rangle$) which belongs to the state $|\gamma\rangle$. For now we suppose that we have a list, where we can find for every index γ the corresponding $Q(\gamma)$ (in practice one initializes this list in the beginning of the simulation). Then we do the following iteration for $Q = 0 \cdots Q_{max}$, where Q_{max} is the maximum quantum number that can be attached to the

states $|\gamma\rangle$ of the system $n+1 \cdots N$ (the maximum number of up spins that can be put into this system).

For $Q_R = 0$ to Q_{max}, first find all index combinations (j, γ) for which $Q(j) + Q(\gamma) = Q_R$. This gives a set $\{(j_1, \gamma_1), \cdots (j_n, \gamma_n)\}$. Second, find all index combinations (α, i) for which $Q(\alpha) + Q(i) = Q - Q_R$. This gives a set $\{(\alpha_1, i_1), \cdots (\alpha_r, i_r)\}$. Now build all pairs $\big((j, \gamma), (j', \gamma')\big)$ of index-pairs out of the above set. For each of these pairs, compute the sum

$$\sum_{\alpha i} \Theta^{ij}_{\alpha\gamma} (\Theta^{ij'}_{\alpha\gamma'})^*$$

(where the sum is taken only over the pairs $(\alpha, i) \in \{(\alpha_1, i_1), \cdots (\alpha_r, i_r)\}$) and store it in a matrix as the element $\big((j, \gamma), (j', \gamma')\big)$. Diagonalize this matrix and store the eigenvalues, eigenvectors and the corresponding Q.

If you have done this, take the χ largest eigenvalues obtained from above and store them as the new λ_β, insert the corresponding Q(β) into the list. For every β take the β-th eigenvector. Every element U^β_k of this vector belongs to a certain index- pair (j, γ), which you should know from above. Now take this element and insert it as new element into the matrix $\Gamma'^{[n+1]j}_{\beta\gamma}$:

$$\Gamma'^{[n+1]j}_{\beta\gamma} = \frac{U^\beta_{(j\gamma)}}{\lambda^{[n+1]}_\gamma}$$

After computation of $\Gamma'^{[n+1]j}_{\beta\gamma}$, the matrix $\Gamma'^{[n]i}_{\alpha_{n-1}\alpha_n}$ can then be computed from eq.(5.6). A side remark: A situation where one can use this is the time evolution of a Heisenberg XXZ model, where $[H, \hat{S}^z] = 0$ and hence S^z is conserved. This is a typical example of an abelian symmetry (rotation around the z axis). Non abelian symmetries, like $[H, \vec{\hat{S}}^2] = 0$ (space rotations), are in general more complicated to implement (see [29] for a discussion on this topic).

Chapter 6

Time Evolution Methods for MPS: Time Evolving Block Decimation (TEBD) Algorithm

6.1 Real Time Evolution of Canonical States

In this section we will explore the first application of MPS. In the following, we will only look at 1-d systems. As is well known from the basic quantum mechanics lectures, the time evolution of a state $|\psi\rangle$ is carried out by the time evolution operator $\hat{U}$ which is the formal solution of the Schroedinger equation

$$i\hbar\frac{\partial\hat{U}}{\partial t} = \hat{H}\hat{U}$$

and can be written

$$\hat{U} = \hat{T}e^{-\frac{i}{\hbar}\int_{t_0}^{t}\hat{H}(t')dt'} \tag{6.1}$$

where $\hat{T}$ is the time ordering operator. If the Hamiltonian $\hat{H}(t)$ commutes with itself for different times, $[\hat{H}(t), \hat{H}(t')] = 0$, one can omit $\hat{T}$ from eq.(6.1). In the following we will assume a time-independent Hamiltonian. In this case, integration of the exponent of eq.(6.1) is trivial, and $\hat{U}$ becomes

$$\hat{U} = e^{-\frac{i}{\hbar}\hat{H}t} = (e^{-\frac{i}{\hbar}\hat{H}\frac{t}{N}})^N \tag{6.2}$$

where we have set the time line origin t_0 to 0 and in the last column used a representation in terms of short-time propagators.

All the information about the time evolution is contained in the Hamiltonian $\hat{H}$, and the more complicated the structure of the Hamiltonian is, the harder it is in general to solve eq.(6.1) or (6.2). We will now make a further

simplification of the many-body problem by assuming, that the Hamiltonian under consideration contains only nearest neighbor interaction terms and has therefore the following form

$$\begin{aligned}\hat{H} &= \sum_i \hat{H}_i \\ \hat{H}_i &= \hat{h}_i \hat{h}_{i+1}\end{aligned}$$

where $\hat{h}_i$ is a local operator, for example the spin 1/2 operator $\vec{\hat{S}}_i$ at site i. Since the operators $\hat{H}_i$ and $\hat{H}_{i+1}$ do not commute, it's in general hard to evaluate the exponential in eq.(6.2). However, for a certain class of operators H_i it is possible to write the operator exponential of the sum of two non-commuting operators A and B as

$$e^{\alpha(A+B)} = e^{\alpha A} e^{\alpha B} + \mathcal{O}(\alpha^2[A,B]) \tag{6.3}$$

where $\mathcal{O}(\alpha^2[A,B])$ denotes multi-comutator terms of order α^2 and higher. In our case, the Hamiltonian decomposes into two non-commuting operators $\hat{H}^{even}$ and $\hat{H}^{odd}$ with

$$\begin{aligned}\hat{H}^{even} &= \sum_{i=even} \hat{H}_i \\ \hat{H}^{odd} &= \sum_{i=odd} H_i.\end{aligned}$$

All operators within $\hat{H}^{even}$ and $\hat{H}^{odd}$ do commute. Using eq. (6.3), we can approximate the time evolution operator $\hat{U}$ by

$$\hat{U} \approx \exp(-\frac{i}{\hbar}\Delta t \sum_{i=even} \hat{H}_i) \exp(-\frac{i}{\hbar}\Delta t \sum_{i=odd} \hat{H}_i) + \mathcal{O}(\Delta t^2[\hat{H}^{even}, \hat{H}^{odd}]) \tag{6.4}$$

where be abbreviated $\frac{t}{N}$ by Δt. Eq (6.4) is the trotter expanded representation of eq.(6.2) up to first order. Since

$$\begin{aligned}[\hat{H}_i^{even}, \hat{H}_j^{even}] &= 0 \\ [\hat{H}_i^{odd}, \hat{H}_j^{odd}] &= 0\end{aligned} \tag{6.5}$$

we can write eq.(6.4) as a product of two site operators $\hat{H}_i$:

$$\hat{U} \approx \prod_{i=even} \exp(-\frac{i}{\hbar}\Delta t \hat{H}_i) \prod_{i=odd} \exp(-\frac{i}{\hbar}\Delta t \hat{H}_i) + \mathcal{O}(\Delta t^2[\hat{H}^{even}, \hat{H}^{odd}]).$$

Applying this operator to a canonical MPS eq.(4.19) amounts to successively applying two site operators first at each odd and then at each even bond, which can be done very easily (see sec. 5.2). We will now outline the algorithm for time evolution of a canonical MPS:

1. For every bond, calculate the according Hamiltonian $\hat{H}_i$ acting between sites i and i+1 and its exponential $\hat{U}_i = \exp(-\frac{i\Delta t}{\hbar}\hat{H}_i)$.

2. For all odd bonds i: apply the operator $\hat{U}_i$ to the bond connecting sites i and i+1. Calculate the new Γ-matrices for these two sites and the new Schmidt eigenvalues λ_α which live on the bond from site i to i+1.

3. Apply 2) to all even bonds.

4. If desired, calculate observables after each trotter time step.

6.2 Finding Groundstates by Imaginary Time Evolution with TEBD

Finding groundstates of strongly interacting quantum many body Hamiltonians has proven itself to be one of the the most difficult problems in physics. The main reason for this is the unpleasantly high number of degrees of freedom which plagues this problem and for sure has been the cause for more than one night's bad sleep of a many of theoreticians. Now the theoretical basics we've developed enable us to approximate these groundstates with low computational cost, and in this section we will describe how this can be achieved with the TEBD algorithm (in section 7, we will learn about an even more accurate algorithm, DMRG, but for the moment, we will stay with the TEBD).

Consider the evolution of an arbitrary state $|\psi\rangle$ under the transformation

$$|\psi'\rangle = \frac{\exp(-\beta \mathrm{H})|\psi\rangle}{||\exp(-\beta \mathrm{H})|\psi\rangle||} \tag{6.6}$$

where β is a real, positive number. By setting $t = -\hbar i\beta$ in eq.(6.2), one sees that eq.(6.6) corresponds to time evolution in imaginary time. The state will converge to the groundstate of the system due to the exponential damping of all states with higher energy than the groundstate. As illustrated before, one could again use the Suzuki Trotter expansion of the imaginary time evolution operator and use the same algorithm as above to approximate the groundstate (at least for infinite time, the state will converge). However, the

operator in eq.(6.6) has the very unpleasant property of not being unitary, and thus we need to modify the algorithm in a certain way. Before we do this, let me explain, why there will arise problems if we apply a non-unitary gate to a canonical state and update it via the procedure outlined in section 5.2. Above we saw, that if a non-unitary one site operator acts on a canonical state, the resulting state obtained by our update procedure will no more be a canonical one. The same holds for the application of a non unitary two site operator under the update scheme for two sites. Lets look at a bipartition of the system at the bond connecting site l and $l+1$. A Schmidt state $|\Phi_{\alpha_l}\rangle$ for the system $1\cdots l$ is itself a superposition of an outer product of Schmidt states $|\Phi_{\alpha_{l-1}}\rangle$ from the system $1\cdots l-1$ and single site states $|i_l\rangle$:

$$|\Phi_{\alpha_l}^{1\cdots l}\rangle = \sum_{\alpha_{l-1}i_l} c_{\alpha_{l-1}i_l}|\Phi_{\alpha_{l-1}}^{1\cdots l-1}\rangle|i_l\rangle$$

We now let an operator $\hat{U}_{l-1}$ act on an arbitrary bond $m < l$ within the left block. This operator acts only in the space of the states $|\Phi_{\alpha_{l-1}}^{1\cdots l-1}\rangle$. The transformation of the states $|\Phi_{\alpha_l}^{1\cdots l}\rangle$ under $\hat{U}$ are found to be

$$\begin{aligned}|\tilde{\Phi}_{\alpha_l}^{1\cdots l}\rangle &= \sum_{\alpha_{l-1}i_l} c_{\alpha_{l-1}i_l}|\tilde{\Phi}_{\alpha_{l-1}}^{1\cdots l-1}\rangle|i_l\rangle \\ &= \sum_{\alpha_{l-1}i_l} c_{\alpha_{l-1}i_l}\hat{U}_{l-1}|\Phi_{\alpha_{l-1}}^{1\cdots l-1}\rangle|i_l\rangle\end{aligned}$$

Let's investigate the case of a unitary gate $\hat{U}_{l-1}$: Since unitary operations conserve orthonormality, the application of a unitary gate will not alter the orthonormality properties of **all** Schmidt eigenstates $|\Phi_{\alpha_{l-1}}^{1\cdots l-1}\rangle$. Above we already found an update algorithm for this case and saw, that it preservers the canonical representation of the state. If in contrast, the operator $\hat{U}_{l-1}$ is a non-unitary two site operator, the states $|\tilde{\Phi}_{\alpha_l}^{1\cdots l}\rangle$ will in general NOT be orthonormal, even if they were before the action of $\hat{U}_{l-1}$. However, if we apply our update algorithm from above to a non-unitary operation at site m and $m+1$, we still get the orthonormal states for systems $1\cdots m$ and $m+1\cdots N$. The point is, that due to the non unitarity of $\hat{U}$, the former Schmidt states for **all other** partitions, that contain the sites m and $m+1$, are no more orthonormal and hence the λ's are no more the Schmidt eigenvalues for this bipartition and therefore the state is no longer in its canonical form, and any manipulation of the state that relies on the orthonormality of the $|\tilde{\Phi}_{\alpha_l}^{1\cdots l}\rangle$ will give wrong results. The problem is visualized in fig.6.1. Though after application of a non unitary gate at a certain bond the states for the left and right block of the corresponding bipartition are orthonormal, this is not the

case for the left block of the left-nearest bipartition and the right block of the right nearest bipartition (and in general, for all blocks which contain the gate at which the non-unitary operator has been applied), because the A-matrices at the sites where $\hat{U}$ has been applied (the ones in black squares in fig.6.1) are not orthonormalized. Recall that a partition is in a Schmidt decomposed representation if and only if all matrices to the left are left orthonormalized, all matrices to the right are right orthonormalized and in between there is a diagonal matrix which is normalized by $1 = \sum_\alpha \lambda_\alpha^2$. Here, this is only the case for the partition, where $\hat{U}$ has been applied.

Now let's address the imaginary time evolution with some arbitrary time evolution operator $\hat{U}$ that decomposes into a product of two site operators $\hat{U}_n$ like in eq.(6.4). Our main problem is, that the update algorithm produces non-orthonormalized states. In the Suzuki Trotter expansion method from above, we first update all even bonds and then all odd bonds of the MPS. If the operator acts on sites n and $n+1$, the states for the blocks $1 \cdots n-1$ and $n+1 \cdots N$ have to be orthonormal for the update algorithm, therefore the matrices need to be left and right orthonormalized respectively. But as indicated in fig.6.1, this cannot be achieved in the even/odd sweep, because if after updating bond $n-(n+1)$ we update $(n+1)-(n+3)$, there is a non orthonormalized A-matrix in the left system. The way out now is that instead of merely shifting the gate by two sites, one first applies the identity operator between the bonds that have to be updated. In fig.6.2 you can see the graphical representation of it.

The algorithm now is:

1. Start with odd bonds at $n = 1$.
2. Apply $\hat{U}_n$ at the bond n.
3. At bond n+1, apply $\mathbb{1}$. If $n < N-3$, set $n = n$+2 and go to 2.
4. If $n >= N-3$, set $n = N$-1.
5. Apply $\hat{U}_n$ at site n.
6. Apply $\mathbb{1}$ at site n-1. If $n > 4$, set $n = n$-2 and go to 5.
7. Apply $\mathbb{1}$ at site $n = 1$.

In this way, we are always shifting the non orthonormal matrices to the bond, at which either $\mathbb{1}$ or $\hat{U}$ acts, and there the non-orthonormality doesn't matter. Of course all the above described algorithms are useless if we don't have a state onto which we can let them act. In the next subsection, we will shortly

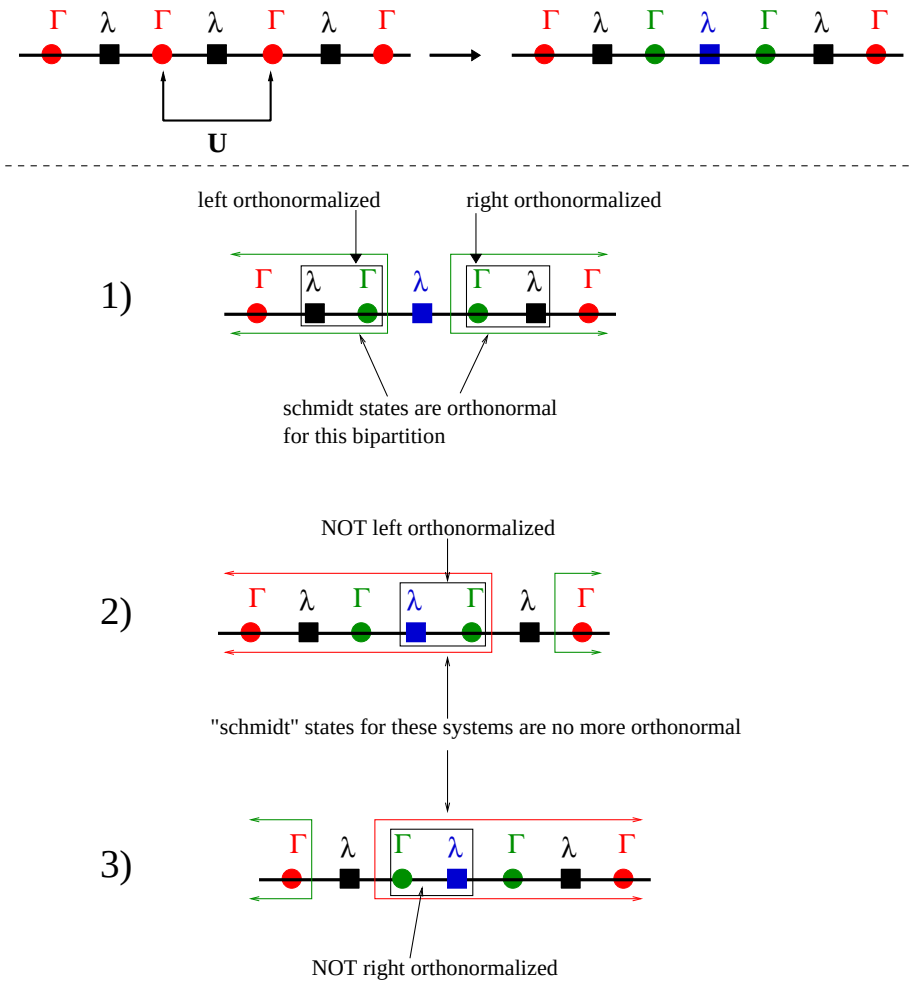

Figure 6.1: Application of a non-unitary gate $\hat{U}$ to a canonical state. Red and green letters label updated matrices. 1) shows the bipartition where the gate has been applied. The factor $\Gamma\lambda$ in the black square corresponds to a right orthonormalized A-matrix, the factor $\lambda\Gamma$ to a left orthonormalized A-matrix. In 2) and 3), the bipartition for the left and right next site is shown. The factor in the black square is not an orthonormal A-matrix, hence the new block states are not orthonormal and are therefore not Schmidt states (which is indicated by the " " sign in the graphics).

describe how a certain class of states, namely pure product states for open boundary conditions, can easily be prepared in a canonical state.

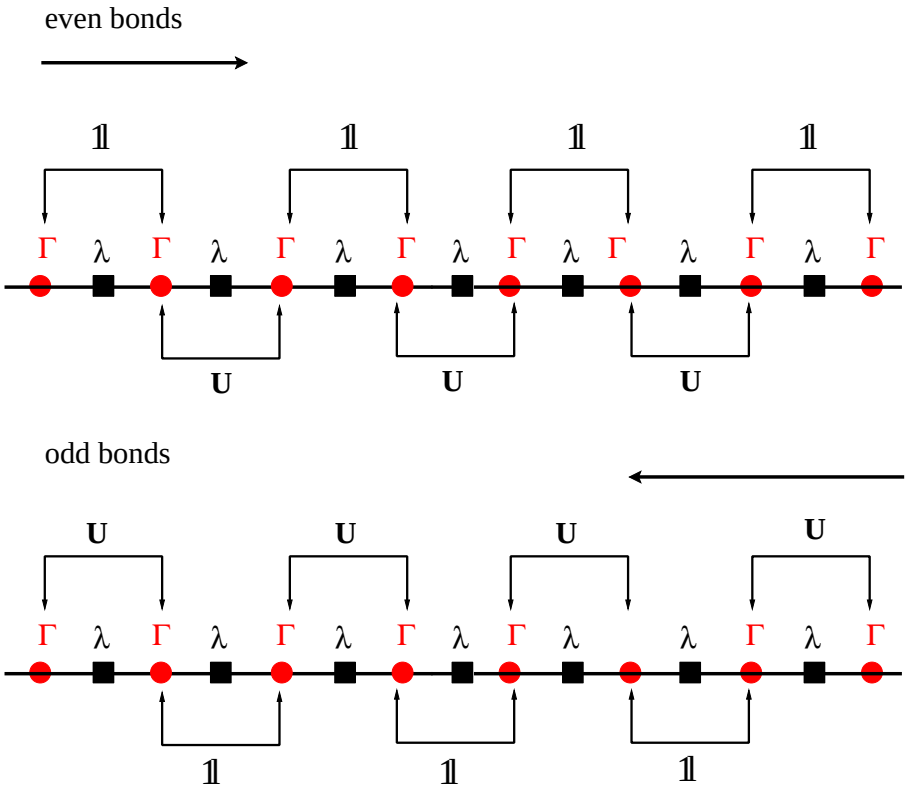

Figure 6.2: Imaginary time evolution with TEBD. First Suzuki Trotter expand the time evolution operator. Start with even bonds. Apply $\hat{U}$ at the first even bond, then apply $\mathbb{1}$ at the neighboring bond, then again $\hat{U}$, then $\mathbb{1}$, and so on. In the backwards sweep, apply this to all odd bonds.

6.3 Matrix Product Representation for Simple Quantum States

The simplest many body state one can think of is a product state of N independent systems. The construction of the canonical representation of such a state is straightforward. Let the state be

$$|\psi\rangle = |j_1 j_2 \cdots j_N\rangle$$

where $|j_n\rangle$ is a local basis for site n, like the eigenstates of $\hat{S}_n^z$. The dimension of the local Hilbert space is d. For such a product state, the canonical

representation is given by

$$\Gamma^{[n]i_n}_{\alpha_n\alpha_{n+1}} = \begin{cases} \begin{pmatrix} \delta_{i_1 j_1} & 0 & \cdots & 0 \end{pmatrix} & n = 1 \\ \begin{pmatrix} \delta_{i_n j_n} & 0 & \cdots & 0 \\ 0 & 0 & \cdots & 0 \\ \vdots & & \ddots & \vdots \\ 0 & \cdots & & 0 \end{pmatrix} & 1 < n < N \\ \begin{pmatrix} \delta_{i_N j_N} \\ 0 \\ \vdots \\ 0 \end{pmatrix} & n = N \end{cases}$$

$$\lambda^{[n]}_{\alpha_n} = \begin{pmatrix} 1 \\ 0 \\ \vdots \\ 0 \end{pmatrix}$$

All manipulations can be carried out on such a state. In particular, quantum numbers can easily be attached to the Schmidt eigenvalues of each bond, allowing for more efficient simulation of the real or imaginary time evolution.

Chapter 7

The DMRG Algorithm

In the last section we introduced a method with which groundstates of quantum many body systems can be approximated, but imaginary time evolution is by far not the best one can do. The best method in one dimension to obtain ground states is DMRG. DMRG is short for Density Matrix Renormalization Group. As the name indicates, it has its roots in renormalization group methods. The details on the subject can be found in [30]. There are also a lot of good reviews available, and we urge the reader who has no experience with DMRG to have a look at [31, 32, 33, 34].

DMRG was introduced as a tool to calculate the energy and other observables of ground states (but also excited states) of a one dimensional quantum system to a very high precision with a very modest amount of computational effort. The key aspect of DMRG is the truncation of the total Hilbert space of the system to a reduced Hilbert space, i.e. one with a small number of states with the property that these states all have a very large overlap with the state we want to describe (for example the ground state). Let's assume for now that we are looking for the ground state properties of a system in the thermodynamic limit. The Hamiltonian of this system shall be of the form

$$\hat{H} = \sum_i \hat{O}^i \hat{O}^{i+1} \tag{7.1}$$

where i denotes the site index. An example would again be the Heisenberg magnet with $\hat{O}^i = \vec{\hat{S}}^i$. DMRG can be applied to infinite and finite systems. We will start with the infinite case because it is conceptually easier to understand and bears all the important aspects of the algorithm. Before we go into the details, we want to add a remarks: DMRG as we will introduce it here is equivalent to matrix product state algorithms, DMRG even produces MPS (we will discuss this in chapter 7.4), and all DMRG algorithms can thus

be reformulted in terms of MPS and vice versa (though the implementation can be complicated).

7.1 Infinite System DMRG

DMRG is an iterative process which converges to an approximation of the ground state of some Hamiltonian. At each iteration step, the system is virtually split up into four distinct areas (see fig.7.1): one block (which consist in general of many site) at the left side, then two single sites in the middle (often called the "free" sides), and one block at the right side (which can also contain many sides). The system is in the ground state $|\psi\rangle$ of the system. For each block we have (for the moment) an exact basis, and $|\psi\rangle$ can be written in this basis as

$$\begin{aligned} |\alpha\rangle &\quad \text{basis for left block} \\ |i\rangle &\quad \text{basis for first site} \\ |j\rangle &\quad \text{basis for second site} \\ |\gamma\rangle &\quad \text{basis for right block} \\ |\psi\rangle &= \sum_{\alpha,i,j,\gamma} c_{\alpha ij\gamma} \, |\alpha ij\gamma\rangle \end{aligned}$$

The principle of DMRG now is to successively enlarge the left and the right block (by adding sites) and then computing the groundstate of this enlarged system. For generic quantum systems, this leads to an exponentially growing Hilbert space for each block. The clue of DMRG now is, that it approximates the ground state of the enlarged system with a very small part of the full Hilbert space basis. So in every block, we do not keep all the basis states of the block system but only a very small number, a so called effective basis. Of course these states have to be carefully chosen in order to get a good description of the true ground state. After these preliminaries, we now look at the details of the algorithm:

1. Set up a system of two blocks and two single sites. At the first step, the two blocks in general consist only of one site. Set up the Hamiltonian and all operators needed for block 1 to 4 (in χ-dimensional representation).

2. From the representation of the Hamiltonian and all operators, form the superblock Hamiltonian of the combination of the two blocks and the two single sites. For our model, this leads to $H_{SB} = H_{B_1} \otimes \mathbb{1}^n \otimes \mathbb{1}^{n+1} \otimes \mathbb{1}^{B_4} + \hat{O}_{B_1}^{n-1} \otimes \hat{O}^n \otimes \mathbb{1}^{n+1} \otimes \mathbb{1}^{B_4} + \mathbb{1}^{B_1} \otimes \hat{O}^n \otimes \hat{O}^{n+1} \otimes \mathbb{1}^{B_4} + \mathbb{1}^{B_1} \otimes \mathbb{1}^n \otimes \hat{O}^{n+1} \otimes \hat{O}_{B_4}^{n+2} + \mathbb{1}^{B_1} \otimes \mathbb{1}^n \otimes \mathbb{1}^{n+1} \otimes H_{B_4}$. n and n+1 denote the single sites of the system. $\hat{O}_{B_1}^{n-1}$ is the representation of the operator $\hat{O}^{n-1}$ in the reduced basis of block 1, similar for $\hat{O}_{B_4}^{n+2}$.

3. Diagonalize this matrix and keep the groundstate $\psi_{\alpha i j \gamma}$. Energy and other observables can now be measured.

4. Compute the reduced density matrix $\hat{\rho}_{\alpha,i_1,\tilde{\alpha},\tilde{i}_1} = \sum_{i_2,\gamma} \psi_{\alpha,i_1,i_2,\gamma} \psi_{\tilde{\alpha},\tilde{i}_1,i_2,\gamma}$ for the system $B_1\bullet$ and diagonalize it. Keep the χ largest eigenvalues w_j^α and eigenvectors λ_α. These eigenvectors are the new basis vectors for the system $B_1\bullet$. If desired, store them (for example for implementation of time evolution algorithms into DMRG, so called tDMRG).

5. Transform all operators of the block+site system $B_1\bullet$ into this new basis, thus you get a representation of all operators for the $B_1\bullet$ system. The reduced Hamiltonian for the new block+site system for example is given by $\tilde{H}_{B_1\bullet} = U H_{B_1\bullet} U^\dagger = U(H_{B_1} \otimes \mathbb{1} + \hat{O}_{B_1}^{n-1} \otimes \hat{O}^n) U^\dagger$ where $U_{\alpha j} = w_j^\alpha$.

6. Replace the old block 1 with the system $B_1\bullet$ ($H_{B_1}^{new} = \tilde{H}_{B_1\bullet}$), and replace the old block 4 with the reflection of $B_1\bullet$.

7. Restart the iteration at 2.

Table 7.1: Infinite DMRG algorithm for 1-d quantum systems

The eigenvectors of the reduced density matrix are those states, which contribute to the state, in which the subsystem is. By taking only the eigenvectors belonging to the highest eigenvalues of the reduced density matrix as new block states, one takes only those states into account, which contribute noticeable to the expectation value of operators. These eigenvectors are thus the new "effective" basis for the block system.

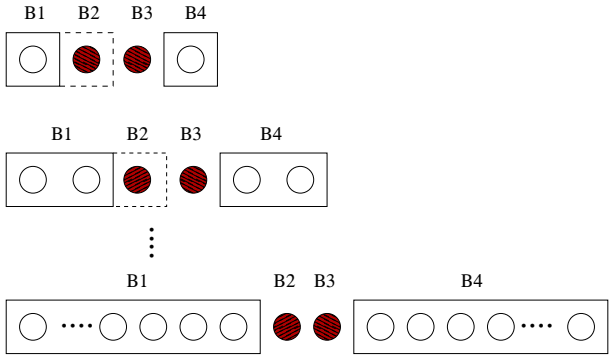

Figure 7.1: Visualization of the infinite DMRG algorithm. Starting from a four blocks setup, one successively adds a site to the left block B_1 and constructs an effective basis for this $B_1\bullet$ system as described in the text.

The infinite system DMRG algorithm can be adapted to finite systems as well, but we have to modify it because we can't reflect the blocks any more.

7.2 Finite System DMRG

The basic idea of the finite DMRG remains the same, but we have to modify the iteration process. The system is still split up into four separate parts, but this time blocks one and four in general do not have the same number of sites any more. Let us look at the algorithm first and then explain the concepts behind it:

1. Apply an infinite system DMRG algorithm until you reach a block size of number $N/2-1$. Store Hamiltonians and operators for each block.

2. Now set $n = N/2-1$ and use the block B_n as the left block 1 and the earlier stored block B_{N-n-2} as the right block 4 (two blocks consisting of a single site are between block 1 and 4).

3. Build the superblock Hamiltonian just as in the infinite system algorithm and diagonalize it.

4. Build the reduced density matrix for the system $B_n\bullet$ and diagonalize it. Take the χ largest eigenvalues and eigenvectors as a new basis for this block and express all relevant operators in this basis. Store the block as B_{n+1}, set $n = n+1$;

5. Got to 3) and proceed until you reach the right end of the system ($n = N-3$).

6. Now reverse direction by taking block B_{N-3} as the new block 4 and three single sites as blocks 1 to 3. Set $n = 1$.

7. Build the super block Hamiltonian and diagonalize it. From the ground state or any other target state compute the reduced density matrix as in 4. and diagonalize it. Take the eigenvectors as the new basis for the block $B_n\bullet$.

8. Transform all operators into this basis and store the resulting block $B_n\bullet$ as new block B_{n+1}. Set $n = n+1$ and proceed until $n = N/2-1$.

9. If $n \geqq N/2$, take block $N-n-2$ (obtained from the previous step where $n < N/2$) as new right block (block 4). Go to 3.

10. Stop after 2 to 3 sweeps through the system.

Table 7.2: Finite system DMRG algorithm

As an example, we programmed a small finite DMRG for the Heisenberg system in Matlab. In fig.7.3 you can see the groundstate energy per site of the isotropic Heisenberg AF (J=1) in one dimension as a function of the iteration step of the finite DMRG. In this simulation only 20(!) states per block were kept. As you can see, the value converges to the exact groundstate energy per site of the $N \to \infty$ periodic Heisenberg AF (obtained from the Bethe ansatz, see [19]) . An estimate for the overall error due to the truncation of eigenvalues is the sum of the discarded eigenvalues. In fig.7.4, the truncation error is plotted with increasing number of iterations. The periodic behavior of the error has the following explanation: If you cut the finite system in the middle, then the reduced densities of the emerging two systems have many more eigenvalues than the one you get if you cut the system at the first (or last) bond. This is because a single site in a Heisenberg spin 1/2 chain can only be in two states, thus the reduced density for this single site (and also the one for the rest of the system) has only two eigenvalues. In finite DMRG one wanders through the chain, from one site to the other and back, computes the reduced density at every site and then discards all but the χ highest values. Clearly then the error is highest in the middle of the system and gets smaller the closer one gets to the borders.

In sec.7.4 we will see that DMRG produces site dependent MPS with auxiliary matrix a dimension χ. Since the amount of entanglement encoded in a MPS is bounded by an upper constant depending on χ, the DMRG representation of the groundstate (and any other state) of the system will get worse with increasing system size unless one keeps an increasing number of states per block, which goes along with an increase in computational time.

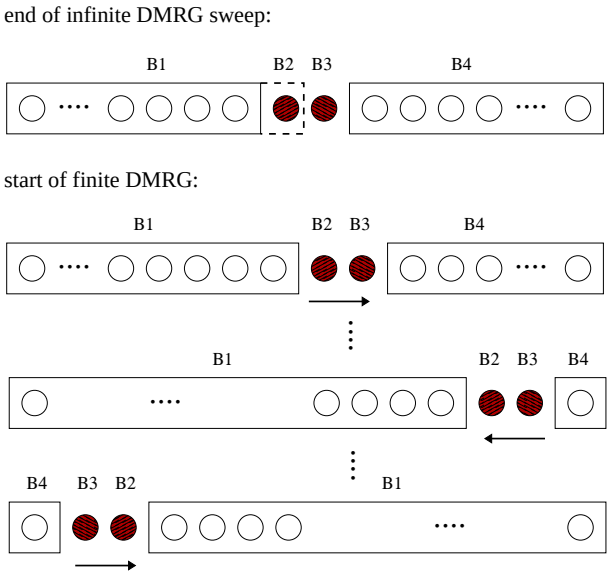

Figure 7.2: Visualization of the finite DMRG algorithm. One sweeps back and forth through the system until a convergence criterion is matched.

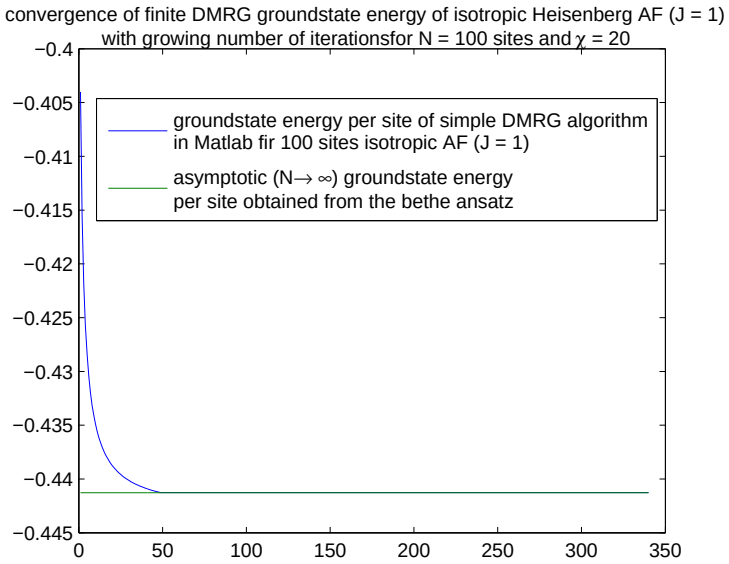

Figure 7.3: Convergence of ground state energy per site with iteration steps of finite system DMRG for 100 sites Heisenberg AF (J = 1). Blue line: groundstate energy obtained by a simple Matlab DMRG. Green line: groundstate energy obtained from the asymptotic (N $\rightarrow \infty$) Bethe ansatz solution for the Heisenberg AF (J = 1)

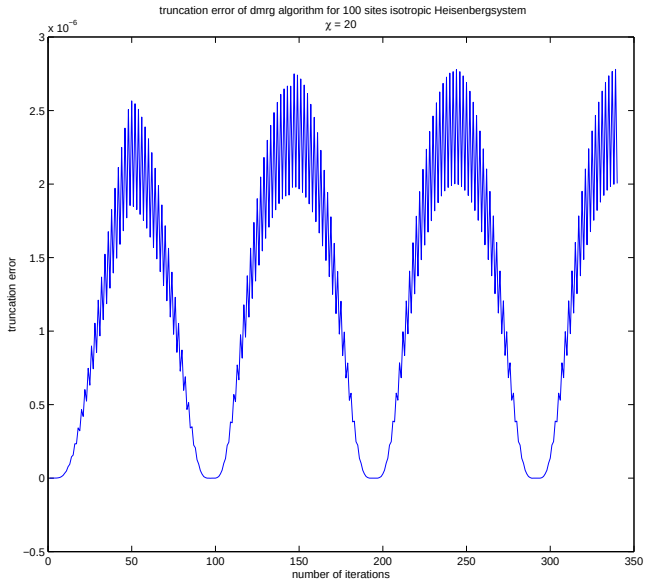

Figure 7.4: Truncation error at each iteration step of a simple finite DMRG in Matlab. When the free sites in the DMRG are in the middle of the system, the truncation error is high because the entanglement of the block $B_1\bullet$ with $\bullet B_4$ is very large and not all Schmidt states can be stored for a given χ. At the edge of the system, the truncation error is small because a small system has only a small number of Schmidt states which can all be stored. If for example the left block B_1 consists only of one spin, then the Hilbert space dimension for the $B_1\bullet$ is 4 (for spin 1/2 systems), which is in general much smaller than χ, and in this case all Schmidt eigenvalues can be stored.

7.3 Calculation of Observables

To calculate observables in DMRG it is necessary to store the operator representation of this observable in every block. The expectation value of any operator is then computed from the target state in a simple matrix multiplication. As an example, we look at the spin density at site n which shall lie in the left block. Assume that we just computed the groundstate $|\psi\rangle$ of the superblock Hamiltonian for a partition $B_1\ i\ j\ B_4$. The state lies in a $\chi^2 d^2$ dimensional Hilbert space:

$$|\psi\rangle = \psi_{\alpha i j \gamma}$$

$\langle\psi|S_n^z|\psi\rangle$ can then be computed by a simple matrix multiplication and is given by

$$\langle\psi|S_n^z|\psi\rangle = \langle\psi|\tilde{S}_n^z \otimes \mathbb{1}_i^d \otimes \mathbb{1}_j^d \otimes \mathbb{1}^\chi|\psi\rangle$$

where $\mathbb{1}_{i,j}^d$ denotes the identity operator in the Hilbert space of sites i and j, $\mathbb{1}^\chi$ denotes the identity in the reduced Hilbert space of the right block and $\otimes$ is the outer product of these operators. $\tilde{S}_n^z$ is the χ dimensional matrix representation of the operator S_n^z in the left block.

In this frame, it is also very easy to create excitations from the ground state. One merely constructs the according operator and applies it to the target state(s) at the end of the finite system sweep. This is especially interesting when one wants to investigate the time evolution of excitations from the groundstate of quantum systems.

7.4 Connection of DMRG to MPS

The DMRG procedure outlined above produces site dependant MPS which was first recognized by Östlund and Rommer ([35]). We first consider the infinite DMRG algorithm. The typical situation encountered here is that at a certain iteration step we have a system of size l and an effective basis $|m_l\rangle$ for it, which is encoded in the matrix representation of all relevant operators. From this basis, we want to construct a new basis set for the $l+1$ sites system where one site has been added to the block of size l. A suitable basis for the $l+1$ sites system would be the set of χd states

$$\widetilde{|m_{l+1}\rangle} \equiv |m_l\rangle|s_{l+1}\rangle.$$

Since want to reduce the dimension of this system to χ, we project these states down to a Hilbert space described by only χ states $|m_{l+1}\rangle$ by

$$|m_{l+1}\rangle \equiv A^{i_{l+1}}_{m_l m_{l+1}}|m_l\rangle|i_{l+1}\rangle. \tag{7.2}$$

If we do so, we get a new effective basis for the $l+1$ sites system. In DMRG, the projection operator (or better, the reduced basis transformation) A is given by the orthogonal matrix U that diagonalizes the reduced density matrix of the system of length $l+1$ according to $\hat{\rho}^{1\cdots l+1} = UDU^\dagger$ (see 4. in table (7.1), page 71), but one can also think of other optimization methods by which one can get such a projection operator (for example minimization of energy of the $l+1$ sites system). We now show, that by building up a system by such a procedure, one arrives at a site dependent MPS. We want to find an approximate basis set of an n-sites quantum system. We start the iteration at the left side of the N-sites system. For a block of length $p \ll n$, we assume to have a set of exact basis states $|z_p\rangle$. If we now apply the above described method, i.e. first add a site to the p-sites system, thus arriving at

$$\widetilde{|m_1\rangle} = |z_p\rangle|i_1\rangle$$

and then project these states down by

$$|m_1\rangle = A^{i_{l+1}}_{m_l m_{l+1}}|m_l\rangle|i_{l+1}\rangle$$

where A is obtained by some minimization procedure, we get an effective approximate basis for the $p+1$ system. We can iterate this by applying the same procedure to the new effective basis states and thus we can construct an approximate basis for the n sites system, and it is given by

$$|m_n\rangle = \sum_{\{i_k\}\{m_k\},z_p} A^{i_1}_{z_p m_1}\cdots A^{i_n}_{m_{n-1}m_n}\cdots|z_p\rangle|i_1\cdots i_n\rangle.$$

In this way, DMRG produces site dependent MPS, although in the standard DMRG, the MPS are implicitly given by the operator representations. The minimization procedure is in general chosen in such a way, that the projected states are suitable for approximating the true ground state of the large system.

The MPS produced by infinite DMRG is by construction left orthonormalized if one starts at the left side of the system, whereas starting at the right side of the system would result in a right orthonormalized MPS. Like already mentioned above, the orthogonality constraint eq.(4.4) provides a necessary and sufficient condition that the projected states $|m_{l+1}\rangle$ are orthonormalized, provided the $|m_l\rangle$ are: if all A matrices satisfy condition eq. (4.4), then the block states of all blocks to the left of any site are orthonormal.

In finite system DMRG, one has both constraints partly satisfied. If we start our infinite DMRG sweep again at the left side of the system, we produce a right orthonormalized MPS. When switching to the finite system sweep, we

again get right orthonormalized A-matrices until we reach the right side of the system, where direction is reversed. In the backwards sweep we now get left orthonormalized A-matrices at each iteration step. The complete finite DMRG MPS is thus a product of a right and left orthonormalized MPS. In other words, we approximate the true ground state within a productbasis of a left orthonormalized MPS, two single sites and a right orthonormalized MPS.

For canonical MPS, there is a relation between the wave function $\psi_{\alpha i_n i_{n+1} \gamma}$ and the matrices Γ^{i_n} and $\Gamma^{i_{n+1}}$ at sites n and $n+1$. It is given by

$$\psi_{\alpha i_n i_{n+1} \gamma} = \sum_{\alpha_{n+1}} \lambda_{\alpha_n} \Gamma^{i_{n+1}}_{\alpha_n \alpha_{n+1}} \lambda_{\alpha_{n+1}} \Gamma^{i_{n+2}}_{\alpha_{n+1} \alpha_{n+2}} \lambda_{\alpha_{n+2}} \tag{7.3}$$

and is proved by expanding the state in the suitable basis set for the corresponding partition of the system (left block $|\alpha_n\rangle$, sites $|i_n\rangle$ and $|i_{n+1}\rangle$, right block $|\alpha_{n+2}\rangle$).

7.5 Adaptive Time Dependent DMRG (tDMRG)

At the same time Vidal proposed his TEBD algorithm [2, 3], it became clear that this time evolution scheme could easily be adopted to DMRG ([36, 4]).

As we saw above, DMRG produces site dependent, orthonormal MPS. In principle, DMRG makes use of the Schmidt decomposition because at each step one builds the reduced density matrix for a bipartition and diagonalizes it. The idea behind tDMRG now is the following: Time evolution of quantum system is connected to entanglement propagation through the system. This means, that the degree of entanglement of two system blocks changes in time. As a consequence, the Schmidt states of each bipartition evolve in time. So if at a site n at $t = t_1$ we identified a good approximate basis set (=Schmidt states), we can not assume that at $t = t_2$ this set still represents a good approximate basis. Thus just keeping one representation of all operators for all times t won't work. A way around this problem is the following observation: We can use a Suzuki Trotter decomposition of the time evolution operator (see section 6.1). Time evolution is then carried out by applying two site operators at each bond, so each bond is independently evolved. If we now apply a Schmidt decomposition directly after the gate application at each bond, we get a new effective basis for the time evolved bond. This is the principle behind tDMRG (and also TEBD).

The approximate time evolution operator $\hat{U} = \prod_n \hat{U}^{[n]}$ is obtained from a Suzuki Trotter decomposition of $\exp(\frac{-it}{\hbar}\hat{H})$. As already discussed, at some point of each iteration step (namely after the diagonalization of the

superblock Hamiltonian), the DMRG wave function of the complete chain is given in a product basis of two χ dimensional Hilbert spaces (the two big blocks) and two d dimensional one (the free or single sites) as $\psi_{\alpha ij\gamma}$. At this point, one can apply the bond operator $\hat{U}^{[l]}$ to the free sites, giving

$$\psi'_{\alpha' i' j' \gamma'} = \sum_{\alpha i j \gamma} U^{[l],\alpha' i' j' \gamma'}_{\alpha i j \gamma} \psi_{\alpha i j \gamma}.$$

From $\psi'_{\alpha' i' j' \gamma'}$, compute the reduced density for system $\alpha' i'$, diagonalize it and transform operators into the new basis. In the next step, you need to shift the free sites by two and then apply the gate at the free sites. This shift of the free sites is done with White's state prediction method ([23]). For the state prediction, one needs to store reduced basis transformation matrices that transform operators in to the reduced basis. In essence, they contain the eigenvectors of the reduced density. In the following these matrices are termed $A^{i_{l+1}}_{\alpha_l \alpha_{l+1}}$ for site $l+1$.

We will only state the results for a shift by one site to the left and refer the reader to [36] for the detailed calculation. The state in the shifted representation is

$$\psi_{\alpha_{l-1} i_{l-1} i_l \alpha_l} = \sum_{\alpha_{l-1} \alpha_{l+1} i_{l+1}} \psi_{\alpha_{l-1} i_l i_{l+1} \alpha_{l+1}} A^{i_{l+1}}_{\alpha_l \alpha_{l+1}} A^{i_{l-1}}_{\alpha_{l-2} \alpha_{l-1}}. \tag{7.4}$$

A similar formula holds if you want to shift the bond by one to the right side. The basic tDMRG algorithm thus contains the following parts:

1. One does a finite DMRG system sweep to get the ground state of the system.

2. One creates an excitation by applying some operator to the ground state.

3. Now comes the time evolution part: compute the bond operator $\hat{U}_l = e^{\frac{-i\Delta t}{\hbar}\hat{H}_l}$ acting at bond l from the matrix representation of $\hat{H}_l$ (in the reduced basis). Then run a sweep

   (a) Apply $\hat{U}_l$ to an odd bond. This is a matrix multiplication of the target state $\psi_{\alpha ij\gamma}$ with the time evolution operator.

   (b) Build the reduced density with the evolved state and diagonalize it. Like in standard DMRG, transform all operators into the basis set consisting of the eigenvalues of the reduced density matrix.

   (c) If you have not yet reached the boundaries of the system, shift the free sides by two using the prediction method by White and go again to (a).

4. If you have reached the end of the system, reverse the direction and apply 3 to all even sides of the system.

5. Evaluate operators after every Trotter time step.

Table 7.3: tDMRG algorithm for finite systems

This has been a very brief discussion of tDMRG and intended to show the reader the similarity of TEBD and tDMRG. DMRG and MPS in general are very close connected, which is the reason why we included this chapter. For further introductory material and reviews look at the bibliography.

Part III

Results

Chapter 8

Testing the TEBD Algorithm for the 1-d Heisenberg Chain Against the Exact Solution

For small system sizes, the Heisenberg chain can be exactly diagonalized, and the time evolution can then be compared to the MPS approximation. We did this for a system of 12 sites. At t = 0, we chose as initial state a product state with 7 up spins on the left side and 5 down spins on the right side of the chain. We then let this state evolve and compared it to the MPS-time evolution. In fig.(8), the difference of the spin-density at site 6 obtained from the exact solution to that from TEBD is plotted for different values of the auxiliary dimension χ. With increasing χ, the difference gets smaller. Small oscillations remain due to the Trotter expansion. These can be suppressed by using either a smaller time step or a higher order Trotter expansion. In appendix D, the reader finds a study on the error convergence for TEBD simulations of two spin chains which are connected at one site.

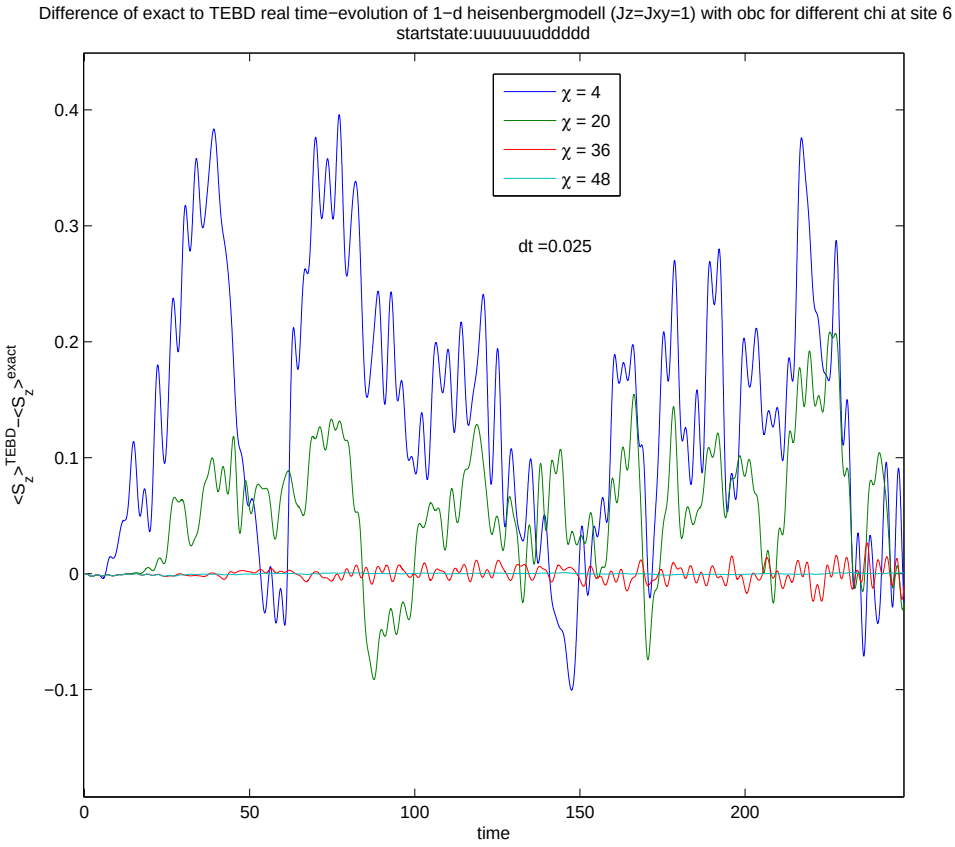

Figure 8.1: Difference of $\langle S_z \rangle^{exact} - \langle S_z \rangle^{TEBD}$ of exact time evolution of the isotropic Heisenberg AFM to the TEBD approximation at site 6 of the system. System size is 12, as initial state 7 up spins are located at the left side of the system and 5 down spins at the right side of the system (this is a pure product state). For bipartitions where the left and the right block have approximately the same number of sites (effectively this means cutting the system into half), the number of non-zero eigenvalues of the reduced density matrix has a maximum. This means that the effect of discarding some eigenvalues on local observables is best observed in the middle of the system. Here we plotted the difference of the approximative TEBD time-evolution to the exact one for site 6 of a 12 sites system with 7 up spins. With increasing χ, the error gets smaller, and one can see that beyond certain value of χ the time evolution with TEBD is nearly exact (apart from the error due to the Suzuki Trotter expansion of the time evolution operator).

Chapter 9

Measuring the Time Evolution of Entanglement in Heisenberg Spin Chains

As already mentioned above, MPS can only contain a limited amount of entanglement entropy. The time evolution of a quantum system is a process where this entangled entropy grows. The time evolution of a quantum system with TEBD (or similar with TDMRG) allows one to easily calculate the entanglement of a certain bipartition of the system because the basis states of the Hilbert space are chosen to be the eigenvectors of the reduced density matrix and all the according eigenvalues are stored. So by inserting these eigenvalues into eq (4.26), one gets the entanglement entropy for the respective blocks of the bipartition. To be precise, this entanglement entropy is only a measure of the entanglement of the two blocks and not of how "much" entanglement there is within each block. In the following section, we will look at how the entanglement entropy of a MPS depends on χ and how fast it converges as a function of time.

9.1 Entanglement Entropy of Matrix Product States as a Function of Auxiliary Dimension χ

In this section we look at how the entanglement entropy for two blocks depends on the auxiliary dimension χ of a MPS. This is important for error estimates. In general one can make several runs of a simulation with different χ and look at the convergence of different observables. The entanglement en-

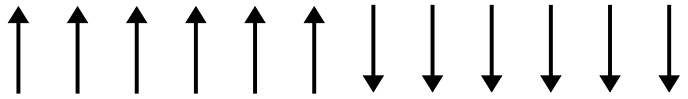

Figure 9.1: Inital state at t = 0.

tropy for example gives you a criterion when your simulation is reliable and when it's not.

I prepared a 50 sites Heisenberg chain in a initial state with no entanglement where on the left side there are 25 up-spins and on the right side 25 down spins (see fig.9.1). During time evolution we looked at the entanglement of the two blocks which emerge from cutting the system into two half at the up-down boundary. I did this for two different sets of parameters for the Heisenberg model, first for the XX model and second for the isotropic AFM (J = 1). Fig.9.2 (a) shows the time evolution of the afore described initial state in the XX-Heisenberg chain for $\chi = 50$.

In fig (9.2) (b) we plotted the entanglement entropy of the left block as a function of time for several values of χ. There is a smooth increase of S_{vN} for short times and at t = 50 there is a sudden jump. At this time, reflections from the walls of the system have propagated back to the site 25 which results in a strong increase in entanglement of the two blocks, similarly at t = 100. For $\chi = 25$ S_{vN} reaches a saturation value which is not the case for larger χ. For $t \leq 50$, all simulations yeald approximately the same time evolution of S_{vN}. For larger times, the increase of entanglement due to the reflection at the boundaries forces one to use high values of χ to get reliable results. One thing to learn from this is that the simulation time should be short enough so that reflections cannot propagate through the system. As a second measure we looked at the sum squared error (SSE) of the magnetization density obtained from comparing simulations for different χ. It is given by

$$SSE = \frac{1}{N} \sum_i | \langle S_i^z \rangle^{\chi_1} - \langle S_i^z \rangle^{\chi_2} |.$$

For the XX and the isotropic Heisenberg chain (J=1), we plotted this quantity in fig.9.4 (a) and (b). The SSE computed from the difference of simulations with $\chi = 100$ and $\chi = 75$ shows that at $t \approx 50$ the two simulations start to differ. One also can see that for the XX chain, the SSE is much higher than for the isotropic Heisenberg chain.

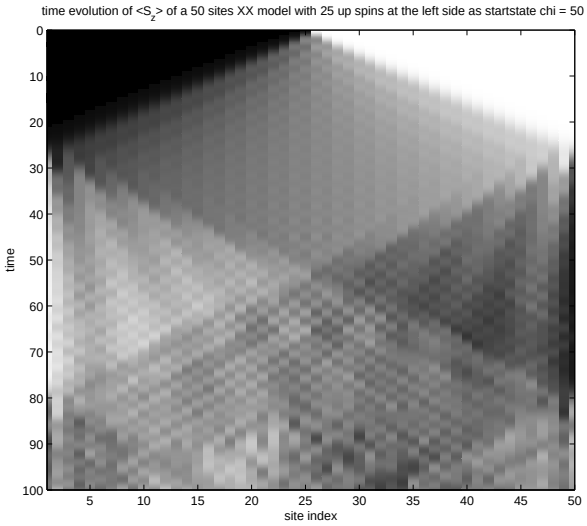

(a) $\langle S_z \rangle(t)$

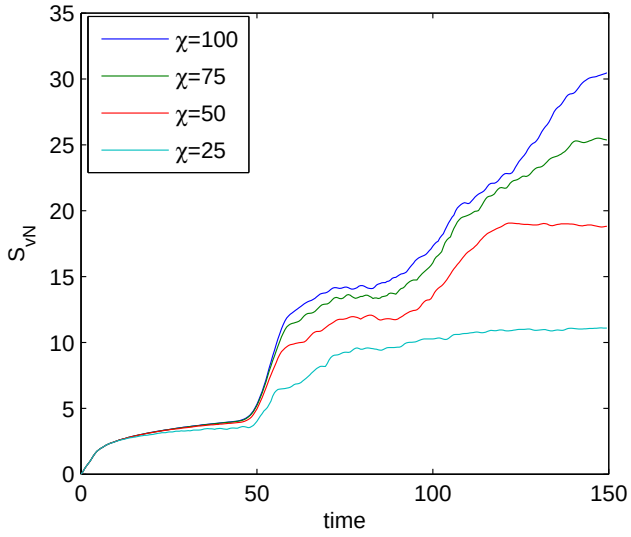

(b) evolution of entanglement for different χ

Figure 9.2: (a) Time evolution of a $|\uparrow \cdots \uparrow\downarrow \cdots \downarrow\rangle$ initial state with 25 up and 25 down spins in XX Heisenberg chain ($J_{xy} = 1$) obtained from TEBD with $\chi = 50$. (b) Entanglement of the block $1 \cdots 25$ with the block $26 \cdots 50$ as a function of time for different values of auxiliary dimension χ. For small χ, the entanglement saturates at small values of S_{vN}. For higher values of χ, one observes a sudden increase of S_{vN} at t ≈ 50 which comes from back propagation of reflections at the boundaries of the system.

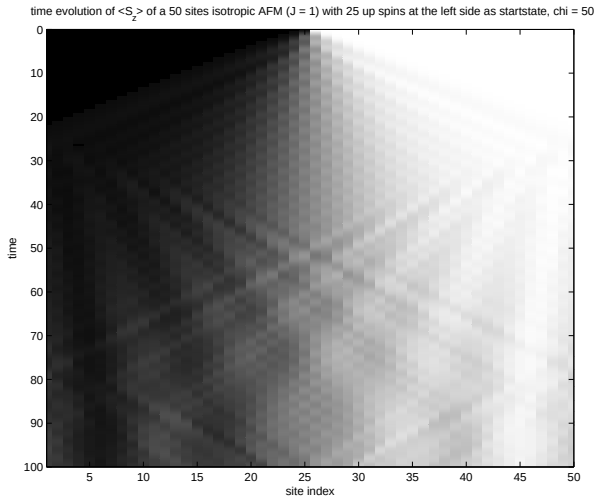

(a) $\langle S_z \rangle(t)$

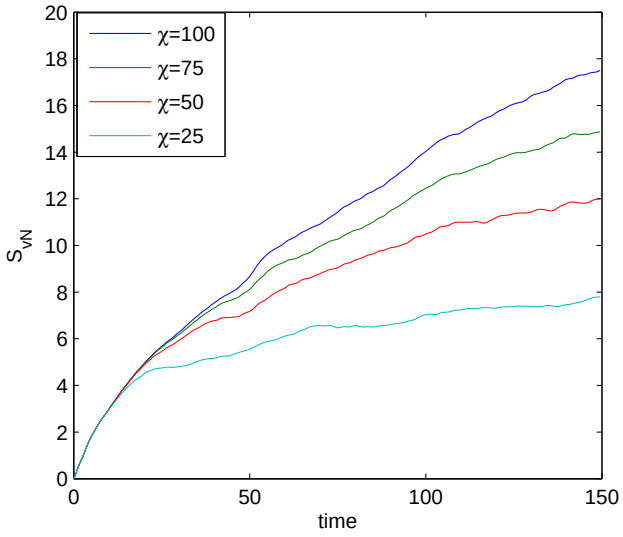

(b) evolution of entanglement for different χ

Figure 9.3: (a) Time evolution of a $|\uparrow \cdots \uparrow\downarrow \cdots \downarrow\rangle$ initial state with 25 up and 25 down spins in isotropic Heisenberg chain ($J = 1$) obtained from TEBD with $\chi = 50$. (b) Entanglement of the block $1 \cdots 25$ with the block $26 \cdots 50$ as a function of time for different values of auxiliary dimension χ. Like in the XX case (fig:9.2, one observes saturation of the entropy at small values of χ. The increase due to reflections much smaller than in the XX chain.

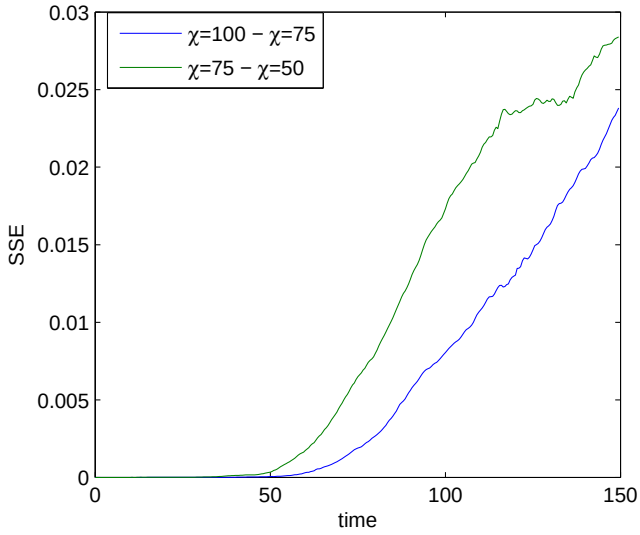

(a) Isotropic Heisenberg chain

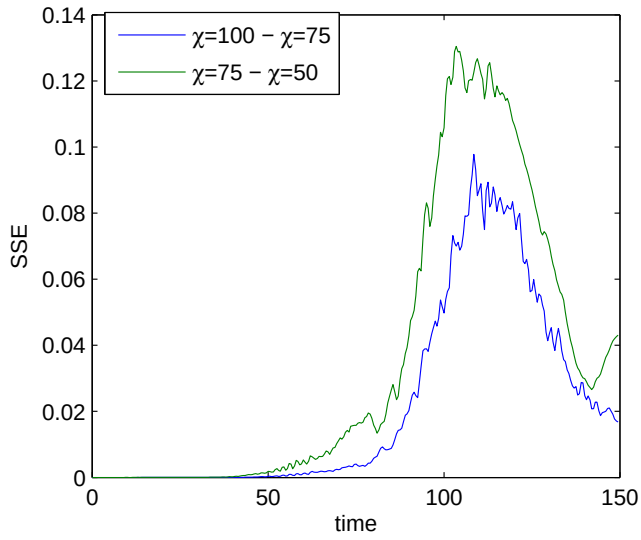

(b) XX Heisenberg chain

Figure 9.4: We compare the sum squared error $SSE = \frac{1}{N}\sum_i |\langle S_i^z\rangle^{\chi_1} - \langle S_i^z\rangle^{\chi_2}|$ of magnetization density for different values of auxiliary dimensions χ_1, χ_2. (a) SSE for isotropic Heisenberg chain ($J = 1$). (b) XX chain ($J_{xy} = 1$).

9.2 Time Evolution of Entanglement for Different Values of J_z

The behavior of the entanglement of a block of spins with the rest of the chain depends on the coupling constants of the Heisenberg system. The following section is a short study of how the entanglement of a block 25 of sites, in the beginning filled with up spins, evolves as a function of time if at t = 0 it is connected to a 75 sites chain with initially only down spins present. Fig.9.5 shows the time evolution of $\langle S^z \rangle(t)$ for different values of J_z ($J_{xy} = 1$ for all simulations) for this setup. Fig.9.6 and 9.7 show S_{vN} as a function of time. As in the previous section, reflections again manifest themselves in a sudden increase of the entanglement at t = 50. For $J_z > 1$, the entanglement of the two blocks saturates at a finite value. For a much more thorough discussion of entanglement in spin chains, we refer the reader to the review[26] and [10] where entanglement properties of ground states of quantum systems are investigated.

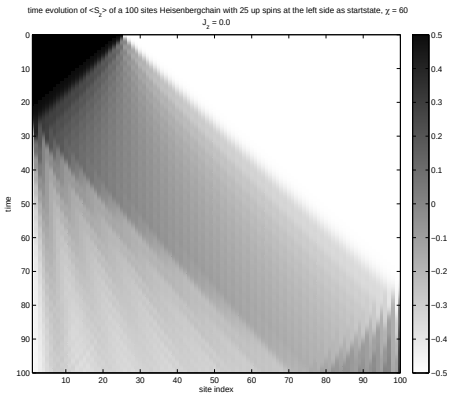

(a) $J_z = 0$

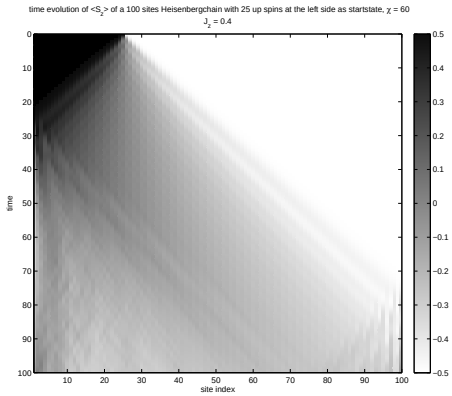

(b) $J_z = 0.4$

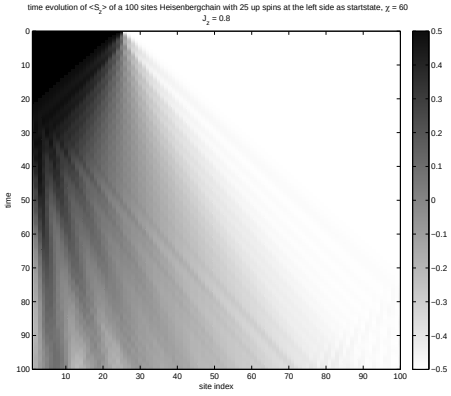

(c) $J_z = 0.8$

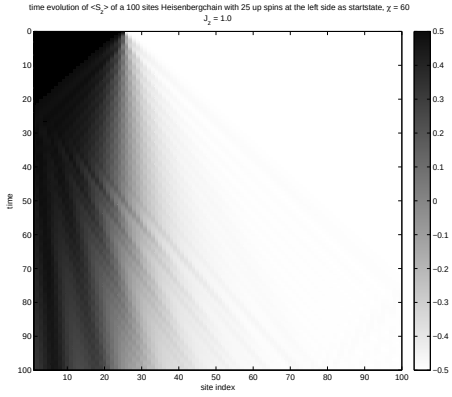

(d) $J_z = 1$

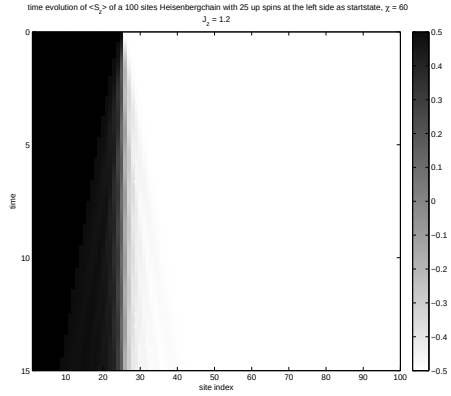

(e) $J_z = 1.2$

Figure 9.5: Time evolution of $\langle S_i^z \rangle$(t) with TEBD algorithm for a 100 sites Heisenberg with $\chi = 60$. From (a) to (e), the J_z coupling is varied, $J_{xy} = 1$ for all figures. The initial state for all figures was a product state with 25 up-spins on the left side and 75 down-spins everywhere else. Values for t>100 have been discarded.

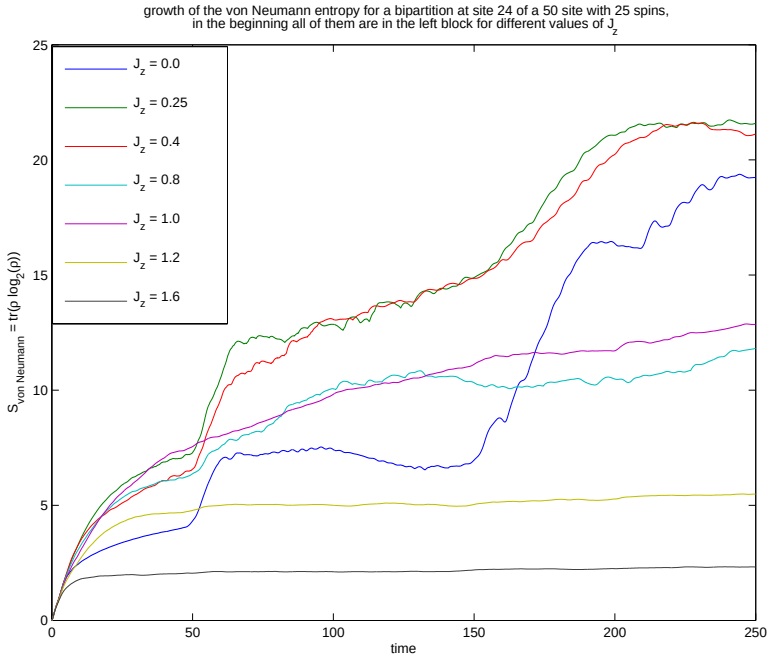

Figure 9.6: Growth of the entangled entropy of the block with sites $1 \cdots 25$ in a 100 sites Heisenberg model for the setup of fig.9.5. The system was initially prepared in a product state where 25 up-spins were on the left side of the chain and down-spins were everywhere else. Simulations were obtained from TEBD with $\chi = 60$. For $J_Z > 1$, one observes that the entanglement saturates at a small value. Comparison to fig.9.5 (e)shows, that in this case, the spins "stay" in the block and do not want to travel away from it.

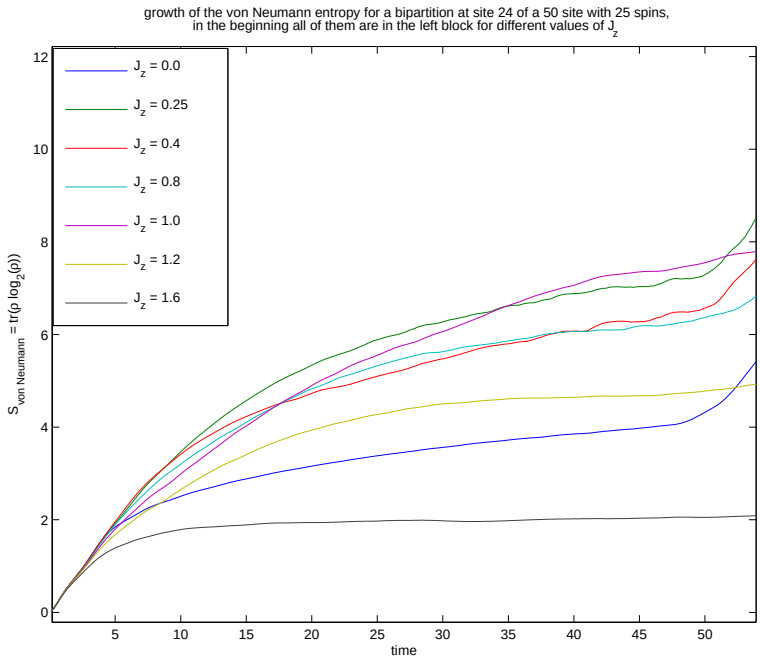

Figure 9.7: Fig.9.6 for t$\leq$50. At $J_z = 1$ the form of S_{vN} is consistent with a logarithmic function. Please note that due to the finite number of spins in the block, the entanglement of the block will saturate at a certain time because in equilibrium, the spins will be distributed all along the chain.

Chapter 10

Propagation of Bound States in the Ferromagnetic Heisenberg Chain

In this section we will present the results of the simulated time evolution of excitations of the ferromagnetic ground state of the Heisenberg chain. We restrict ourselves to the case $\Delta > 0$ because the time evolution of observables for initial states $|\psi_0\rangle$ with purely real coefficients,

$$|\psi_0\rangle = \sum_{\{i_k\}} \alpha_{\{i_k\}} |\{i_k\}\rangle$$
$$\alpha_{\{i_k\}} \in R$$

is invariant under the transformation $\Delta \to -\Delta$. In the following we will sketch the proof for this statement: Let's assume an even number of sites on the lattice. Rotating every second spin of the system by an angle π around the z-axis transforms H according to H(Δ) $\to$ -H($-\Delta$) and is equivalent to a unitary transformation G (see [17]). This transformation does not commute with H, since the total z-magnetization on the sub lattice is not conserved in time translations. The time dependent expectation value of an arbitrary operator $\hat{O}$ transforms then as

$$\langle\psi_0|e^{\frac{it}{\hbar}H(\Delta)}\hat{O}e^{-\frac{it}{\hbar}H(\Delta)}|\psi_0\rangle \to \langle\psi_0|e^{\frac{it}{\hbar}(-H(-\Delta))}\hat{O}e^{-\frac{it}{\hbar}(-H(-\Delta))}|\psi_0\rangle.$$

Since the operator $\hat{O}$ hermitian, this expectation value is real. By taking the complex conjugate of the above equation and using that the coefficients of

$|\psi_0\rangle$ are real, one shows that

$$\begin{aligned}\left(\langle\psi_0|e^{\frac{it}{\hbar}(-H(-\Delta))}\hat{O}e^{-\frac{it}{\hbar}(-H(-\Delta))}|\psi_0\rangle\right)^* = \\ = \langle\psi_0|e^{\frac{it}{\hbar}(H(-\Delta))}\hat{O}e^{-\frac{it}{\hbar}(H(-\Delta))}|\psi_0\rangle \\ = \langle\psi_0|e^{\frac{it}{\hbar}(-H(-\Delta))}\hat{O}e^{-\frac{it}{\hbar}(-H(-\Delta))}|\psi_0\rangle\end{aligned}$$

which proofs the statement (see also [13]). In the following, we prepared states with different number of adjacent up-spins in the middle of the system and then let these states evolve in time and measured the expectation value of $\hat{S}^z$ for each site. For system sizes of n up to 51 and one or two up-spins, the time evolution was carried out by exact diagonalization of the Heisenberg system, but since the implementation of some observables is easier in TEBD, we also simulated such systems with TEBD. In appendix B fig.B.0 we compare the exact results for the two up-spin system with those obtained from TEBD. We also did simulations for three and more up spins in the middle of the system. These were done with the TEBD algorithm as described above.

10.1 Propagation of Single Particle Excitations

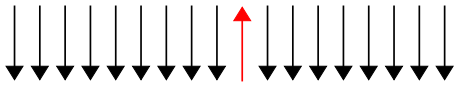

Figure 10.1: Startstate for the single spin propagation.

The simplest case one can look at is when at t=0, a single spin is flipped from the totally aligned state (see fig.10.1). This case can be handled by exact diagonalization (for $N \approx 50$ in our case). In fig.10.3 you can see the propagation of a single up spin in a Heisenberg chain. In all simulations, only one typical group velocity $v = 1$ is observed. This can be understood from eq.(2.4). By differentiation, we obtain

$$v(k) = \frac{dE(k)}{dk} = -J_{xy}\sin(k)$$

which is the definition of the group velocity v (if one linearized E(k) from eq.(2.4) around a value k* and then, with this linearized dispersion, constructed a state with k-values gauss-distributed around this value k^*, then this would give a gauss package in real space travelling at the speed $v(k^*)$).

The maximum of v occurs at k $= \pi/2$ and takes on the value $J_{xy} = 1$ which is the maximum speed we observe. One may ask why we only see this propagation speed and not also slower waves. The reason is as follows: We can look at the density of states $\rho(v)$ at a certain velocity v. It is given by

$$\rho(v) = \frac{N}{2\pi} \int_0^{2\pi} dk \; \delta(v - \frac{dE}{dk})$$

where the pre factor of the integral is the density of states. For our dispersion (2.4), this yields the result

$$\rho(v) = \frac{N}{2\pi} \int_{k=0}^{2\pi} dk \; \delta(v + \sin(k)) = \frac{N}{2\pi} \frac{1}{\sqrt{1 - v^2}}$$

where we have set $J_{xy} = 1$. In fig.10.2, we plotted the function $\rho(v)$. $\rho(v)$ has a singularity at $v = \pm 1$. Our initial state $\psi(x, t = 0)$ in fig.10.3 at t $= 0$ is of the form

$$\frac{1}{2\pi} \int_0^{2\pi} dk \exp(-ik(x - N/2)) = \delta_{x,N/2}$$

which is a superposition of plane waves with uniform coefficients. The part of the wave function which belongs to the $k = \pi/2$ area will give a wave package that is stable due to the linearity of the dispersion at this point which travels at the speed $v = 1$. Other parts (belonging to $k \notin U(k = \pi/2)$ will dephase quickly and hence do not contribute to $\langle S^z \rangle (t)$. The spin density at the site of the flipped spin also performs a damped oscillation from which several propagation branches emerge. Also note that the simulations for $J_{xy} = \pm 1$ yield the same results because of the above mentioned symmetry.

As long as no reflections occur, the qualitative behaviour of all four cases in fig.10.3 is the same. Only when the spin is reflected at the boundaries, the J_z coupling leads to a different behaviour. In the $J_z = 0$ case, a complicated interference pattern emerges, whereas in the $J_z = 1$ case, the spin-reflection resembles that of a localized particle. For high values of J_z, the interference pattern again emerges. It is not clear why the reflection properties of the system depend on the J_z coupling.

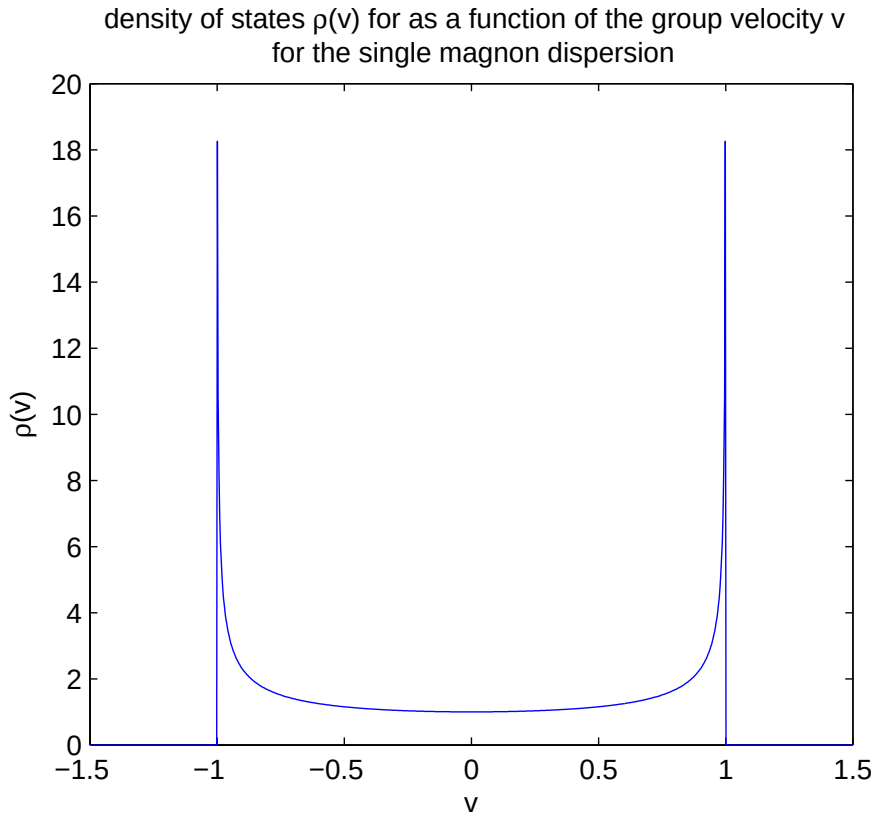

Figure 10.2: Density of states $\rho(v)$ as a function of group velocity for the single particle dispersion relation.

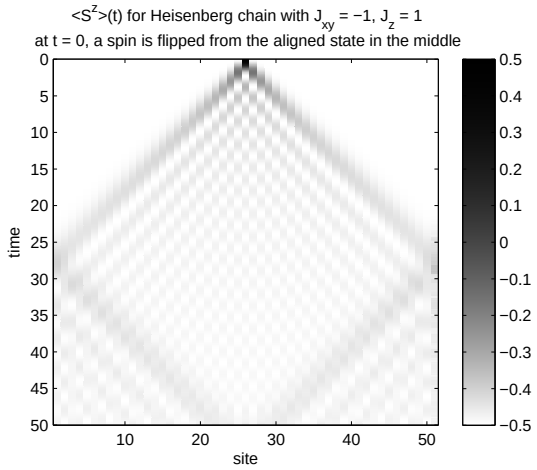

(a) $J_z = -1$, $J_{xy} = -1$

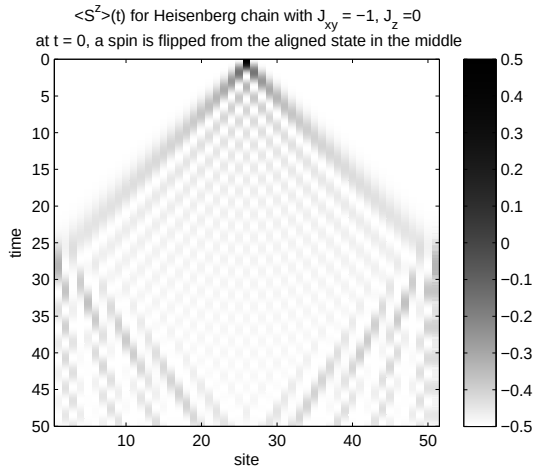

(b) $J_z = 0$, $J_{xy} = -1$

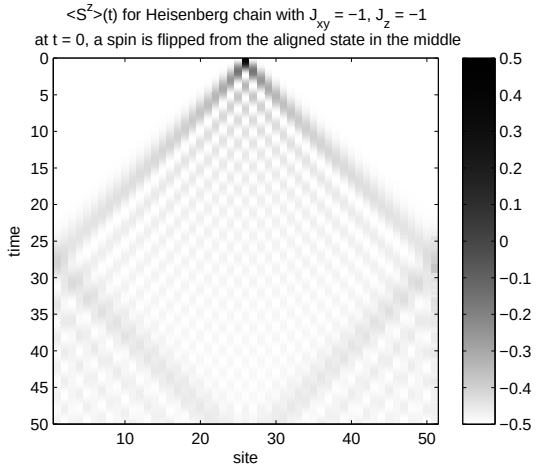

(c) $J_z = 1$, $J_{xy} = -1$

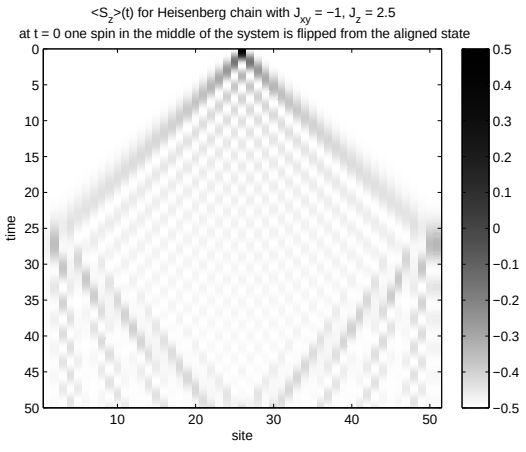

(d) $J_z = 2.5$, $J_{xy} = -1$

Figure 10.3: Exact time evolution of a Heisenberg chain with 51 sites. At t = 0, in the middle of the system a single spin is flipped from the aligned state. From (a) to (d), the J_z coupling is varied. The propagation of the spin is qualitatively the same for all couplings. At the boundaries, the different couplings lead to different reflections. Also note, that the simulations (a) and (c) yield the same results due to the mentioned invariance of the time evolution of states with real coefficients under $\Delta \to -\Delta$.

10.2 Propagation of Two Particle Excitations in the FM Heisenberg Chain

In fig.(10.4) (a) to (c), the exact time evolution of $\langle S^z \rangle(t)$ for initially two up spins in the middle of the system is plotted for different values of the J_z coupling. In all simulations, $J_{xy} = 1$. With increasing J_z-coupling in the chain, one observes a transition from a single spin propagation wave to a two-branch propagation. Simulations for different values of J_z show, that the speed of this second branch depends on J_z, see fig.10.4. The origin of this two-fold spin propagation can be understood in terms of the Bethe ansatz of the previous section. The eigenstates in the space of two-particle excitations split up into bound states and scattering states. The bound states have a dispersion relation eq.(2.13) from which we obtain the group velocity $v(k)$ by taking its derivative:

$$v(k) = \frac{dE(k)}{dk} = -\frac{1}{2J_z}\sin(k)$$

The highest speed that can be observed from these states is given by $v_{max} = \frac{1}{2J_z}$ and varies linearly in $1/J_z$ which is consistent with our numerical results. This can again be derived from the density of states for the two magnon bound states. The density of states $\rho(v)$ at a certain group velocity v is

$$\rho(v) = \int_{k=0}^{2\pi} dk \delta(v + \frac{1}{2\Delta}\sin(k)) = \frac{2\Delta}{\sqrt{1-(2\Delta v)^2}} \tag{10.1}$$

and has a singularity at $v = \frac{1}{2\Delta}$, which again means, that most states of the system have the speed of this singularity. From the exact calculations, we measured the propagation speed of the second branch as a function of J_z and compared it to the maximum group velocity $v(k = \pi/2) = 1/(2\Delta)$ eq.(2.13) of the two magnon bound states (see fig.10.5). This suggests, that the second branch of the wave consists of two spin up particles which are bound by the interaction potential $S_i^z S_{i+1}^z$. To gather further evidence for this we measured for the same spin setup the probability that two nearest neighbors are in a $|\uparrow\uparrow\rangle$ configuration. This is shown in fig. (10.6) (see appendix C for details on how such a probability can be measured). Comparing this to the evolution of $\langle S^z \rangle(t)$ clearly shows, that spin transport in the second branch is carried by two magnon bound states. For large values of J_z, the two spins behave like a single particle excitation (fig.10.4 (d)).

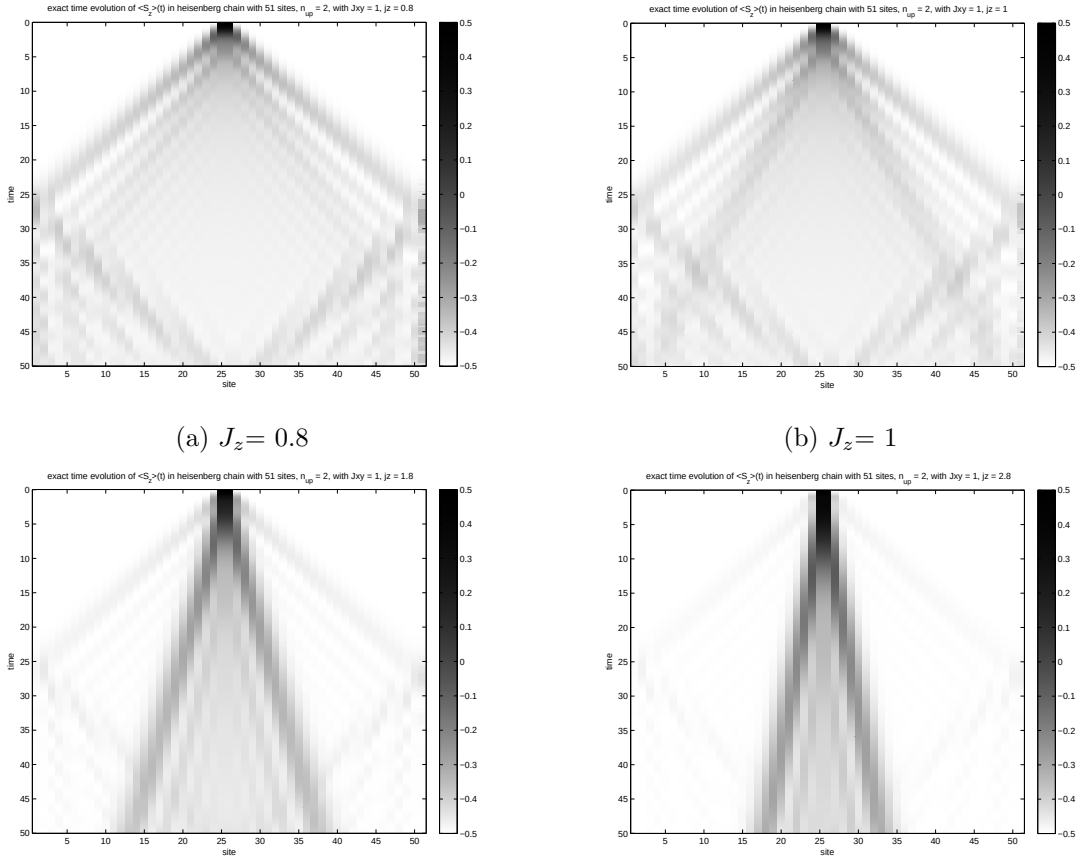

(a) J_z= 0.8

(b) J_z= 1

(c) J_z= 1.8

(d) J_z= 2.8

Figure 10.4: Exact time evolution of $\langle S_i^z \rangle(t)$ for an initial state with two up-spins in the middle of the system and down-spins everywhere else. In figures (a) to (d), the J_z-coupling has been varied from 0.8 to 2.8. The speed of the upper branch does apparently not depend on J_z, whereas the speed of the lower one decreases with increasing J_z. Beyond $J_z \approx 0.9$, the second branch starts to disappears because for values of $\Delta < 1$, bound states exist not for all k but only for k above a certain threshold (see text).

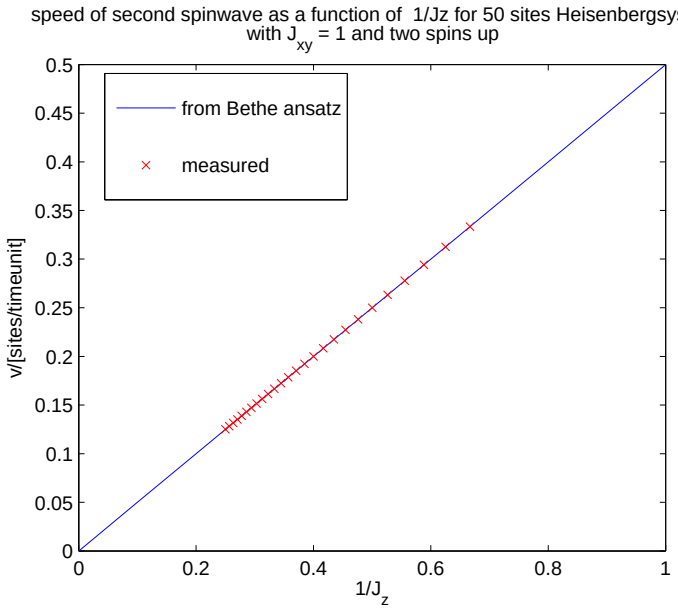

Figure 10.5: red crosses: Variation of the speed of the slower branch of the spin propagation with the inverse of J_z measured from exact time evolution (see fig.10.4). One observes a linear dependence on $1/J_z$. Comparing to eq.(2.13) shows, that the group velocity $v(k) = \frac{dE(k)}{dk}$ of two magnon bound states has the same dependence on the coupling, which indicates, that the spin-current of this branch is largely carried by such states. Solid blue line: variation of the group velocity v at $k = \pi/2$ from the Bethe ansatz with J_z. v is given by the derivative of eq.(2.13). At $k = \pi/2$, $v(\pi/2) = 1/(2\Delta)$. We measured the speed by looking at which time t the two-particle branch hit the boundaries of the system (when the value of $\langle S^z \rangle$ at site 1 had its maximum). From this time we computed v by taking the fraction l/t where l is the site where the first spin was put at $t = 0$.

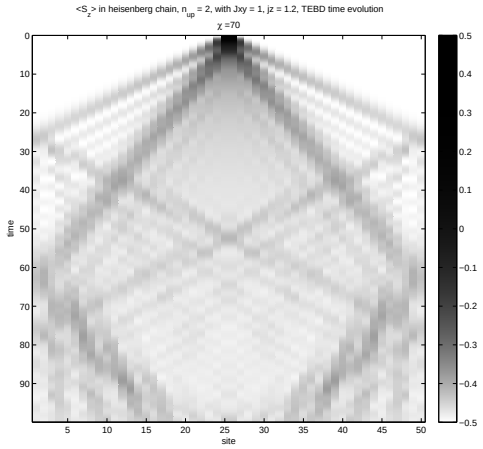

(a) $\langle S^z \rangle(t)$

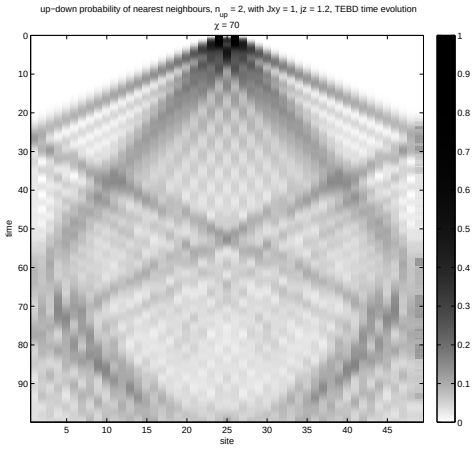

(b) P($|\uparrow\downarrow\rangle$)

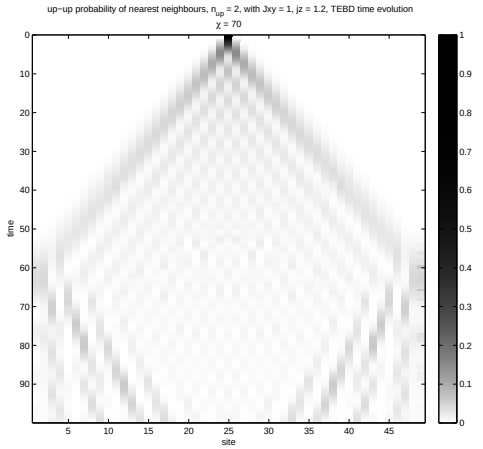

(c) P($|\uparrow\uparrow\rangle$)

Figure 10.6: TEBD study of Heisenberg model for $J_z = 1.2$ and $J_{xy} = 1$.(a) Time evolution of two $|\uparrow\rangle$-spins placed in the middle of a $|\downarrow\rangle$ saturated spin chain. The time evolution is the same as the one derived by exact diagonalization. (b) Probability of finding a nearest neighbor pair of spins in a $|\uparrow\downarrow\rangle$ or $|\downarrow\uparrow\rangle$ configuration. (c) Probability of finding a nearest neighbor pair of spins in a $|\uparrow\uparrow\rangle$ configuration. This clearly shows that the upper propagation branch is associated with movement of a single spin.

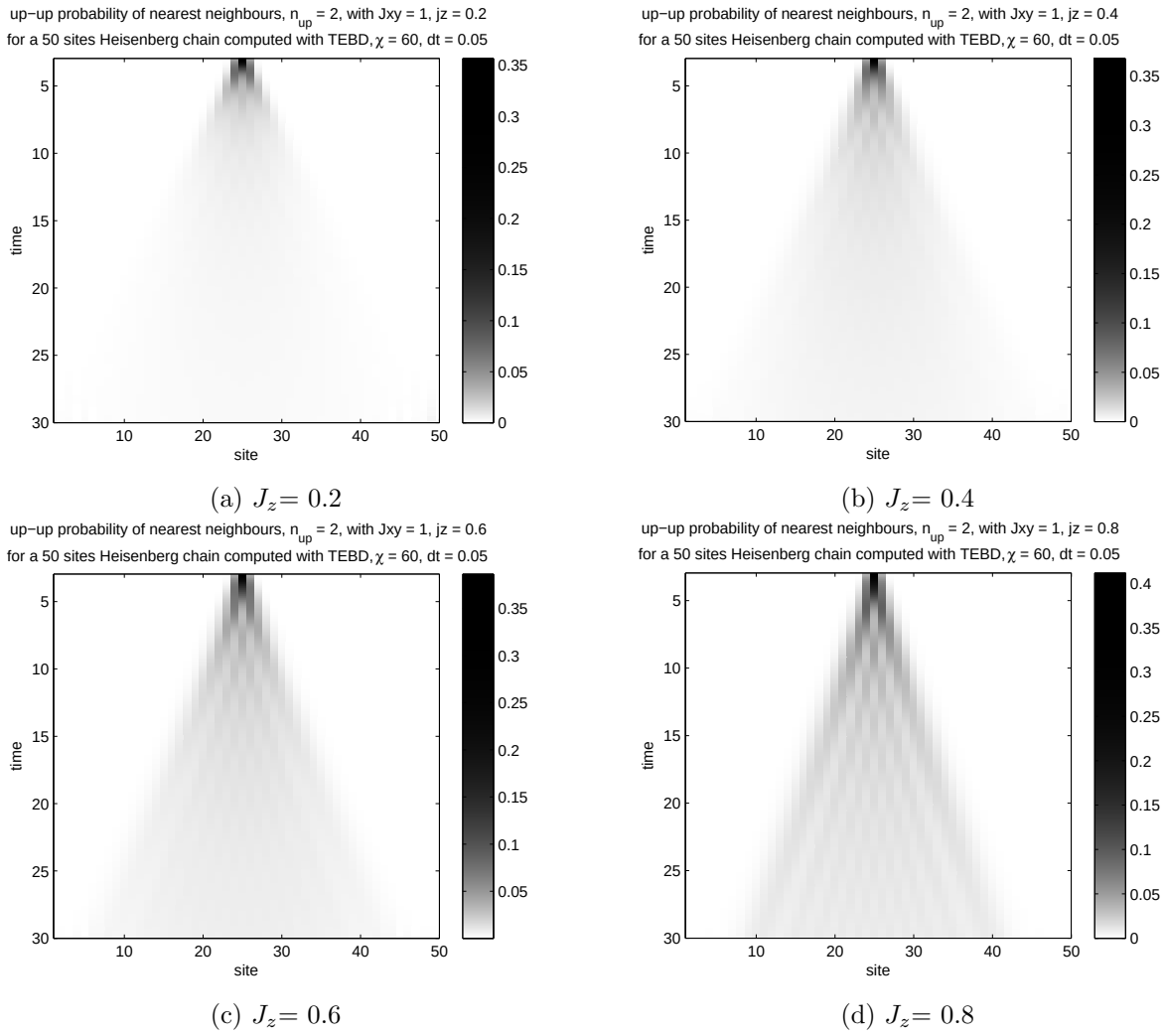

(a) $J_z = 0.2$ (b) $J_z = 0.4$

(c) $J_z = 0.6$ (d) $J_z = 0.8$

Figure 10.7: Time evolution of the probability of finding two nearest neighbors in a $|\uparrow\uparrow\rangle$ configuration. From (a) to (d), the J_z coupling has been varied. For small J_z (< 0.6), the behaviour of the two spins is diffusion like, for $J_z > 0.6$, long lived two-spin packets start to emerge.

The disappearance of the lower propagation branch for decreasing J_z can be explained by the fact, that for $|\Delta| < 1$ bound states do not exist for all values of k (see sec.2.3). However, for $\Delta < 1$, some k are not allowed. If Δ is so small that the allowed k values are between $k \in (\pi/2, 3\pi/2)$, then the singularity disappears (since $\sin(k)$ has no extremum in this area). Using eq.(2.14), this gives the critical value $\Delta_c = \frac{1}{\sqrt{2}} \approx 0.7071$ beyond which the distinct propagation branch for two spins should start to disappear. In fig.10.7 you can see the probability of finding two nearest neighbors in a

$|\uparrow\uparrow\rangle$ configuration. For $J_z < 1/\sqrt{2}$, the behaviour of the two spins is indeed diffusion like.

Fig.10.8 (a) shows the total spin transported by the single particle branch as a function of J_z. At t = 20 we integrated the spin density of the first peak for different J_z. Increasing J_z leads to decrease of this quantity.

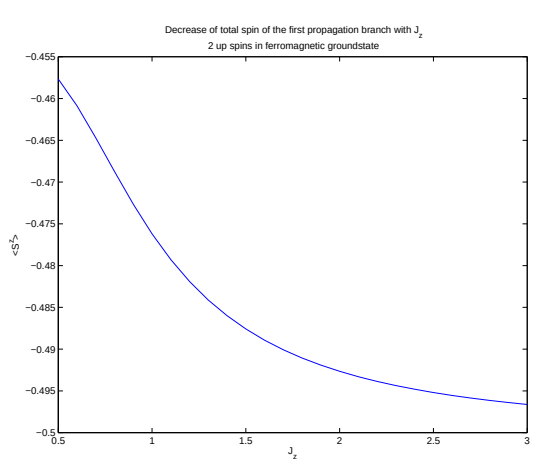

(a)

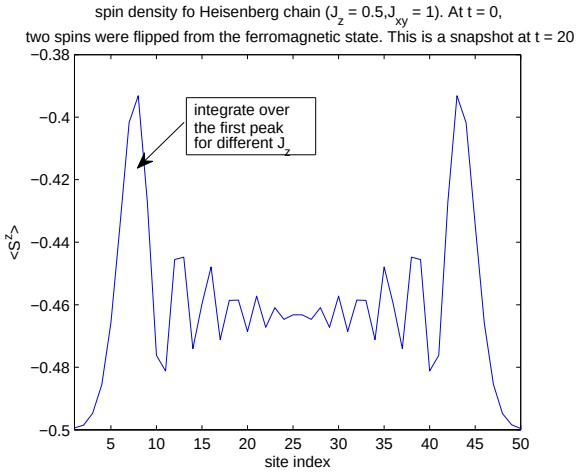

(b)

Figure 10.8: (a) Integrated spin density of the single particle propagation branch ("fastest peak") as a function of J_z. At t = 0, two spins were flipped from the aligned state, at t = 20 we integrated the spin density. (b) Illustration of the peak over which we integrated. Results are obtained from exact diagonalization.

10.3 Propagation of Three Particle Excitations in the FM Heisenberg Chain

Now we are going to explore the propagation properties of three particle excitations from the aligned groundstate of the ferromagnet. In fig.10.9 one can see the results for the propagation of a three spin excitation for $J_z = 1.2$ and $J_{xy} = 1$ (values were chosen in hindsight of the phenomenon of multi propagation speeds in the 3 particle case). At t=0, the three spins are flipped from the aligned ground state. This time, there are three branches corresponding to three different propagation velocities. This is shown in fig.10.9 (a) where we plotted $\langle S^z \rangle (t)$ as a function of time for every site on the lattice. We can apply the same analysis as for the two particle case and look at the probabilities of finding nearest and next nearest neighbors in a certain configuration. In fig.10.9 (b) and (c), we plotted the probabilities P($|\uparrow\downarrow\rangle$) and P($|\uparrow\uparrow\rangle$) of finding nearest neighbors in a $|\uparrow\downarrow\rangle$ or $|\uparrow\uparrow\rangle$ configuration. This shows, that the up most branch again belongs to single particle propagation (see previous section). Fig.10.9 (d) shows the time evolution of the probability of finding three nearest neighbors in a $|\uparrow\uparrow\uparrow\rangle$ configuration. Since the middle branch is not visible, one concludes that it belongs to a two-particle propagation and that the lowest branch corresponds to the propagation of three particles (the probability of finding the three particles all side by side is however very small). In section 2.3 we remarked, that the lowest energy eigenstates of a n particle excitation are bound complexes of these particles for different values of the total momentum k. It is thus very likely, that we observe propagation of such a bound complex for three spins. In fig.10.10 we plotted P($|\uparrow\uparrow\uparrow\rangle$) for different J_z, ranging from 0.6 to 1.2. The low-J_z behaviour in fig.10.10 (a) is very similar to a diffusion driven process with an initially Gaussian distribution, where one expects a linear growth of the width of the peak with time. For larger J_z, this behaviour disappears. Instead, one gets long lived density excitations (in this case probability excitations) which travel at constant speed. Simulations for different J_z showed that the third branch appears at $J_z \approx 1$. From these simulations, we also inferred the speed of the lowest propagation branch as a function of J_z. This is plotted in fig.10.11. In contrast to the two particle case, the propagation speed is not linear in $\frac{1}{J_z}$, but there is rather a $\frac{1}{4J_z^2-1}$ dependence of v on J_z. Error bars come from the fact, that the speed was estimated from the slope of the propagation branches. You can also see the speed obtained from the exact dispersion of the 3-string (eq.(2.15)). We stress, that the calculations leading to eq.(2.15) were done by [17] who took $|\Delta| \leq 1$. However, if we neglect this and assume the dispersion to be valid as well for $|\Delta| > 1$ we get the red line in fig.10.11

from the same calculation as for the two particle case by taking the maximum of the derivative $dE(k)/dk$. The calculation yields

$$v = \frac{dE}{dk}^{3-\text{string}}_{max} = \frac{1}{4\Delta^2 - 1}. \tag{10.2}$$

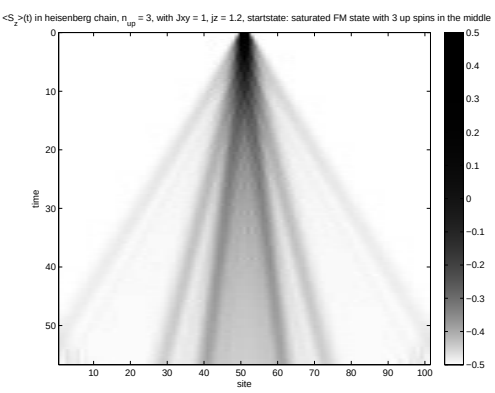

(a) $\langle S^z \rangle(t)$

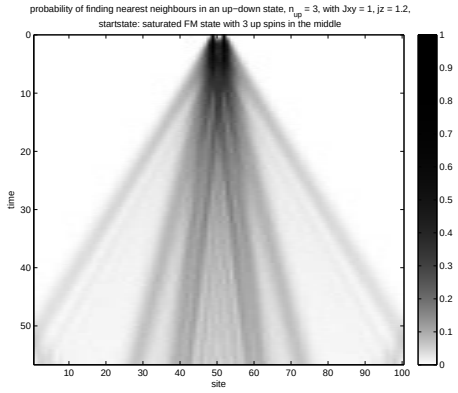

(b) P($|\uparrow\downarrow\rangle$or$|\downarrow\uparrow\rangle$)

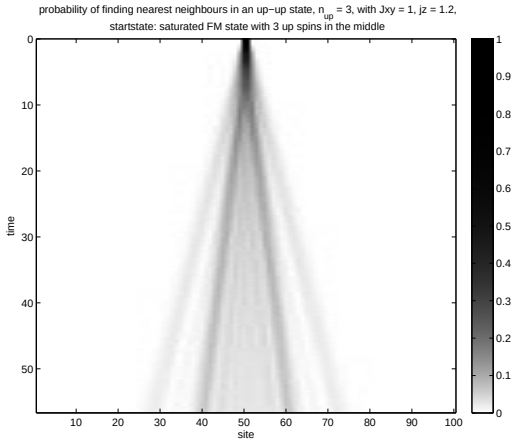

(c) P($|\uparrow\uparrow\rangle$)

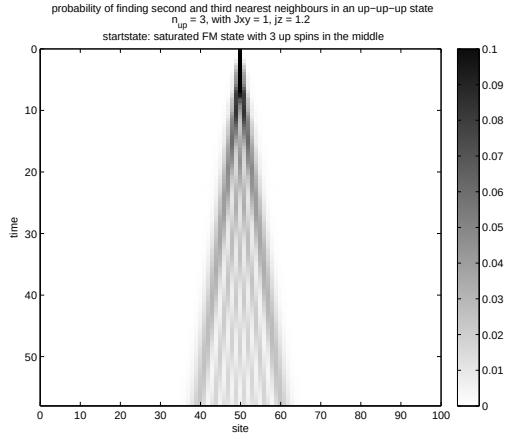

(d) P($|\uparrow\uparrow\uparrow\rangle$)

Figure 10.9: Heisenberg chain with $\Delta = 1.2$, $J_{xy} = 1$. (a) Time evolution of $\langle S^z \rangle(t)$. At t = 0, three spins are flipped from the ferromagnetic (aligned) groundstate of the Heisenberg ferromagnet. (b) Probability of finding two nearest neighbors in either $|\uparrow\downarrow\rangle$ or $|\downarrow\uparrow\rangle$ configuration. (c) Probability of finding two nearest neighbors in a $|\uparrow\uparrow\rangle$ configuration. (d) Probability of finding three nearest neighbors in a $|\uparrow\uparrow\uparrow\rangle$ configuration.

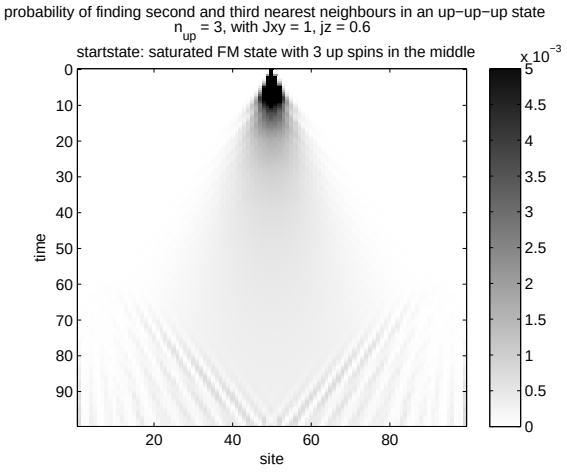

(a) P($|\uparrow\uparrow\uparrow\rangle$), $J_z = 0.5$, $J_{xy} = 1$

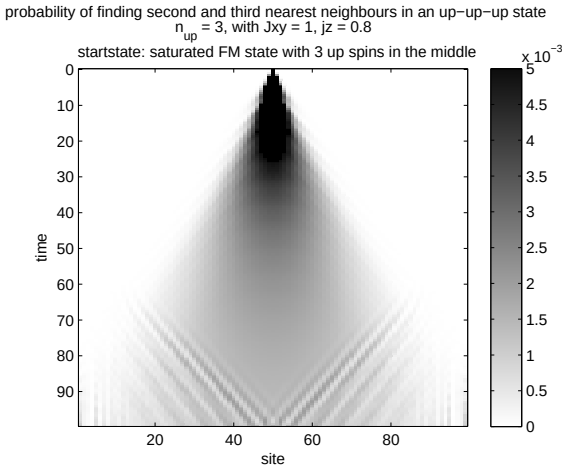

(b) P($|\uparrow\uparrow\uparrow\rangle$), $J_z = 0.9$, $J_{xy} = 1$

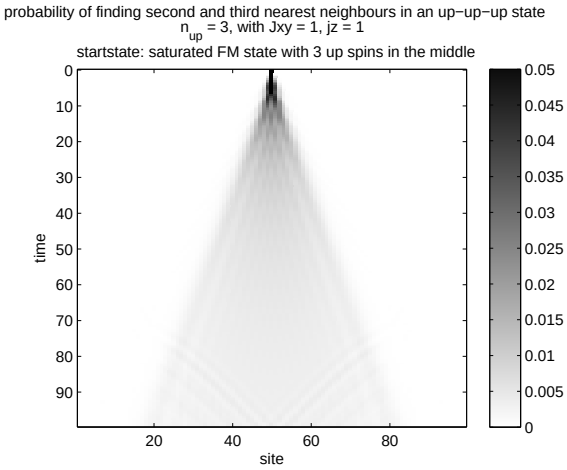

(c) P($|\uparrow\uparrow\uparrow\rangle$), $J_z = 1.0$, $J_{xy} = 1$

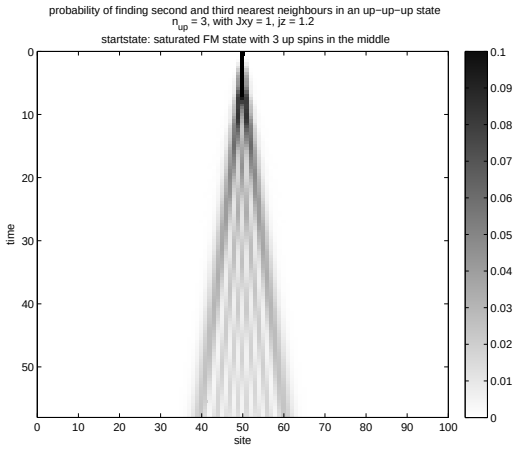

(d) P($|\uparrow\uparrow\uparrow\rangle$), $J_z = 1.2$, $J_{xy} = 1$

Figure 10.10: Time evolution of the probability of finding 3 adjacent up spins on the chain for increasing J_z coupling. (a): small J_z leads to diffusion like behaviour of P($|\uparrow\uparrow\uparrow\rangle$). (b) to (d): due to increase in J_z, the particle are more and more bound and their propagation speed decreases. In (d), long lived excitations emerge.

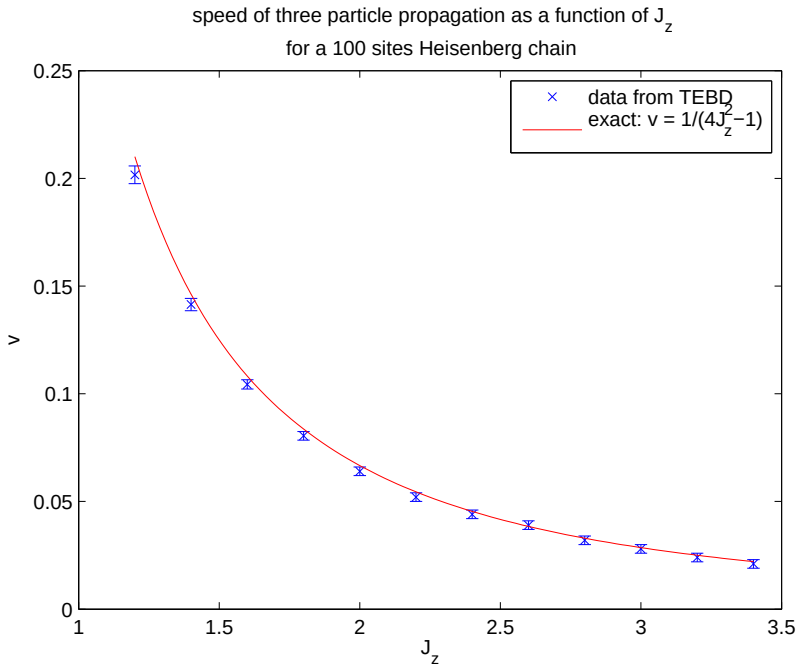

Figure 10.11: Speed of the three particle excitation as a function of J_z. Like in the two particle case, the speed of the three bound particles depends on J_z, but in contrast to the two bound particle case, the speed of the three particles varies not linearly in $1/J_z$ but with $1/(4J_z^2 - 1)$. The data was obtained by TEBD, with $\chi = 40$. $J_{xy} = 1$ in all simulations. The exact data is obtained from [17].

Chapter 11

Spin Scattering at $\vec{\hat{S}}\vec{\hat{S}}$ Impurities

In this section we look at the scattering of magnetization excitations at the connection of two Heisenberg chains. The system setup is shown in fig.11.1. On the chains we set $J_z = 0, J_{xy} = 1$. We are interested in the scattering of spin density excitations from the groundstate at half filling at the coupling between the chains (blue line in fig.11.1). The excitation is created by switching on an external magnetic field in z direction with a Gaussian shape and doing imaginary time evolution. The total spin of the system is set to 0 (half filling). The Hamiltonian for this setup is

$$\begin{aligned} H = & \sum_{i \in \text{chain } 1} \frac{1}{2}(S_i^+ S_{i+1}^- + S_i^- S_{i+1}^+) + B_z(i) S_i^z + \\ & + \sum_{i \in \text{chain } 2} \frac{1}{2}(S_i^+ S_{i+1}^- + S_i^- S_{i+1}^+) + B_z(i) S_i^z \\ & + J_z^c S_m^{z,1} S_m^{z,2} + \frac{1}{2}(S_m^{+,1} S_m^{-,2} + S_m^{-,1} S_m^{+,2}) \end{aligned} \tag{11.1}$$

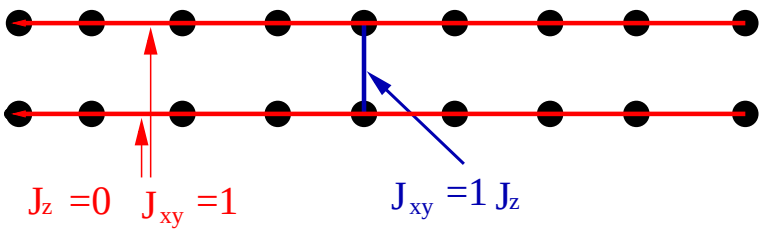

Figure 11.1: Schematic picture of the single connected ladder. Black circles are spins.

where $B_z(i)$ is the magnetic field strength at the sites i of the upper and lower chain and the last row of eq.11.1 is the coupling. The B-field on both chains has the form

$$B_z(i) = B_0 \exp(-\frac{(i-i_0)^2}{2\sigma^2}) \tag{11.2}$$

with $i_0 = 60$, $\sigma = 2.3$ and $B_0 = -1$. $\hbar = 1$ in all simulations. The length of each chain is $N = 128$, and the connection index $m = 90$. We then computed the groundstate for the system for various values of J_z^c and J_{xy}^c and evolved them in time. The perturbation potential acting between the chains contains a spin flip and a density-density interaction term and is therefore highly non trivial to analyze. Figs.11.2 and 11.3 show to simulations for $J_z^c = 0$, $J_{xy}^c = 1$ and $J_z^c = 1$, $J_{xy}^c = 0$, respectively. We plotted only the spin density of the upper chain since its evolution is the same as that of the lower chain. As one can see, there is nearly no scattering at the impurity. In a next step, we set both coupling parameters to a finite value and again let the spin density scatter at the connection. The couplings for this simulation were chosen $J_z^c = 1$, $J_{xy}^c = 1$ and $J_z^c = 2$, $J_{xy}^c = 1$ (fig.11.4 (a) and (b)). The gauss package now gets scattered, and the intensity of the transmitted wave is smaller than before the barrier. The transmittivity apparently depends on the J_z coupling strength. By tuning the coupling constant J_z^c, one can thus change the transmittivity of the system. Interestingly, a pure J_{xy} or J_z coupling gives much weaker scattering than a combination of the two. The interplay of J_z^c and J_{xy}^c coupling therefore leads to different scattering behaviour. In fig.11.5 you can see a 3d space-time plot of the scattering at the $J_z^c = 2$, $J_{xy}^c = 1$ connection. We also added a 3d plot of the entanglement entropy in fig.11.6. We treated the system as a 1d chain where on each site the local Hilbert space dimension is 4 instead of 2. As you can see from comparing fig.11.2 and 11.3, the J_{xy}^c coupling leads to strong entanglement increase when the density excitation crosses the connection which is not the case for $J_{xy}^c = 0$. In fig.11.5 you can see the time evolution of the entanglement entropy for a coupling of $J_z^c = 2, J_{xy}^c = 1$. Apparently, the combination of both couplings leads to stronger increase of the entanglement between the left and right system than the $J_z^c = 0$, $J_{xy}^c = 1$ and $J_z^c = 1$, $J_{xy}^c = 0$ case. One also observes a backscattering in the magnetization density for these parameters.

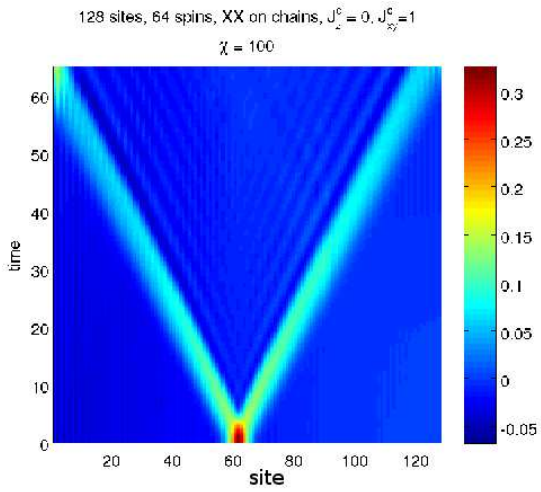

(a) $\langle Sz \rangle$

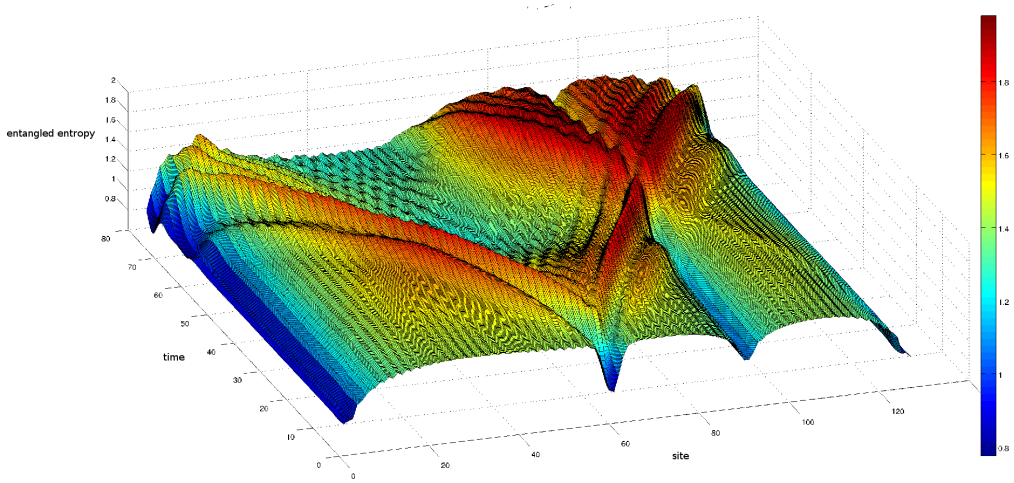

(b) entanglement entropy $S_{vN}(t)$

Figure 11.2: (a) Time evolution of a gauss shaped magnetization excitation ($\sigma = 2.3$) from the ground state at half filling in a system as depicted in fig.11.1. We plotted $\langle S_i^z \rangle (t)$ of the upper chain. On each chain $J_z = 0, J_{xy} = 1$. The chains are connected via a $J_z^c = 0, J_{xy}^c = 1$ coupling at site 90. To get a smoother plot, we averaged the density over three sites.There is no visible scattering of the spin density. (b) Time evolution of the entanglement entropy S_{vN}. At t = 0, the J_{xy}^c coupling leads to a decrease in the entanglement of the system left of the connection with the system to the right side of the connection. Due to the magnetic field, the entanglement around site 30 is reduced. When the magnetic field is switched off, a entanglement wave propagates through the system. When the density excitation reaches the coupling, there is a strong increase of the entanglement.

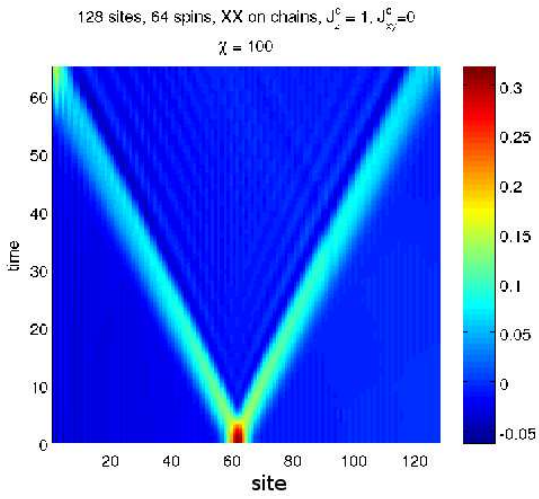

(a) $\langle Sz \rangle$

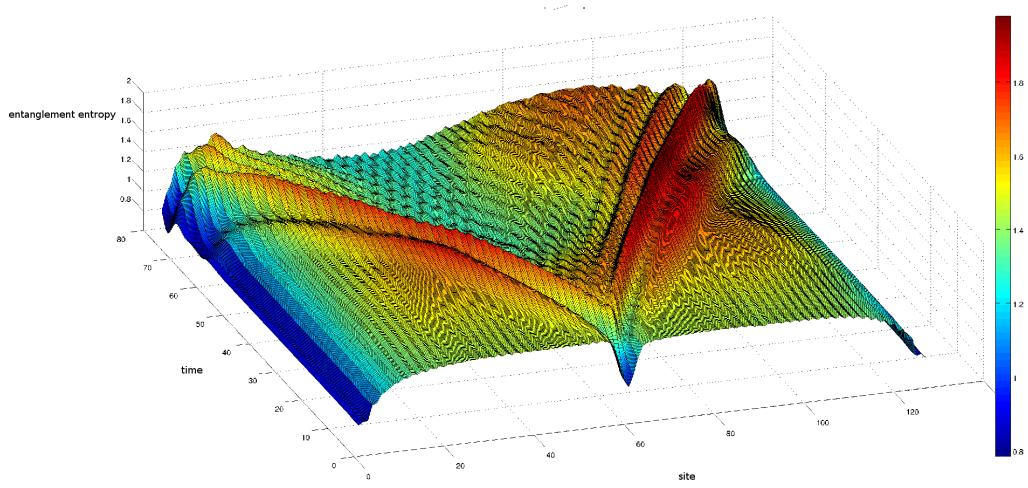

(b) entanglement entropy $S_{vN}(t)$

Figure 11.3: (a) Time evolution of a gauss shaped magnetization excitation for system fig.11.1 at half filling. On the chains there is an XX coupling. Only the upper chain is plotted. The two chains are coupled with $J_z^c = 1, J_{xy}^c = 0$ at site 90. Again, there is no visible scattering at the connection. To get a smoother plot, we averaged the density over three sites. The initial gaussian width is $\sigma = 2.3$ sites. (b) Time evolution of the entanglement entropy S_{vN}. The J_z^c coupling apparently has no influence on the entanglement of the subsystems to the left of the connection and the one to right of the connection for the initial state at t = 0. When the density excitation reaches the connection there is only a small increase in the entanglement of the two subsystems.

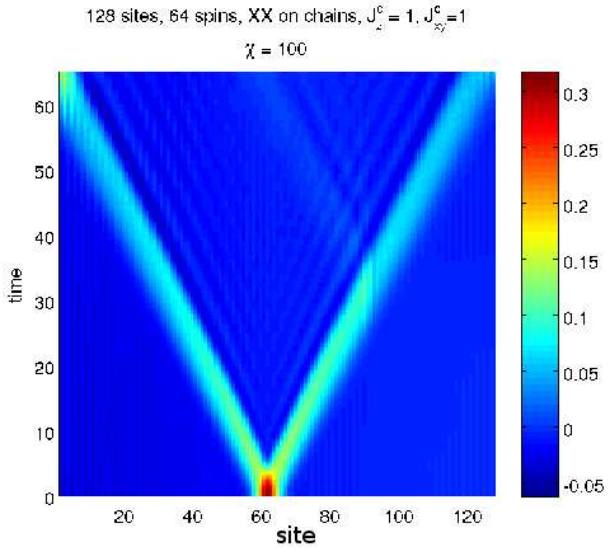

(a) $J_z^c = 1, J_{xy}^c = 1$

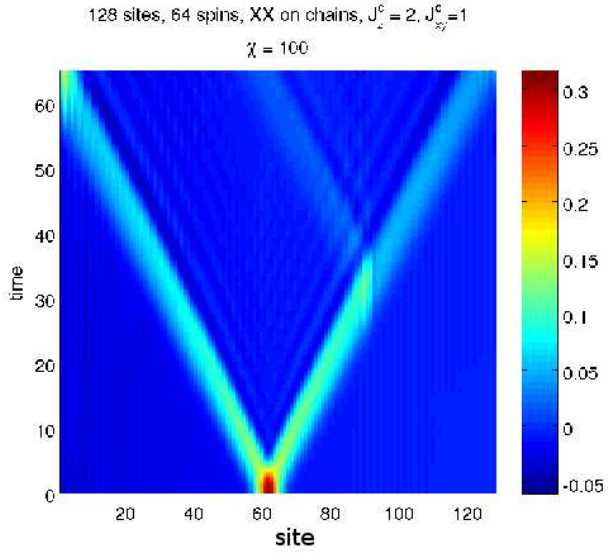

(b) $J_z^c = 2, J_{xy}^c = 1$

Figure 11.4: Time evolution of a Gauss shaped magnetization excitation for system fig.11.1 of the upper chain. (a) The chains are coupled with $J_z^c = 1, J_{xy}^c = 1$ at site 90. The amplitude of the transmitted ray gets smaller, and a part of the density is reflected. To get a smoother plot, we averaged the density over three sites. The initial gaussian width is $\sigma = 2.3$ sites (b) The setup is the same as in (a), the coupling strength between the two chains is set to $J_z^c = 2, J_{xy}^c = 1$. As one can see, there is an increase in the intensity of the back scattered magnetization.

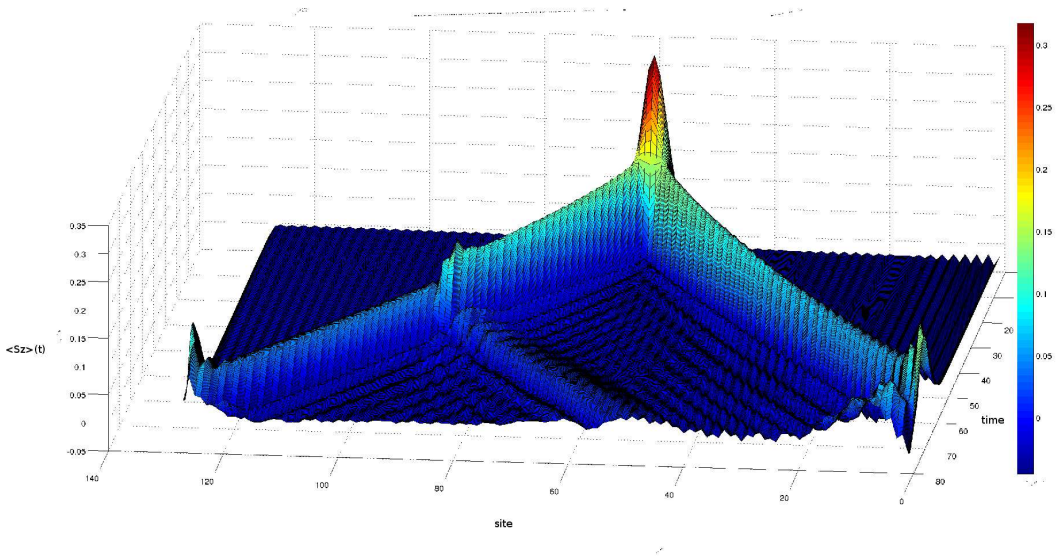

Figure 11.5: 3d plot of fig. 11.4. Only the upper chain is plotted. Note that site numbering is right to left (different from fig.11.6)

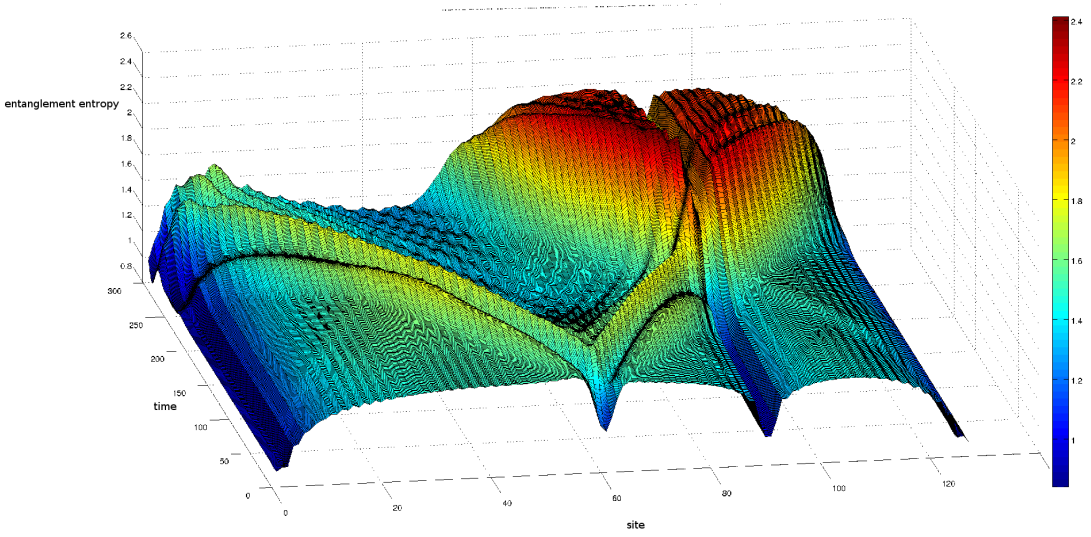

Figure 11.6: Entanglement entropy for bipartitions at different sites. Data is from same simulation as 11.4 (b). The two chains are connected with $J_z = 2$ and $J_{xy} = 1$. H-system is treated as a 1-d system with a Hilbert space dimension of 4 at each site. Initial state: Gauss shaped density excitation at site 60. Due to the connection at site 90, the entanglement increases when the density excitation crosses it.

Chapter 12

Conclusions

We investigated spin transport in a XXZ Heisenberg chain in real time using full diagonalization and TEBD. In the first part, we looked at the time evolution of one, two and three spin excitations above the ferromagnetic phase of the system for different coupling strengths J_z and J_{xy} on the chains. We chose open boundary conditions for all simulations. Single particle excitation show similar behaviour for different values of J_z ranging from -1.5 to 1.5 and $J_{xy} = 1$ as long as there are no reflections at the boundaries. The reflected waves however show wave like interference for values $J_z \neq 1$, whereas for $J_z \approx 1$, a particle like reflection is observed (see fig.10.3). The two-particle excitations show a different behaviour. If at t = 0, two adjacent spins are flipped from the ferromagnetic phase, one observes a fast propagation branch where a spin density wave propagates at a speed v = 1, and for large enough J_z there also emerges a second branch where spins travel at a speed which depends on J_z. The analytical solution for such a system is available, and we compared our numerical results with the analytical one from the Bethe ansatz. The data suggests, that the two flipped spins decay into bound and unbound two-spin states (fig.10.6). These states have different propagation properties. The spectrum of the two-spin bound states depends on $1/J_z$ and forms a continuous branch (in the limit $N \to \infty$, see fig.2.1, class C_3). The corresponding group velocity for these two particle bound states has a maximum value of $v_{max} = 1/(2J_z)$. Numerical results of the propagation speed of the slower propagation branch are in perfect agreement with this (see fig.10.5). In the fast propagation branch the spins travel at a speed of $v = 1$, which suggest that this branch corresponds to two unbound particles, where the one is at rest with $k_1 = 0$ and the second has a momentum $k_2 = k$ where k is the total momentum. These states also form a continuous excitation branch (fig.2.1, class C_1). The bound-state branch disappears for small $|J_z| < 1/\sqrt{2}$ becaus for these parameter values, the states are restricted to a

subset of k values (see fig.2.2). If one calculates the DOS $\rho(v)$ of the group velocities v from the dispersion of the bound states, one can see that it has two singularities (see eq.10.1) which coincide with the observed propagation speed of the bound states. These singularities vanish for $|J_z| < 1/\sqrt{2}$, which results in a decrease of the amplitude of the two particle propagation branch.

We also looked at three particle excitations from the ferromagnetic phase where at $t = 0$ three adjacent spins were flipped from the ground state. One observes three different propagation branches which correspond to one, two and three particle propagation (see fig.10.9). The numerical evaluation of the speed of the three particle branch is in good agreement with the theoretical result $v = \frac{1}{4\Delta^2-1}$ (see eq.10.2 and fig.10.11)

Interestingly, the time evolution of our initial states is indipendent from the sign of the anisotropy $\Delta = J_z/J_{xy}$ (see 97). In the case of positive J_z, the spins interact via repulsive interaction, whereas in the case of $J_z < 0$ there is an attractive interaction between the spins. In both cases however, two and more spins form bound states. For $J_z > 0$, the spins are thus bound by a *repulsive* interaction.

As a second system, we investigated two Heisenberg spin 1/2 XX chains which are connected at a single site (see fig.11.1 for system details). As initial state for the time evolution, the system was prepared in its ground state at half filling with a Gaussian magnetic field added to the Hamiltonian of both chains. The ground state was obtained by imaginary time evolution. At t = 0, the magnetic field was switched off and we looked at the scattering of the Gauss shaped density excitation at the connection of the two chains for different connection strengths. Depending on the coupling constants between the chains the transmissivity over the connection can be varied. The strongest effect was observed if both J_z^x and J_{xy}^c had finite values (see fig.11.4, whereas nearly no scattering is observed if either J_v^c or J_{xy}^c is set to 0 (fig.11.2 and 11.3).

Appendix A

Orthonormality Properties of Matrix Product States

We want to establish that the states in eq.(4.5) are orthonormal if the A-matrices of this state are orthonormalized according to eq.(4.4). We will show this for the states $|\phi_{\alpha_n}\rangle$ of the left system. The prove for the right-side states is analog to this case. Inserting the full representation in terms of the A-matrices, we get (n site index $[n]$ is ommited)

$$\begin{aligned}
\langle\phi_{\alpha'_n}|\,\phi_{\alpha_n}\rangle &= \sum_{\{i_k\}\{i'_k\}}\sum_{\{\alpha_k\}\{\alpha'_k\}} A^{*i'_1}_{\alpha'_1} A^{*i'_2}_{\alpha'_1\alpha'_2}\cdots A^{*i'_n}_{\alpha'_{n-1}\alpha'_n} A^{i_1}_{\alpha_1} A^{i_2}_{\alpha_1\alpha_2}\cdots A^{i_n}_{\alpha_{n-1}\alpha_n} \underbrace{\langle i'_1\cdots i'_n|\, i_1\cdots i_n\rangle}_{\delta_{i_1 i'_1}\cdots\delta_{i_n i'_n}} = \\
&= \sum_{\alpha_1\alpha'_1}\underbrace{\sum_{i_1} A^{*i_1}_{\alpha'_1} A^{i_1}_{\alpha_1}}_{\delta_{\alpha_1\alpha'_1}} \sum_{i_2\cdots i_n}\sum_{\alpha_2\cdots\alpha_n}\sum_{\alpha'_2\cdots\alpha'_n} A^{*i_2}_{\alpha'_1\alpha'_2} A^{i_2}_{\alpha_1\alpha_2}\cdots = \\
&= \underbrace{\sum_{i_2\alpha_1} A^{*i_2}_{\alpha_1\alpha'_2} A^{i_2}_{\alpha_1\alpha_2}}_{=\sum_{i_2\alpha_1} A^{\dagger i_2}_{\alpha'_2\alpha_1} A^{i_2}_{\alpha_1\alpha_2}=\delta_{\alpha'_2\alpha_2}} \sum_{i_3\cdots i_n}\sum_{\alpha_3\cdots\alpha_n}\sum_{\alpha'_3\cdots\alpha'_n} A^{*i_3}_{\alpha'_2\alpha'_3} A^{i_3}_{\alpha_2\alpha_3}\cdots = \cdots
\end{aligned}$$

where we made use of the left handed orthonormalization condition eq.(4.4). Iterating the steps, one ends up with

$$\langle\phi_{\alpha'_n}|\,\phi_{\alpha_n}\rangle = \sum_{i_n\alpha_{n-1}} A^{\dagger i_n}_{\alpha'_n\alpha_{n-1}} A^{i_n}_{\alpha_{n-1}\alpha_n} = \delta_{\alpha_n\alpha'_n}$$

which proves the statement.

Appendix B

Comparison of TEBD to Exact Results

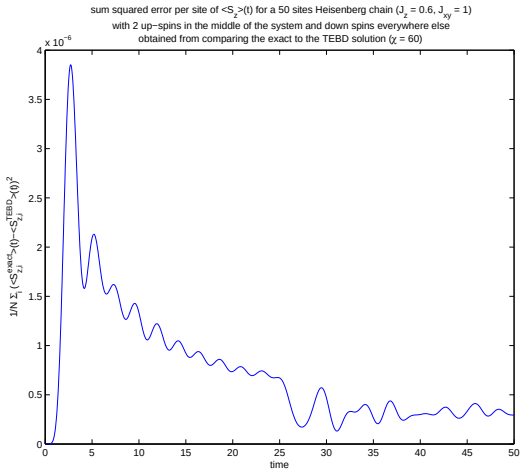

(a) $J_z = 0.6,\ J_{xy} = 1$

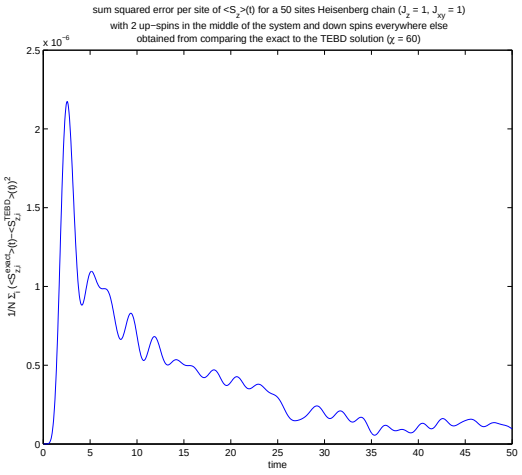

(b) $J_z = 1,\ J_{xy} = 1$

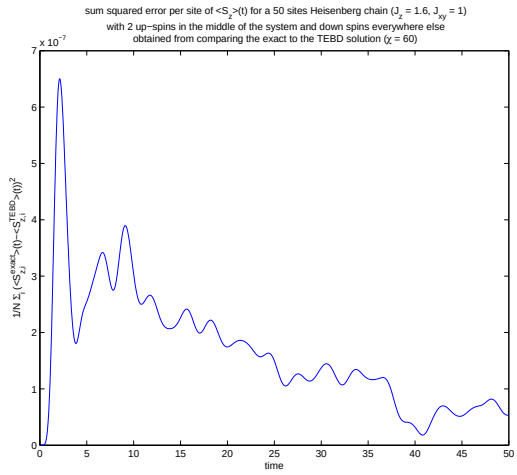

(c) $J_z = 1.6,\ J_{xy} = 1$

Figure B.0: Sum-squared error $\frac{1}{N}\sum_i (S_i^{z,TEBD} - S_i^{z,exact})^2$ as a function of simulation time for a $n = 50$ sites Heisenberg chain in the ferromagnetic state where in the middle of the system two spins are flipped at the beginning. From (a) to (c), the J_z coupling has been varied. The auxiliary dimension for the MPS is $\chi = 60$. Evidently, the error is very small and largely due to the Suzuki-Trotter expansion of the time evolution operator.

Appendix C

Measuring Spin Configurations of Nearest and Next Nearest Neighbors

In the frame work of TEBD, the spin configuration of nearest neighbors can easily be measured by applying a projection operator to the MPS and computing the overlap with the original MPS. An example: Let's assume you want to know the probability P($|\uparrow\uparrow\rangle$) of finding nearest neighbors at bond k in a certain configuration, say $|\uparrow\uparrow\rangle$. Then you have to define the projection operator $\hat{P}r$ that projects the spins at bond k onto this state. In our case $\hat{P}r$ is given by

$$\hat{P}r = |\uparrow\uparrow\rangle\langle\uparrow\uparrow|,$$

and the probability P($|\uparrow\uparrow\rangle$) is simply

$$\mathrm{P}(|\uparrow\uparrow\rangle) = \langle MPS|\hat{P}r|MPS\rangle$$

The generalization to other configurations is straightforward.

Measuring the probability P($|\uparrow\uparrow\uparrow\rangle$) of finding three adjacent spins in a certain configuration, say $\uparrow\uparrow\uparrow$, can be done by applying three projection operators to three adjacent sites. If you are interested in the spins at the sites n, $n+1$ and $n+2$, you can apply a $|\uparrow\rangle$-projector at those sites to the state and then calculate the overlap with the original state. This then gives

$$P(|\uparrow\uparrow\uparrow\rangle) = \langle\psi|\,|\uparrow_n\rangle\,\langle\uparrow_n|\otimes|\uparrow_{n+1}\rangle\,\langle\uparrow_{n+1}|\otimes|\uparrow_{n+2}\rangle\,\langle\uparrow_{n+2}|\,|\psi\rangle$$

which is just a three point correlator and is easily computed in terms of MPS (see section 4.2):

Appendix D

Study of Error Convergence of TEBD Simulations in Heisenberg System

For a system as depicted in fig.D.1, we tested the convergence of the $\langle S^z \rangle(t)$ time evolution.

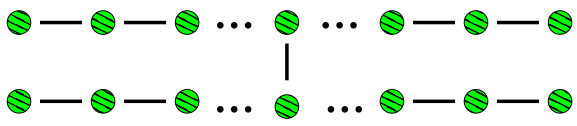

Figure D.1: System setup for convergence study. Two spin chains are connected in via a J_z and J_{xy} coupling. In this case, the couplings on the chains and those of the connection are the same: $J_z = J_{xy} = 1$.

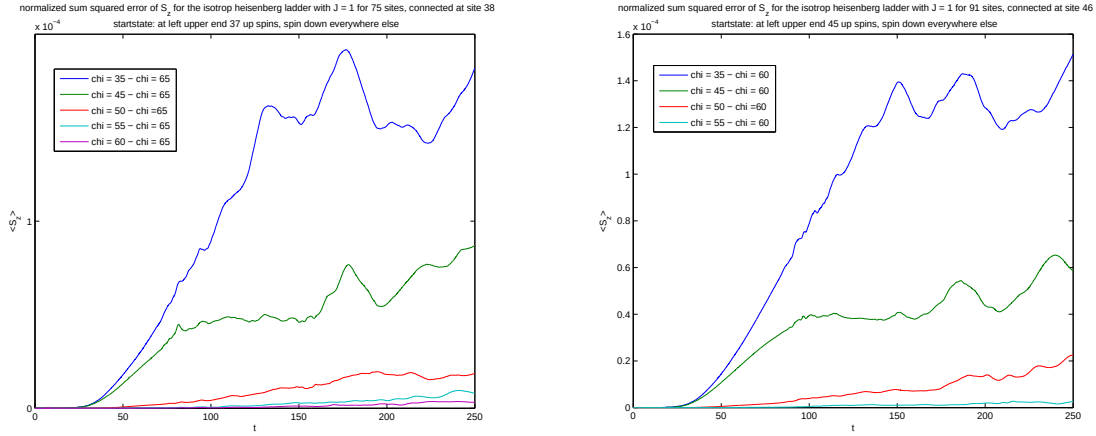

(a) 75 sites

(b) 91 sites

Figure D.2: (a) System setup is like in fig.D.1 with 75 sites on each chain. At the left upper branch of this system, 37 up spins are placed in the else totally aligned state, starting from the very left side. This state is time-evolved with TEBD for different auxiliary dimensions χ. In the figure, we plotted the sum-squared difference $\frac{1}{N}\sum_{i=1}^{N}(\langle S_i^z\rangle_{\chi_1}^{TEBD}(t) - \langle S_i^z\rangle_{\chi=65}^{TEBD}(t))^2$ for $\chi_1 = 35\cdots 60$. (b) Convergence study for a setup as in (a) with 91 sites on each chain. The chains are connected at site 46. At t = 0, 45 spins on the upper chain (starting from left to right) are flipped from the totaly aligned state.

Bibliography

[1] C. Lubich, Quantum Simulations of Complex Many-Body Systems: From Theory to Algorithms **10**, 459 (2002).

[2] G. Vidal, Phys. Ref. Lett. **91** (2003).

[3] G. Vidal, Phys. Ref. Lett. **93** (2004).

[4] S. R. White and A. E. Feiguin, Phys. Ref. Lett. **93** (2004).

[5] M. Greiner, O. Mandel, T. W. Hänsch, and I. Bloch, Nature **419**, 51 (2002).

[6] I. Bloch, Nature Physics **1**, 23 (2005).

[7] M. Greiner, O. Mandel, T. Esslinger, T. W. Hänsch, and I. Bloch, Nature **415**, 39 (2002).

[8] R. H. Crooks and D. V. Khveshchenko, Phys. Ref. A **77**, 062305 (2008).

[9] G. Vidal, J. I. Latorre, E. Rico, and A. Kitaev, Phys. Ref. Lett. **90** (2003).

[10] J. I. Latorre, E. Rico, and G. Vidal, quant-ph/0304098 (2003), Quant.Inf.Comput. 4 (2004) 48-92.

[11] V. Hunyadi, Z. Racz, and L. Sasvari, Phys. Ref. E **69** (2004).

[12] T. Antal, Z. Racz, A. Rakos, and G. M. Schütz, Phys. Ref. E **59** (1999).

[13] D. Gobert, C. Kollath, U. Schollwöck, and G. Schütz, cond-mat/0409692 (2004), Phys. Rev. E 71, 036102 (2005).

[14] S. Langer, F. Heidrich-Meisner, J. Gemmer, I. P. McCulloch, and U. Schollwöck, Phys. Ref. B **79**, 214409 (2009).

[15] W. Dür, L. Hartmann, M. Hein, M. Lewenstein, and H. Briegel, Phys. Ref. Lett. **94** (2005).

[16] T. Giamarchi, *Quantum Physics in One Dimension* (Oxford University Press, 2004).

[17] B. Sutherland, *Beautiful Models* (World Scientific Publishing Co. Pte. Ltd, 2004).

[18] M. Karbach and G. Müller, cond-mat/9809162 (1998), Computers in Physics 11, 36 (1997).

[19] M. Karbach, K. Hu, and G. Müller, cond-mat/9809163 (1998).

[20] M. Karbach, K. Hu, and G. Müller, cond-mat/0008018 (2000).

[21] F. Verstraete, J. I. Cirac, and V. Murg, arXiv:0907.2796 (2009), Adv. Phys. 57,143 (2008).

[22] D. Perez-Garcia, F. Verstraete, M. M. Wolf, and J. I. Cirac, quant-ph/0608197 (2006), Quantum Inf. Comput. 7, 401 (2007).

[23] S. R. White, Phys. Ref. Lett. **77** (1996).

[24] Y. Shi, L. Duan, and G. Vidal, Phys. Ref. A (Atomic, Molecular, and Optical Physics) **74**, 022320 (2006).

[25] R. Orus and G. Vidal, Phys. Ref. B **78**, 155117 (2008).

[26] J. Eisert, M. Cramer, and M. B. Plenio, 0808.3773 (2008), Rev. Mod. Phys. 82, 277 (2010).

[27] I. P. McCulloch, cond-mat/0701428 (2007), J. Stat. Mech. (2007) P10014.

[28] P. Pippan, S. R. White, and H. G. Evertz, cond-mat/0801.1947 (2008), Phys. Rev. B 81, 081103(R) (2010).

[29] S. Singh, H. Q. Zhou, and G. Vidal, cond-mat/0701427 (2007).

[30] S. R. White, Phys. Ref. B **48** (1993).

[31] U. Schollwöck, cond-mat/0502470 (2005), J. Phys. Soc. Jpn. 74 (Suppl.), 246 (2005).

[32] U. Schollwöck and S. R. White, cond-mat/0606018 (2006), in G. G. Batrouni and D. Poilblanc (eds.): Effective models for low-dimensional strongly correlated systems, p. 155, AIP, Melville, New York (2006).

[33] U. Schollwöck, Rev. Mod. Phys. **77** (2005).

[34] R. M. Noack and S. R. Manmana, cond-mat/0510321 (2005), AIP Conf. Proc. 789, 93-163 (2005).

[35] S. Rommer and S. Östlund, Phys. Ref. B **55** (1997).

[36] A. J. Daley, C. Kollath, U. Schollwöck, and G. Vidal, Journal of Statistical Mechanics: Theory and Experiment **2004**, P04005 (2004).

Acknowledgements

Everybody who has written a diploma thesis knows the ups and downs one goes through, the small and big problems one has to deal with, when something does not work as you would like it to, or when it does but you rather would like it not to, the long hours in your office, searching lines and lines of code for some erroneous command. At this point I would like to thank all those people who helped me out with all these problems and gave me new input for what to do next when I had no ideas. First of all, I would like to thank my family, my mother and my brother, and also my girlfriend Antonia for their support and their encouragement. Second, I would like to thank Hans Gerd Evertz for his supervision and for the interesting and helpful discussion on many things. He always had time for my many questions and problems and helped me out more than once. Another person I'm greatly indebted to is Elias Rabel, who's source code I was kindly allowed to use, which saved me many hours of time and nerve-consuming programming. I also would like to thank Michael Krenn at this point for all the discussions he, Elias and me had on so many topics (not all of them of scientific nature) and for helping me out with so many things. It was really a funny time. Of course I also really want to thank Peter Pippan, Ralf Gamillscheg, Michael Knap and Anna Fulterer for always having time for me when I was unable to get even the simplest things to work on my own and for many funny discussion.

Last but not least, I want to thank Andreas Hirczy for his help with my computer whenever it refused to work properly and I wasn't able to fix it.

Of course there are a lot more people I would like to thank, but I think listing all the names would take to many pages, so I want to thank all of them together, especially all my friends in Vorarlberg, Vienna and in the rest of Austria and also those abroad.